



ЕЛЕКТРОТЕХНИЧКИ ФАКУЛТЕТ
УНИВЕРЗИТЕТА У БАЊАЛУЦИ

FACULTY OF ELECTRICAL ENGINEERING
UNIVERSITY OF BANJALUKA

ЕЛЕКТРОНИКА *ELECTRONICS*

FACULTY OF ELECTRICAL ENGINEERING BANJALUKA

Address: Patre 5, 78000 Banjaluka, Republic of Srpska, Bosnia and Herzegovina

Phone: +387 51 211 408, +387 51 212 002

Fax: +387 51 211 408

ELECTRONICS

Editor: Prof. Branko L. Dokić Ph. D.

Faculty of Electrical Engineering, University of Banjaluka

Republic of Srpska

e-mail: bdokic@etf-bl.rstel.net

Program Committee:

- Nikolaos Uzunoglu, National Technical University of Athens, Greece
- Barry Jefferies, University of Hertfordshire, UK
- Vojin Oklobdzija, University of California, Davis, USA
- Bratislav Milovanović, Faculty of Electronics Niš, FR Yugoslavia
- Milić Stojić, Faculty of Electrical Engineering Beograd, FR Yugoslavia
- Vojislav Aranđelović, Institute "Vinča" Beograd, FR Yugoslavia
- Veljko Milutinović, Faculty of Electrical Engineering Beograd, FR Yugoslavia
- Ilija Stojanović, SANU Beograd, FR Yugoslavia
- Vladimir Katić, Faculty of Technical Science Novi Sad, FR Yugoslavia
- Aleksandar Ilišković, Faculty of Electrical Engineering Banjaluka, RS
- Milorad Božić, Faculty of Electrical Engineering Banjaluka, RS

Secretary: Goran Ninković, M. Sc., Faculty of Electrical Engineering

University of Banjaluka, Republic of Srpska

e-mail: ngogi@etf-bl.rstel.net

Language editors: Milena Mandić

Radomir Kosić

Publisher:

Faculty of Electrical Engineering, University of Banjaluka, Republic of Srpska

Address: Patre 5, 78000 Banjaluka

Phone: +387 51 211 408, +387 51 212 002

Fax: +387 51 211 408

Printed in:

GLAS - SRPSKI, Banjaluka

Number of printed copies: 300

Editorial

We are pleased to offer our readers the latest issue of our journal *Electronics*. I invited the authors of distinguished papers presented at the symposium INDEL '98 (Banja Luka, October 1998) to share in the publication and give their permission to publish their papers, either in full or abridged. All of them kindly welcomed the idea. Most of the authors abridged or expanded their papers, such as: Vladimir Katić, Predrag Petković, Saša Ristić, Milun Jevtić. The paper *Failure Mechanism in Power MOSFETs in Radiation Environment* by Predrag Habaš and Ninoslav Stojadinović was accepted at INDEL '98 as invited paper. The authors, however, were not able to attend the symposium so the paper was not presented. The papers by Danilo Mandić, Bratislav Danković, Petar Marić and Milojko Jevtović do not pertain to INDEL '98.

I hope that our readers will be satisfied with the quality of the papers. I shall be particularly happy and obliged if some of them decide to share with us in the future publications of our journal and thus give us the honour of offering their papers to our readership for the first trial of their quality.

Branko L. Dokić, *Editor*

Failure Mechanisms in Power MOSFETs in Radiation Environment

Predrag Habaš and Ninoslav Stojadinović

Abstract— Degradation mechanisms in power MOSFETs (VD and LDMOS structures) and IGBTs subjected to irradiation are briefly reviewed. Two qualitatively different classes of failures are observed: 1) silicon bulk-related, and 2) gate and insulation oxide-related failures. Bulk effects are caused by upset of ionized (charged) particles or secondary charged particles generated by upset of high energy neutral particles (e.g. neutrons), and thereby created electron-hole pairs in the form of charge wake and burst in silicon. The generated free carriers may lead to: (1) triggering of internal parasitic structures inherent in VDMOSFET (bipolar transistor), and IGBT (thyristor) - single event burnout (SEB), and (2) discharging of the charge collected at the oxide/silicon interface through the gate oxide - single event gate rupture (SEGR). Both effects (1) and (2) result in a catastrophic device failure. Moreover, particle bombarding causes silicon lattice damage, resulting in increased concentration of bulk recombination centers. The oxide-related failures occur when high energy particles or photons pass through the oxide, which leads to a sequence of complex, but today relatively understood processes in the SiO_2 matrix. These finally result in trapping of charge in the oxide and in creation of electrically active traps at the oxide/silicon interface. Both effects do not lead to MOSFET catastrophic failure, but derivate device characteristics, which may result in a faulty circuit operation. In this paper, we concentrate on the techniques used for electrical characterization of the gate-oxide and interface damage in power VDMOSFETs exposed to radiation. In particular, various current-voltage, charge-pumping and capacitance-voltage techniques are briefly reviewed with respect to their (possible) application on power VD(LD)MOSFETs.

I. INTRODUCTION: POWER MOSFETs AND RADIATION ENVIRONMENT

POWER MOSFETs are exposed to radiation in several applications: aerospace (satellite, spacecraft), airplanes, military, and some medical, nuclear and industrial environments ([1]). The effects may even occur in everyday commercial use due to cosmic rays and natural radiation. Radiation represents a serious reliability

P. Habaš is with IMEC, Kapeldreef 75, B-3001 Leuven (B), and Institute for Solid State Electronics, Vienna University of Technology, Floragasse 7, A-1040 Vienna (A). E-mail: habas@imec.be and phabas@fkesserver.fke.tuwien.ac.at.

N. Stojadinović is with Faculty of Electronic Engineering, University of Niš, Beogradska 14, 18000 Niš (Yu). E-mail: nino@unitop.elfak.ni.ac.yu.

concern in technology design and application of power MOSFETs, particularly for the aerospace use. For the aerospace applications compact high-frequency switching power supplies (SPS) with small and light inductive and capacitive components are required. Thanks to their fast switching speed, high input resistance (relatively easy drive circuit), negative temperature coefficient of the drain saturation current and the absence of the classical second breakdown, power VDMOSFETs are very suitable for switches in these SPSs. In the space, VDMOSFETs are exposed to very high cosmic radiation; they can accumulate an ionization dose up to 10–100 krads over the 10 years satellite mission ([2],[3]). A simple protection by shielding is inefficient, and the devices have to be designed to tolerate the large radiation dose for a certain period of time (desired lifetime). Primary cosmic rays are isotropic and consists of 89% protons, 10% α -particles and 1% heavy ions. Their huge energies range up to 10^{19} eV [4]. After entering Earth's atmosphere the primary rays collide with atmospheric atoms producing secondary rays of: electrons, protons, neutrons, neutrinos, muons, photons, etc. The energy of secondary rays spreads from low 1 eV to still high 100 GeV ranges. The flux of secondary cosmic rays is significantly larger at the aircraft altitudes than at the sea level (occ. 100 times [5]). The environmental conditions may be simulated in the laboratory characterization of the radiation hardness of semiconductor devices by the use of various artificial sources: neutron beams [4], α -particle sources and heavy ions sources (to replace neutron beams [6],[7]) for investigation of bulk-related failures, and γ rays [3],[8],[9],[10], high energy UV light [11], β rays (electrons) [12] and X rays [9],[13] for studies of oxide-related failures.

In this paper, a brief overview of the silicon bulk-related failures in power MOSFETs exposed to radiation is given in Section II. Section III considers the gate-oxide degradation of irradiated power MOSFETs. The impact of oxide damage on power MOSFET characteristics, and the techniques used to measure the oxide damage in irradiated devices are shortly reviewed in Section IV. Section V provides a few examples of

the characterization of irradiated power MOSFETs by using techniques in Section IV.

II. BULK-RELATED FAILURES: SINGLE EVENT UPSET

The upset of high-energy charged particles (protons, electrons, α -particles, ions) into silicon bulk (single event upset; SEU) causes ionization and generation of a large amount of free electron-hole pairs along the particle trajectory in silicon - charge wake. Since the particles are highly energetic, they normally pass through the device active area. After the upset which lasts only a few fs (may be estimated as device dimension/light speed), the generated electrons and holes separate due to internal electric field in the device and flow towards the oxide/silicon interface and terminal contacts (it is assumed that power MOSFET (IGBT) is normally biased, with large drain (anode) bias in the off-state - low gate bias). This process lasts in ps to ns range. In DRAMs and SRAMs, the generated charge may induce the *soft error*; a well known failure mechanism, traditionally caused by α -particles emitted from the package material. Typically, α -particles deposit about $16fC/\mu m$ in silicon, while protons (H^+), electrons and muons generate less charge per μm . Energetic heavy ions, however, can deposit much larger charge than α -particles. On the other side, high-energy neutrons normally pass the device without interaction. Rarely, they collide with *Si* nucleus inducing secondary particles in the silicon bulk: protons, α -particles, neutrons, and recoiling nucleus of silicon or a lighter element, Fig.1. Since the recoiling nucleus are heavy, they have short travel distance in silicon, but are highly ionizable. They can deposit up to $154fC/\mu m$ in silicon (which is at least 10 times larger than the charge generated by α and other charged light particles) [4]. Due to their short path in silicon (about $5\mu m$ for $10MeV$ energy) and high ionization rate, they produce a localized charge burst in the bulk (rather than a charge wake). Note that the charge collection due to the upset of high energy neutrons and heavy ions is considered as the major source of soft errors in DRAMs and SRAMs today, but not due to the α -particles from the package [4].

Heavy ions generated by neutron bombarding may be recoiling charged *Si* nucleus, or parts of *Si* nucleus as *Al*, *Mg*, *Na*, *F*, etc. The large free charge in the bulk generated by the upset of a heavy ion or by a recoil nucleus may cause the following two effects in power MOSFETs and IGBTs: single event burnout (SEB) and single event gate rupture (SEGR).

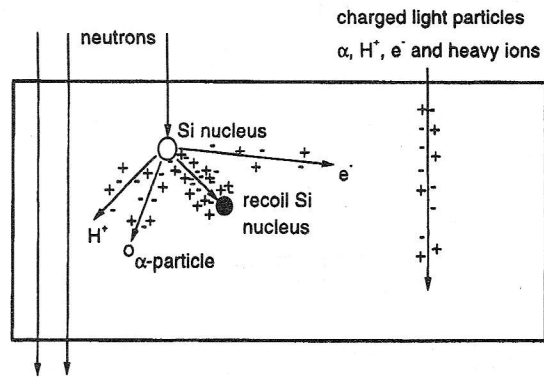


Fig. 1. Schematic view of the effects of upset of neutrons, and charged light particles and heavy ions into the silicon bulk. High energy neutrons typically pass the material without interaction, but some of them collide with *Si* nucleus producing charged light particles and highly ionizable recoiling nucleus of silicon or a lighter element.

A. Single event burnout (SEB):

Parasitic bipolar transistor inherent in VDMOSFET structure (Fig.2) can latch-up. The hole current due to a total amount of N generated e-h pairs in the device may be calculated by $I_h(t) = e \cdot v_{sat}^p \cdot N$, where v_{sat}^p is the hole saturation drift velocity (the electric field is sufficiently high for nominal high drain bias). The collected hole current I_h pass the n⁻-epi/p junction and flows towards the external p⁺ contact, causing a direct polarization of the n⁺-source/p⁻ (E-B) junction due to the lateral series resistance of p⁻ region. If I_h is sufficiently large, it can sustain: the direct polarization of the E-B junction, electron injection into the base (p⁻ region) and flow towards the collector (n⁻ region) due to transistor effect, and impact ionization in the B-C depleted region. The later effect increases the initial base hole current, and results in the breakdown of bipolar structure (breakdown voltage of bipolar transistor with a resistor in the base branch BV_{CER}) Fig.2, finally leading to device destruction. The turn-off of the MOSFET channel cannot stop this regenerative process. Note that the probability that a neutron pass through a VDMOSFET and collides with a silicon nucleus is very small, but if this event happens, the probability of the device burnout is very high. By proper design of device geometry and doping profiles (n⁺ and p⁺ regions) the susceptibility of VDMOSFETs to SEB failure can be minimized [14]. An equivalent burnout effect may occur in IGBTs due to latch-up of parasitic thyristor structure which consists of p⁺ anode, n⁻ region (MOSFET drain), p (MOSFET bulk) and n⁺ cathode (MOSFET source), as well as in the other power devices [15].

Remember that the latch-up of the parasitic transistor is a well known catastrophic failure of IGBTs in short-circuited load conditions. In both VDMOSFETs and IGBTs the SEB effect causes a short between the drain (anode) and source (cathode).

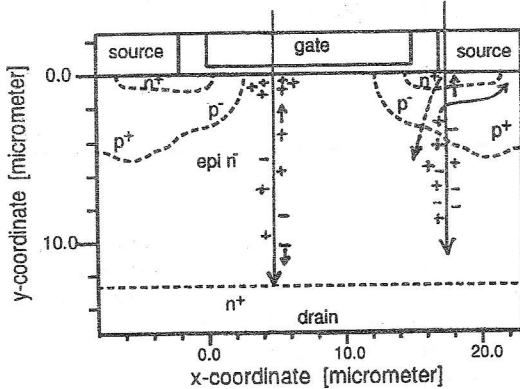


Fig. 2. The geometry of power VDMOSFET across two half-cells. Charge collection causing single event burnout (SEB) due to latch-up of parasitic bipolar transistor, and the charge collection causing single event gate rupture (SEGR) due to gate oxide breakdown are denoted. The electron-hole pairs generated by upset of a high energy particle (SEU) separate in the electric field due to high drain bias applied. The shown doping profile is calculated by numerical process simulation for device EFLIN10 produced by El-Microelectronics (Niš).

B. Single event gate rupture (SEGR):

After a high energy ionizing particle pass through the device in the region of the gate oxide, the holes generated in the bulk flow towards the oxide/silicon interface because of the drain bias. Moreover, the generated electrons flow towards the drain contact. Note that an enhanced carrier generation can occur by impact ionization process when the drain bias is high and the induced dipole charge in the bulk is large ([15]). The build-up of the excess positive charge at the interface due to holes lasts typically in the μs range (E.g. for $U_{DS} = 100V$ and epitaxial layer thickness of $20\mu m$, an average field of $50kV/cm$ results in saturation drift velocity $v_d \approx v_{sat}^p = 9 \times 10^6 cm/s$ at $300K$, and transit time in the order of $10\mu m / 9 \times 10^6 cm/s \approx 100ps$). As a consequence of the charge build-up, a transient increase in the oxide field occurs, which vanishes in time with the flow of the collected holes towards the p region of the VDMOSFET (bulk region of the channel). If the transient field peak is sufficiently large, carriers may be injected into the gate oxide by a short Fowler-Nordheim tunneling (in this case, for n^+ type of gate, electrons are injected from the gate conduction band towards the n^- substrate). If the injected charge exceeds the charge-

to-breakdown (Q_{BD}) a catastrophic breakdown of the gate oxide occurs, resulting in a short between the gate and substrate: single event gate rupture effect (SEGR). The steady-state oxide field E_{ox} is rather insensitive to the drain bias in power VDMOSFETs (for high U_{DS} the interface is inverted (holes), so the surface potential is limited). The steady-state E_{ox} depends directly on the gate bias, but the transient field peak is strongly affected by the vertical electric field due to U_{DS} . If the gate oxide breakdown occurs at a critical oxide field of E_{ox}^c , the steady-state oxide field which will be enhanced up to the value of E_{ox}^c due to the upset of an ion with a linear transfer energy LET may be empirically expressed as $E_{ox}^c/(1+c \cdot \text{LET})$ [7]. This relationship nicely reflect the experimental data for different heavy ions as shown in Fig.3. Note that LET is the stopping power divided by the mass density of the target material.

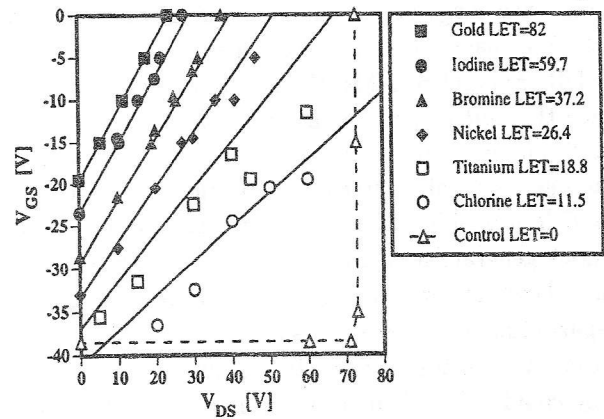


Fig. 3. Measured critical gate and drain biases for which the critical transient oxide field E_{ox}^c occurs in power VDMOSFET as a consequence of upset of different energetic ions with characteristic linear energy transfer: SEGR effect (LET in $MeVcm^2/mg$). From [7].

C. Silicon lattice damage in the bulk:

Silicon atoms can be displaced from their equilibrium position in the crystal lattice by: collision of neutrons with Si atoms (damage forms as clusters with size $\leq 10nm$), irradiation with high energy β -particles, and γ -recoil due to transmutation reactions. Displacement of Si atoms results in vacancies and interstitials in the lattice. Vacancies may be stable in silicon as phosphorus-vacancy and vacancy-vacancy complexes. Moreover, bombarding of ^{14}Si nucleus with neutrons may cause nuclear reactions which result in ^{13}Al (acceptor in silicon) and ^{12}Mg (deep recombination center in silicon). Increased concentration of crystal defects and recombination centers after irradiation reduces the carrier life-time in the silicon bulk. The latter may

change some device electrical characteristics (leakage current and breakdown characteristics). Neutron irradiation is also used in power devices to produce uniform low doped n-type silicon by transmutation of *Si* into *P* (transmutation doping by neutron absorption), but low energy (thermal) neutrons are used in this case.

III. OXIDE-RELATED FAILURES

Passing an ionized particle or photon through the SiO_2 (gate oxide, insulation oxides) triggers sequences of relatively complex and still not completely understood phenomena. These processes take place during irradiation, but also last long time after the radiation stops (seconds, hours, years); the later we call post-irradiation effects. All these processes finally result in four classes of damage in irradiated oxides:

1. Trapped charge in the oxide N_{ox} ,
2. Traps at the oxide/silicon interface N_{it} ,
3. Switching states (traps deeper in the oxide, but close to the oxide/silicon interface): border traps,
4. Increased concentration of electron and hole trapping sites in the oxide.

A. Classes of damage in irradiated oxides

1) Total trapped charge (fixed charge) in the oxide is given by $N_{ox}^{tot} = \int_0^{t_{ox}} \rho_{ox}(y) dy$. Note that MOSFET characteristics are not influenced by N_{ox}^{tot} , but by the effective charge reduced to a charge sheet at the oxide/bulk interface $N_{ox} = \int_0^{t_{ox}} y \cdot \rho_{ox}(y) dy / t_{ox}$. Both electrons and holes can be trapped, but *trapped holes is a typical effect for irradiated oxides* (positive N_{ox}). This charge does not communicate with the underlying silicon bulk (except for tunneling effects - detrapping). The oxide vacancy in silicon matrix $O_3 \equiv Si \bullet \bullet Si \equiv O_3$, known as E' center, is an important and the best studied deep trapping site for holes in SiO_2 [19],[20] (double donor-like trap). It is the dominant hole trap in thermally grown SiO_2 used for gate oxides in MOS technology. Hole trapped on E' is stable. The physics of other hole traps in SiO_2 is not completely understood at present, but there is a clear evidence for the role of sites different than E'. Known defects are non-bridging oxygen: $O_3 \equiv Si - O \bullet$ (donor-like hole trap), and *Si* vacancy (induces shallow acceptor and donor-like traps in SiO_2).

2) Interface traps at the SiO_2/Si interface communicate with conduction and valence band of silicon in a broad time scale (from $\sim ps$ for traps close to the band edges, up to $\sim 100ms$ for traps at the midgap - about intrinsic level). The trap occupancy depends

on the rates of four processes: electron capture and emission, and hole capture and emission with respect to the conduction and valence band in silicon, respectively. For interface traps classical Shockley-Read-Hall statistics is assumed to hold. In equilibrium, the trap population is governed by the Fermi-level at the interface. Today, it is accepted that the free dangling bond of the surface Si atom $Si_3 \equiv Si \bullet$, where \bullet represents an weakly bonded electron, is the major source of traps at the SiO_2/Si interface. This defect is called P_b center (on (111) surface; on (100) P_{b0} and P_{b1} defects are detected). After thermal gate oxide grown, the interface contains a large concentration of P_b defects, but most of them are passivated by hydrogen in a regularly applied subsequent high-T forming gas anneal by the reaction: $Si_3 \equiv Si \bullet + H_2 \rightarrow Si_3 \equiv Si - H + H^0$ (with activation energy $E_a = 2.6V$). Some of P_b centres remain or are generated by depassivation in subsequent very high-T steps during device processing (in junction and other anneals, by the reaction: $Si_3 \equiv Si - H \rightarrow Si_3 \equiv Si \bullet + H^0$). They represent low N_{it} which is measured in devices after final processing (today in the order of $10^{10} \text{ cm}^{-2} \text{ eV}^{-1}$). Radiation causes depassivation of passivated P_b centres by the reactions described in the next subsection, which results in the N_{it} increase. From the electrical point of view, it is believed that the P_b defect is amphoteric [19],[20]. It induces two trapping levels in the band gap: an acceptor-like trap in the upper half and a donor-like trap in the lower half of the band gap. Both traps can accept and release one electron. Acceptor-like trap is neutral when empty and charged with one negative elementary charge when occupied by electron, while donor-like trap is charged with one positive elementary charge when empty, and neutral when occupied. The energy levels of trapping sites spread across the whole upper and lower half of the band gap. When the Fermi-level at the interface coincides with the intrinsic level in silicon (midgap) the charge in interface traps due to trap occupancy should be zero for all traps related to P_b centres (so-called neutral point). This assumption is the basis for the often used midgap technique (Section IV). The accuracy of this assumption is, however, never confirmed. Apart from the P_b defect, experiments show the evidence for other defects acting as interface traps, but they seem to be of less importance. Their physical structure and electrical nature is not clear at present.

3) Switching states (also called border traps) are fixed charges in the oxide, but which communicate with the underlying silicon on long time scales (ms to

days). Their population can be changed by applying gate bias in a sufficiently long time. In thin oxides, switching traps represent an important fraction of oxide trapped charge, and cannot be neglected in analysis. It is demonstrated that some (if not all) switching states are E' centres located close to the SiO_2/Si interface [18],[20]. Switching states are those traps observed in random-telegraph-signal (RTS) and low-frequency noise. Today, it is finally established that they cause $1/f$ noise in MOSFETs. Switching traps can be created in a large amount in irradiated thin oxides. It is important to note that they may contribute to the value of N_{it} which is extracted by low-f and DC techniques for measurement of interface trap density (QS C-V, HF C-V stretch-out and I-V methods), but are not sensed by medium/high-f techniques (like charge pumping).

4) Generation of neutral electron and hole traps in the oxide by irradiation is confirmed by experiments in which Fowler-Nordheim (FN) and substrate or channel hot carrier injections are applied on the previously irradiated oxides (see e.g. [13]). Enhanced charge trapping is observed in irradiated with respect to control oxides, which may be attributed to defect creation by breaking of bonds during irradiation. On the other side, it is known from uniform substrate electron and hole injection studies that high electric field in the oxide during carrier injection strongly enhances the generation of neutral traps in the oxide bulk [16]. Contrary to FN injection conditions, the oxide field is relatively low in radiation studies because they are performed for nominal biases under moderate oxide fields. Consequently, electrons are not strongly heated in the oxide after their generation by incident radiation, so hot electrons do not cause defect creation in irradiated oxides. Moreover, the oxide field in power VDMOSFETs for nominal bias conditions is much smaller than the oxide field in submicron CMOS devices. E.g. for power VDMOSFET with $t_{ox} = 100nm$ at $U_{GS} = 10V$ it follows $E_{ox} \approx 1MV/cm$ (a low field), while for a $0.18\mu m$ MOSFET with $t_{ox} = 4.0nm$, a nominal gate bias of $U_{GS} = 1.8V$ results in $E_{ox} \approx 4.5MV/cm$ (relatively high field).

B. Chemical/electrical phenomena in irradiated oxide

The present understanding of the effects occurring after high-energy photons pass the oxide is summarized in the following. A photon with energy $h\nu$ produces e-h pairs and e-h excitons in the SiO_2 . Note that thermally grown oxides on silicon have vitreous structure (fused silica), not of quartz or amorphous. Fused silica

contains a lot of non-bridging oxygen atoms. In these processes various weaker bonds are broken in SiO_2 : $\equiv Si-O-Si \equiv + h\nu \rightarrow \equiv Si-O\bullet + \equiv Si\bullet + e^- + h^+$, $\equiv Si-H + h\nu \rightarrow \equiv Si\bullet + H^0 + e^- + h^+$, and $\equiv Si-OH + h\nu \rightarrow \equiv Si\bullet + \bullet OH + e^- + h^+$. Oxide field is sufficiently high to remove generated electrons in a short time (for oxide thickness $t_{ox} = 100nm$, it follows $\tau = t_{ox}/v_{sat}^{n,ox} \approx 0.7ps$, where $v_{sat}^{n,ox} = 1.5 \times 10^7 cm/s$ is the electron saturation velocity in conduction band of SiO_2). Contrary to electrons, generated holes flow very slowly through the oxide under the influence of electric field due to their very large effective mass in the valence band of SiO_2 . They become easily trapped on oxide vacancies $O_3 \equiv Si\bullet \bullet Si \equiv O_3 + h^+ \rightarrow O_3 \equiv Si\bullet + Si \equiv O_3$, non-bridging oxygen $O_3 \equiv Si-O + h^+ \rightarrow O_3 \equiv Si-O^+$, and trivalent Si in the oxide $O_3 \equiv Si\bullet + h^+ \rightarrow O_3 \equiv Si^+$. The holes move towards the polysilicon-oxide/oxide or oxide/silicon-bulk interface mostly by hopping process, dependent on the oxide field polarity. Consequently, radiation produces a lot of trapped holes in the bulk of oxide, resulting in positive N_{ox} . After irradiation, N_{ox} may decrease in time due to slow postirradiation effects:

- electron tunneling from the silicon valence band into trapped holes in oxide,
- thermal recombination of electrons from the SiO_2 valence band (hole emission into the oxide valence band) - T -activated process,
- reaction with atomic hydrogen [23]:
 $O_3 \equiv Si^+ \bullet Si \equiv O_3 + H^0 \rightarrow O_3 \equiv Si\bullet \bullet Si \equiv O_3 + H^+$, and
 $O_3 \equiv Si^+ + H^0 \rightarrow O_3 \equiv Si\bullet + H^+$.

The generation of interface traps involve more complex processes. In "hole transport and trapping model" generated holes move towards the oxide/silicon interface, and become deeply trapped close to the interface. These holes may turn into interface traps by reaction: $Si_3 \equiv Si-H + h^+ + e^- \rightarrow Si_3 \equiv Si\bullet + H^0$. The "hole trapping" mechanism is believed to be dominant in thermally dry-grown gate oxides in some studies [2],[28]. The second class of models give the dominant role to "hydrogen transport" [11],[12],[19],[22]. Neutral hydrogen atoms H^0 are generated in the bulk of oxide by breaking of $Si - H$ bonds (given above), or by breaking of OH in the reaction which involves e-h excitons: $Si-OH + \text{exciton energy} \rightarrow Si-O\bullet + H^0$. Hydrogen atoms diffuse towards the interface (the process is T -activated in the range $90 - 120K$, and gate bias independent). At the interface H^0 can react with a passivated P_b center (depassivation) in the exothermic

reaction with practically no energy barrier:

$Si_3 \equiv Si-H + H^0 \rightarrow Si_3 \equiv Si\bullet + H_2$. Thus, interface defect P_b ($Si_3 \equiv Si\bullet$) is generated. This H^0 process accounts for a smaller part of the generated interface traps, and occurs relatively short after the irradiation. A more important role in the N_{it} creation plays the drift of H^+ ion (proton). It is related to the T -activated processes in the range $> 200K$, and is strongly gate bias dependent. For positive gate bias, H^+ ion drifts towards the SiO_2/Si interface, where it may produce interface trap ("proton transport model") by the reaction: $Si_3 \equiv Si-H + H^+ + e^- \rightarrow Si_3 \equiv Si\bullet + H_2$. Here, an electron e^- is consumed from the silicon bulk. The model of H^+ drift can explain the experimental observation that the N_{it} build-up during postradiation anneal is accelerated by applying positive gate bias, and rather suppressed by applying negative gate bias. Fig.4 shows the famous experiment by Saks [12], which supports the H^0 and H^+ models. Note that the postradiation N_{it} increase depends strongly on the anneal T . The build-up of N_{it} during postradiation annealing, from small densities immediately after the radiation up to large densities which may exceed the density of N_{ox} , is called "rebound effect" [25]. The H^+ may be produced in oxide by:

1. cracking of H_2 molecules generated in other processes on positive charged centres, as E' center ($E_a = 0.3eV$ only) and broken $Si-O$ bonds with trapped h^+ , in a reaction of type
 $A^+ + H_2 \rightarrow A-H + H^+$,
2. reaction of H^0 with a self-trapped hole:
 $trapped h^+ + H^0 \rightarrow H^+$,
3. reaction of H^0 with a hole trapped on trivalent Si :
 $O_3 \equiv Si^+ + H^0 \rightarrow O_3 \equiv Si\bullet + H^+$.
4. reaction of H^0 with an E' center:
 $O_3 \equiv Si\bullet + Si \equiv O_3 + H^0 \rightarrow O_3 \equiv Si\bullet\bullet Si \equiv O_3 + H^+$.

The "hydrogen model" assumes that hydrogen is present in the gate oxide, but why is it present? Oxide (even thermally grown) contain hydrogen because it can easily penetrate during various technology processes. Moreover, hydrogen is used to passivate free dangling bonds after oxide grown (reaction is given in Subsection III-A). Oxide may also contains water, mostly in the form of OH . Note that a more complete model should also account for the following passivation reactions $Si_3 \equiv Si\bullet + H^0 \rightarrow Si_3 \equiv Si-H$ (essentially no energy barrier, $E_a = 0.3 - 0.6eV$), and $Si_3 \equiv Si\bullet + H_2O \rightarrow Si_3 \equiv Si-OH + H^0$, and for $H^0 + H^0 \rightarrow H_2$. The depassivation reaction $Si_3 \equiv Si-H \rightarrow Si_3 \equiv Si\bullet + H^0$ normally does not

occur, because it requires very high T .

It is well-known from experiments that the interface trap generation after irradiation is more pronounced in wet than in dry-grown oxides. This fact may be attributed to the presence of a large amount of OH group which is involved in the H^0 and, indirectly, H^+ generation (as described above). Due to problems in the proton transport model, advanced considerations have involved H_3O^+ in the processes; details may be found in [19].

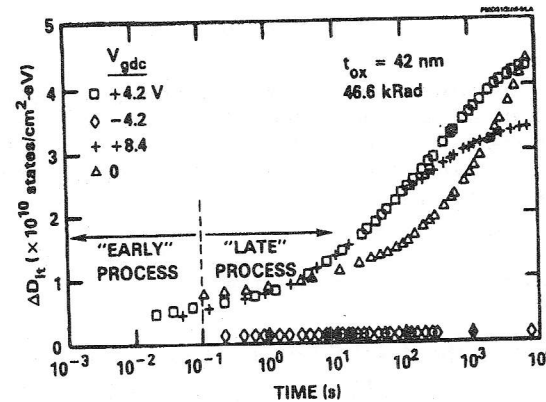


Fig. 4. Increase in density of interface traps ΔD_{it} in four irradiated MOSFET's with different gate biases during postradiation thermal anneal. The "early" build-up of traps is bias independent and may be attributed to the near-interface trapped hole and H^0 processes. The "late" process is strongly gate bias-dependent and is caused by the proton drift (H^+). Note that the initial trap density in the devices before irradiation was about $1.2 \times 10^{10} cm^{-2}eV^{-1}$; only the charge pumping technique is able to resolve small ΔD_{it} in the early phase. The figure is taken from [12].

The N_{ox} and N_{it} are not proportional to the total irradiation dose. Measurements, like those shown in Fig.5, show a power-law relationship ([2],[3],[40],[47]). The power (the slope in the log-log scale) is ≤ 1 . This sub-linear relationship is regularly found in the hot-carrier injection experiments, as well. A clear explanation is presently not available.

IV. EFFECT OF OXIDE DAMAGE AND ITS CHARACTERIZATION IN POWER VDMOSFETS

In all MOS devices, radiation induces spatially rather uniform charge trapping in the oxide and traps at the oxide/silicon interface ([1]). Damaged devices show:

- shift in the threshold voltage U_{th} (Fig.6),
- reduced transconductance g_m and drain current I_D (Fig.9),
- increased subthreshold slope (Fig.6),
- increased subthreshold leakage current (Fig.6), and
- degraded breakdown characteristics ([3]).

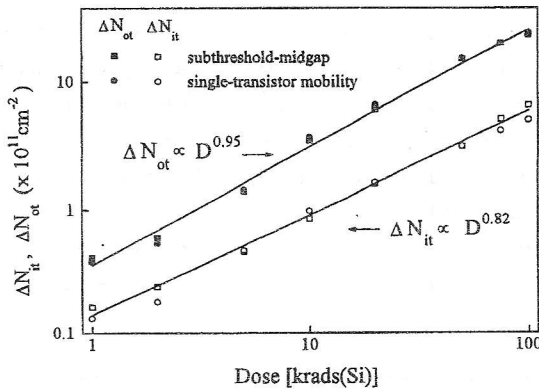


Fig. 5. Measured increase in the oxide fixed charge and interface trap density in power VDMOSFET as a function of applied ^{60}Co γ -ray dose in the rate $4\text{ rads(Si)}/\text{s}$ [40]. The gate is positively biased at $U_{GS} = 9\text{ V}$ during the irradiation, and the postirradiation anneal is not performed. The data is extracted by using the midgap technique and the μ_s -degradation technique. The experimental data can be fitted by a power-law relationship with a power less than 1.

The shift in the threshold voltage has two components $\Delta U_{th} = \Delta U_{th,ox} + \Delta U_{th,it}$: a constant shift due to fixed charge N_{ox} (gate bias independent), and a shift due to charge captured on interface traps N_{it}^\pm which depends on the surface Fermi level (gate bias). As well known, for uniform surface charge $\Delta U_{th,ox(it)} = q \cdot N_{ox(it)}/C_{ox}$ holds, where $C_{ox} = \epsilon_{ox}/t_{ox}$. The drain current decreases as a consequence of decrease in the surface mobility μ_s due to surface charge coulomb or enhanced surface roughness scattering. For irradiated n -channel power VDMOSFETs particularly critical is the large negative shift in the threshold voltage due to positive fixed charge accumulated in the oxide (Fig.6), which causes a catastrophic failure of the switching circuit (the switch cannot be turned-off). Moreover, the transconductance degradation and eventually, a positive threshold voltage shift due to interface trap buildup during long-term anneal (rebound effect) may result in improper device operation point.

Similar to irradiation, various electrical stress also result in a nearly uniform spatial distribution of oxide trapped charge and interface traps in MOSFET: Fowler-Nordheim tunneling, substrate electron or hole injection, optically induced injection, etc. In numerous studies of uniform gate oxide degradation in the literature, several experimental techniques have been developed for a separate extraction of uniform ΔN_{ox} and ΔN_{it} after stress. Usually monitored quantities are:

- threshold voltage shift ΔU_{th} [27],[28],[29],
- subthreshold slope decrease [30],[31],[32],

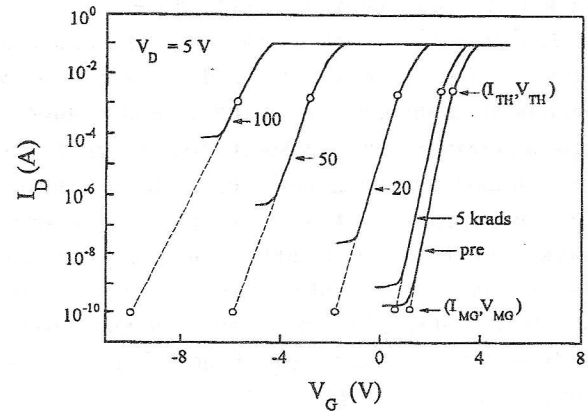


Fig. 6. Subthreshold characteristics in saturation of power VD-MOSFET subjected to ^{60}Co γ -irradiation [40]. The gate is positively biased at $U_{GS} = 9\text{ V}$ during the irradiation, and the postirradiation anneal is not performed. The drain current at the threshold voltage I_{TH} and the midgap conditions I_{MG} is denoted. The radiation causes negative shift in the characteristics due to positive fixed charge trapped in the oxide, and the stretch-out of the characteristics (subthreshold slope increase) due to interface trap generation.

- surface mobility degradation, observed either as MOSFET gain-factor β change [28],[29] or MOSFET transconductance g_m change [27],
- midgap voltage shift [8],[33],[34],
- gate C-V and G-V characteristics [35],[36],[37], and
- charge-pumping characteristics [13],[38],[39].

The dual-transistor mobility [34], and the dual-transistor charge-pumping methods [33] represent advanced approaches.

These techniques are used routinely for measurement of the spatially uniform damage in irradiated conventional bulk and SOI MOSFETs. Most of them have also been applied on irradiated power VDMOSFETs:

- the threshold voltage shift ΔU_{th} in combination with the gain factor β change [2],[40],
- the midgap method [26],[40],[41], and
- the ΔU_{th} in combination with the subthreshold-slope method [3].

Limitations of these commonly used techniques are known. The subthreshold-slope methods have a low sensitivity, and are not applicable on short-channel devices, as well as on devices with high leakage current. They become inaccurate in the presence of lateral nonuniformities ([31]). The methods are affected by the surface potential fluctuations [42], which result in inaccurate values of the interface trap density [30]. The accuracy of the subthreshold slope method for VDMOSFETs which have a strongly nonuniform lateral channel profile, has never been studied.

The surface-mobility techniques are sensitive to values of the model coefficients [2],[29] (the parameters should be adjusted for a particular technology). They are inaccurate in the presence of spatial nonuniform N_{it} and N_{ox} . The surface mobility is not only affected by interface traps ([27]), but also by charge trapped in the oxide [28],[29],[37],[41],[43], in the strength which strongly depends on the distance of the trapped charge from the interface [43],[44],[45]. Moreover, a controversial behavior has been reported that positive fixed oxide charge increases surface mobility, but not decreases [28],[41],[46].

The midgap method is strongly based on the assumption on the acceptor-like and donor-like nature of traps in the upper and lower half of the band gap, respectively. This physical picture reflects the P_b centres, but several authors have proposed the existence of donor-like and acceptor-like traps also in the opposite part of the gap. The midgap method is affected by the spatial nonuniformities [8],[33]. An exact determination of the midgap current is difficult for non-uniform channels, like those in VDMOSFETs. This method is not applicable on devices with high leakage and anomalous subthreshold current (often the case for power MOSFETs). We have confirmed by numerical modeling with MINIMOS-6 [57],[59] that the midgap method is inaccurate if interface traps are localized in the energy space and the density of fixed oxide charge is small.

The dual-transistor methods have overcome some limitations of the single transistor techniques, but require n -channel and p -channel devices with simultaneously processed gate oxides [33],[34]. This is never the case for power MOSFETs.

The limitations of the well established C-V and G-V techniques when applied on conventional MOSFETs are fully clarified, and may be found in e.g. [24],[36]. The C-V techniques can also be applied on VDMOSFETs, even in the form of the split C-V measurements. These novel results will be presented in [48].

Charge pumping (CP) enables accurate, extremely high sensitive and direct measurements of N_{it} [49],[50], independently of N_{ox} in various MOS devices (bulk MOSFETs, SOI MOSFETs, SOI *pin*-diodes, thin-film transistors, EPROMs). The CP current is given by $I_{cp} = q \cdot f \cdot S_G \cdot N_{it}$, where f is the gate-pulse frequency, q the elementary charge, S_G the active gate area, and $N_{it} = \int D_{it}(E)dE$ an average areal trap density across the part of the band gap which is active in CP effect. Recently, a method is developed by the authors of this paper for the application of CP techniques directly on

standard power VDMOSFETs [10],[51],[52]). In several further studies, this method has been used on standard VDMOSFETs [53],[56], or special four-terminal VDMOS structures are used [54]. The method proposed in [10] can be applied on power LDMOSFETs, as well. The main problem which has delayed the application of the CP technique on VDMOS structure in the research community was the absence of a separate bulk contact. In VD and LDMOSFETs, the source and bulk of the channel are always short-circuited as shown in Fig.7. This fact can, however, be used to perform CP effect at the oxide/epitaxial-region interface [10]. The source contact can play a role of the bulk contact and supply holes, unless the n^+ -source region is inactive. In CP measurements these conditions are fulfilled if the channel is always biased under the device threshold voltage during the excursion of the gate bias. Electrons which recombine by trapped holes are supplied by the drain contact. In that cases, n -channel VDMOS structure behaves like a conventional p -channel bulk MOSFET (n^+ source is inactive), which enables all common CP measurements (see Figs.8,10). The applicability of the method has been justified by theoretical, numerical modeling and experimental considerations [10],[51]. It

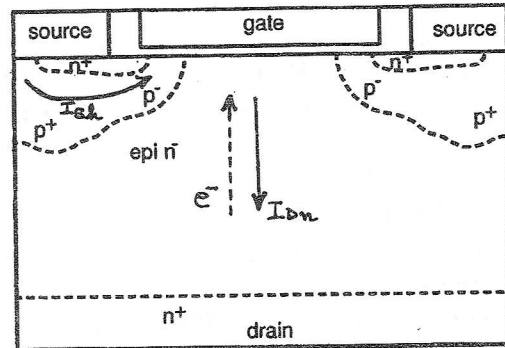


Fig. 7. Charge pumping effect in a power VDMOS cell. The arrows denote the DC-component of the drain electron current I_{Dn} and source hole current I_{Sh} due to net recombination of electrons and holes at the oxide/epitaxial- n^- interface.

should be pointed out that the interface above the channel region is of the primary interest for VDMOSFET characterization. This CP method senses the interface above the n^- -epitaxial region and in a part of the channel, but not directly in the channel. The epitaxial-region interface is of small importance for VDMOS operation. The described CP approach is, however, useful for the evaluation of an overall gate oxide quality in VDMOSFETs and its hardness against the radiation.

V. A GLIMPSE ON EXPERIMENTAL RESULTS

Commercial power VDMOSFETs of 100, 150 and 200V produced by "Ei-Microelectronics" (Niš) are irradiated with γ -rays from ^{60}Co source. Devices have the gate oxide thickness $t_{ox} = 100\text{ nm}$, thermally grown in dry oxygen at 1100°C ; n^+ -polysilicon gate; (100) wafer thickness $400\mu\text{m}$ and wafer doping 10^{19} cm^{-3} . They consist of about 860 hexagonal cells which are arranged in a hexagonal geometry with the distance between the cell centers of $33\mu\text{m}$. The geometry of the structure across two half-cells is shown in Fig.2.

Since the current measured on power VDMOSFETs in the charge-pumping active region (in the channel subthreshold region) is proportional to the density of traps at the gate-oxide/epi- n^- interface, it can be used to measure this density after irradiation. Moreover, the charge trapped in the oxide during irradiation is expected to shift the complete characteristics by its electrostatic effect. CP measurements are carried out with electrometer Keithley 617 placed either in the source or drain branch; the other terminal was grounded (it can also be biased such that the p^-/n^- junction is reverse polarized). Trapezoidal pulses are applied on the gate (HP8116A). Above U_{th} the channel of VDMOSFET's is open during the gate-pulse top level and the measurements are invalid. Figs.8 show experimental CP characteristics of a VDMOSFET before and after γ -irradiation. In virgin device (before irradiation), from the maximum of I_{cp} we calculate $N_{it} = 2.9 \times 10^9\text{ cm}^{-2}$, while N_{ox} cannot be directly extracted. From the increase in the maximum I_{cp} and the shift on the voltage axis, the damage in the irradiated transistor can be extracted: $N_{it} = 1.1 \times 10^{10}\text{ cm}^{-2}$, and $\Delta N_{ox} = 1.8 \times 10^{12}\text{ cm}^{-2}$, respectively. These values correspond to the oxide/epi- n^- interface, but not to the channel region. Remark that $N_{ox} \gg N_{it}$, which is typical for oxides immediately after radiation. In this case the impact of the charge captured in interface traps on the voltage-axis shift is negligible, which enables accurate determination of N_{ox} . The characteristics of the irradiated device is stretched-out in sub-CP-threshold region (Fig.8), for which an explanation is proposed in [10].

In the second example, 100V VDMOSFETs were exposed to ^{60}Co γ -radiation in the dose of 500 Gy , with dose rate 0.037 Gy/s , and the gate bias $U_{GD} = 10\text{ V}$. After irradiation the devices were separated into three groups and annealed during 350 days at 140°C with the gate biased at $+10\text{ V}$, 0 V and -10 V . Figs.9 show the transfer and subthreshold characteristics of the devices

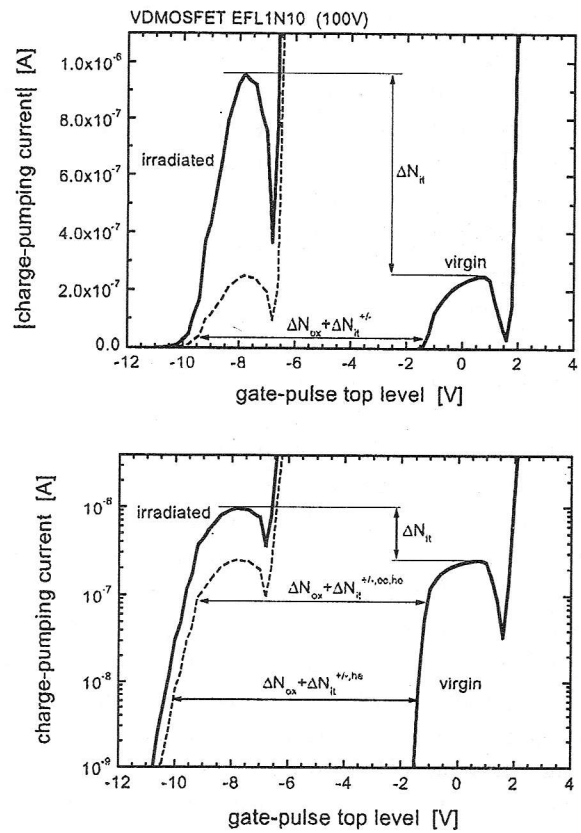


Fig. 8. Charge-pumping characteristics of a power 100V VDMOSFET measured before and after irradiation. Upper figure: linear current scale. Lower figure: logarithmic scale. Trapezoidal gate pulses are applied: $f = 100\text{ kHz}$, 50% duty-cycle, rise and fall time $t_r = t_f = 1\mu\text{s}$, amplitude $\Delta U_G = 3\text{ V}$, $U_{DS} = 0\text{ V}$, and $T = 300\text{ K}$.

in saturation before the irradiation (the spread of the characteristics is small), and after the anneal. It is crucial to point out that these I-V characteristics reflect the oxide trapped charge and interface traps generated in the MOS channel close to the source junction. For all three gate bias polarities during anneal a large amount of positive fixed charge remains trapped in the gate oxide. The interface trap build-up is, however, much enhanced for positive gate bias ($+10\text{ V}$) than for 0 V and negative bias (-10 V). A decrease in the current in the overthreshold region caused by the decrease in the surface mobility due to build-up of N_{it} may be observed for $+10\text{ V}$ curve in Fig.9. Using the midgap technique, by considering the differences in the threshold voltage shift and the midgap voltage shift, the following oxide damage is obtained from data in Figs.9 for $N_{ox}[\text{cm}^{-2}]$ and $N_{it}[\text{cm}^{-2}]$: 3.9×10^{11} and 6.9×10^{10} for -10 V , 1.8×10^{11} and 2.6×10^{10} for 0 V , and 1.6×10^{11} and 1.65×10^{11} for $+10\text{ V}$, respectively. It is evident that after long high- T anneal, particularly for $+10\text{ V}$ on the

gate, N_{it} becomes of the same order, and eventually, dominates over N_{ox} (rebound effect).

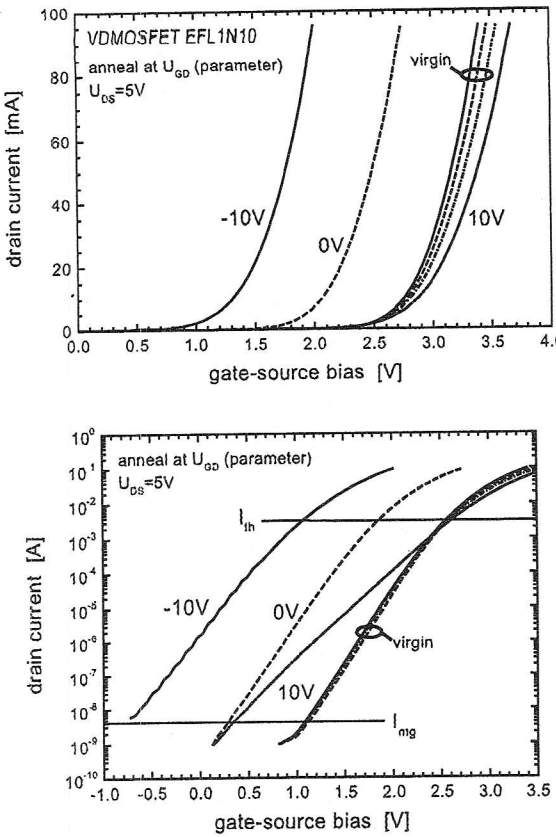


Fig. 9. Transfer and subthreshold characteristics in saturation for 100V VDMOSFETs exposed to ^{60}Co γ -irradiation in the dose of 500Gy with the gate biased at $U_{GD} = 10\text{V}$. The devices were annealed during 350 days at 140°C with the gate at $+10\text{V}$, 0V and -10V . In measurements $U_{DS} = 5\text{V}$.

In cases with significant ΔN_{it} the shift in the CP characteristics (I_{cp} vs. gate-pulse base or top level) is not only determined by ΔN_{ox} , but also by the charge in interface traps. The processes which determine the rising edge of the CP characteristics are rather complex, and are out of scope of this paper. They are fully clarified in a complete theoretical model recently [10],[55],[58]. The shift in the CP characteristics due to electron capture in interface traps (N_{it}^{ec} in Fig.8) is negligible in the deep-CP-subthreshold region. The most important fact is that in this region a part of interface traps, N_{it}^{he} , is charged by hole emission at the gate-pulse top level. The shift in the CP characteristics is, therefore, not only due to N_{ox} , but also due to a constant contribution of N_{it}^{he} . Note that this conclusion cannot follow from common simple model of the CP characteristics. Consequently, in cases with high ΔN_{it} simple extraction of ΔN_{ox} from the shift in the

CP characteristics is not possible without knowledge on the $D_{it}(E)$ profile in the lower part of the band gap and the trap nature.

Experimental data for cases with high interface trap densities is shown in Figs.10. These characteristics are measured on devices considered in Fig.9 before irradiation and after the anneal. From the maximum I_{cp} the N_{it} in particular devices is obtained, and denoted in the figure. These values of N_{it} correspond to the oxide/epi- n^- interface, but not to the channel close to the source (like for I-V methods). The N_{it} values obtained by the CP method differ significantly from the N_{it} values obtained by the I-V methods (midgap and U_{th} shift) due to the following possible reasons:

- This CP technique measures the total trap density in a portion of the band gap which is determined by the electron and hole emission levels (see e.g. [50],[55],[58]). For the CP current the nature (charge) of traps is irrelevant. The U_{th} -shift and midgap methods sense the effective electrical effect of the charge trapped in interface traps. These I-V methods do not detect traps which are neutral at the threshold conditions (assuming P_b centres, for Fermi level in the upper half of the gap the traps in the lower half are neutral). In addition, the interval in the band gap which contributes to the signal is different in CP and I-V methods.
- Oxide degradation could be different in the channel close to the n^+ junction than for the epi-interface. Several reasons related to technology may be proposed. The simple explanation that the oxide field is different in these regions during irradiation and annealing should be ruled-out, because the surface potential varies only slightly along the interface from n^+ region to the center of the epi- n^- region for $+10\text{V}$ and -10V gate biases.
- A possibility for a systematic error in one of these techniques should be seriously considered. This is particularly true for the midgap technique.

The same discrepancy between the midgap- ΔU_{th} and the CP technique is found for these VDMOSFETs after stress by FN injection, where also C-V method is applied [48]. Before considering this problem on VDMOSFETs, we suggest that a systematic study of the I-V, different C-V and CP methods on the same uniformly stressed long-channel conventional MOSFETs has to be done. In these conditions, the problem is 1D, and all these techniques sense the same part of the interface. Such a study is still missing in the literature.

From the results in Fig.10, it follows (like for data in

Fig.9) that the trap density strongly increases with applying positive gate bias in anneal. In Fig.10, the shift in the CP characteristics in the deep-CP-subthreshold region corresponds to an interface charge of about $8 \times 10^{11} \text{ cm}^{-2}$, which is of the same order as the measured N_{it} . According to the discussion above, in this case the nature and trap profile $D_{it}(E)$ in the lower half of the gap ought to be known for the calculation of the ΔN_{ox} . The profile $D_{it}(E)$ can be measured by advanced CP techniques [50],[55].

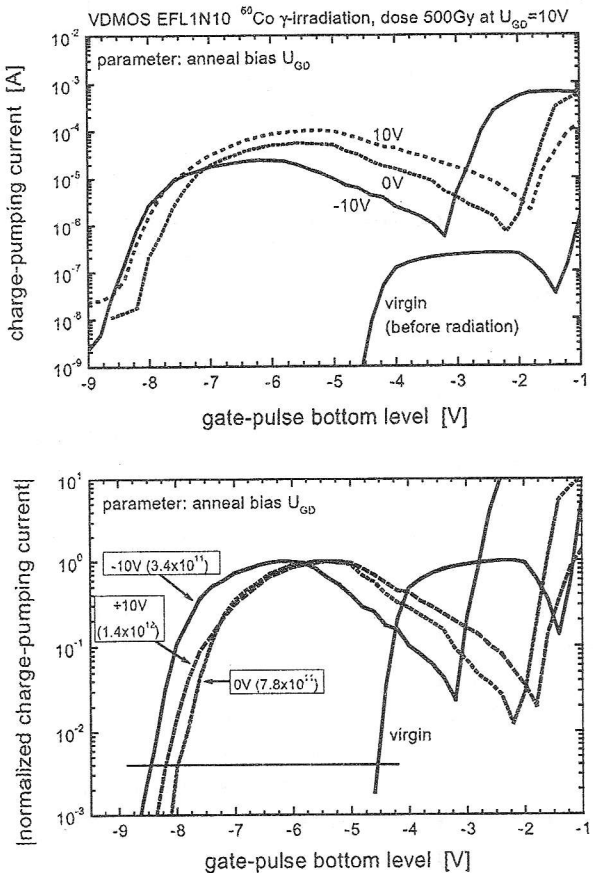


Fig. 10. Charge-pumping characteristics of VDMOSFET's from Fig.9 before irradiation and after the anneal. Upper figure: as measured; lower figure: normalized with maximum I_{cp} values. The extracted $N_{it}[\text{cm}^{-2}]$ in the devices are given in the brackets. Gate pulses in measurements are as for Fig.8.

REFERENCES

- [1] T.P.Ma and P.V.Dressendorfer, *Ionizing Radiation Effects in MOS Devices and Circuits*, Wiley-Interscience, 1989.
- [2] N.Stojadinović, S.Golubović, S.Djorić and S.Dimitrijev, "Analysis of gamma-irradiation induced degradation mechanisms in power VDMOSFETs", *Microelectron. Reliab.*, vol.35, no.3, pp.587-602, 1995.
- [3] T.Sakai and T.Yachi, "Effects of gamma-ray irradiation on thin-gate-oxide VDMOSFET characteristics", *IEEE Trans.Electron Devices*, vol.38, no.6, pp.1510-1515, 1991.
- [4] W.R.McKee et al., "Cosmic Ray Neutron Induced Upsets as a Major Contributor to the Soft Error Rate of Current and Future Generation DRAMs", in Proc. of *Int. Reliab. Phys. Symp. (IRPS)*, pp.1-6, 1996.
- [5] Z.F.Ziegler and W.A.Lanford, "The effect of sea level cosmic rays on electron devices", *J.Appl.Phys.*, vol.52, pp.4305-4312, 1981.
- [6] T.J.Aton, J.Seitchik and H.Shichijo, "Comparison of Charge Collection from Energetic Ions Typical of Neutron-Recoil Events with Charge Collection from Alpha Particle Strikes", in Proc. of *Int.Reliab.Phys.Symp. (IRPS)*, pp.7-11, 1996.
- [7] M.Allenspach, J.Brews, K.Galloway, G.Johnson, R.Schrimpf, R.Pease, J.Titus and C.Wheatley, "SERG: A Unique Failure Mode for Power MOSFETs in Spacecraft", *Microelectron. Reliab.*, no.11/12, pp.1871-1874, 1996.
- [8] P.J.McWhorter and P.S.Winokur, "Simple technique for separating the effects of interface traps and trapped-oxide charge in metal-oxide-semiconductor transistors", *Appl.Phys.Lett.*, vol.48, no.2, pp.133-135, 1986.
- [9] D.M.Fleetwood, P.S.Winokur and J.R.Schwank, "Using laboratory X-ray and Co-60 irradiations to predict CMOS device response in strategic and space environments", *IEEE Trans.Nuclear Science*, vol.35, no.6, pp.1497-1505, 1988.
- [10] P.Habaš, Z.Prijić, D.Pantić and N.D.Stojadinović, "Charge-Pumping Characterization of SiO_2 Interface in Virgin and Irradiated Power VDMOSFETs", *IEEE Trans.Electron Devices*, vol.43, no.12, pp.2197-2209, 1996.
- [11] J.F.Conley and P.M.Lenahan, "Radiation Induced Interface States and ESR Evidence for Room Temperature Interactions Between Molecular Hydrogen and Silicon Dangling Bonds in Amorphous SiO_2 Films on Si", in Proc. of *Int. Conf. on Insul. Films on Sem. (INFOS)*, pp.215-218, 1993.
- [12] N.S.Saks, C.M.Dozier and D.B.Brown, "Time Dependence of Interface Trap Formation in MOSFETs Following Pulsed Irradiation", *IEEE Trans. Nuclear Science*, vol.35, no.6, pp.1168-1177, 1988.
- [13] A.Balasinski, W.Chen and T.P.Ma, "Effects of combined X-ray irradiation and hot-electron injection on NMOS transistors", *J.Electron.Mat.*, vol.21, no.7, pp.737-743, 1992.
- [14] G.H.Johnson, J.H.Hohl, R.D.Schrimpf and K.F.Galloway, "Simulating Single-Event Burnout of n-Channel Power MOSFET's", *IEEE Trans. Electron Dev.*, vol.40, no.5, pp.1001-1008, 1993.
- [15] H.L.Zeller, "Cosmic Ray Induced Failures in High Power Semiconductor Devices", *Microelectron. Reliab.*, vol.37, no.10/11, pp.1711-1718, 1997.
- [16] G.Groeseneken, R.Bellens, G.Van den bosch and H.E.Maes, "Hot-carrier degradation in submicrometre MOSFETs: from uniform injection towards the real operating conditions", *Sem.Science and Techn.*, vol.10, pp.1208-1220, 1995.
- [17] N.S.Saks and R.B.Klein, "Effect of Hydrogen Annealing after Channel Hot Carrier Stress", in Proc. of *Int.Conf.on Insul.Films on Sem. (INFOS)*, pp.265-268, 1993.
- [18] D.M.Fleetwood, M.Shaneyfelt, W.Warren, J.Schwank, T.Meisenheimer and P.Winokur, "Border Traps: Issues for MOS Radiation Response and Long-Term Reliability", *Microelectron. Reliab.*, vol.35, no.3, pp.403-428, 1995.
- [19] E.H.Poindexter, G.J.Gerardi and D.J.Keeble, "Hydrogen Speciation in Electronic Silica", in Proc. of *The Physics and Chemistry of SiO_2 and Si- SiO_2 Interface*, vol.96-1, pp.172-183, The Electrochemical Society, 1996.
- [20] J.F.Conley, Jr., "Application of Electron Spin Resonance as a Tool for Building in Reliability (BIR)", in Proc. of *Mat.Res.Soc.Symp.*, vol.428, pp.293-309, 1996.
- [21] R.E.Stahlbush, "Slow and Fast State Formation Caused by Hydrogen", in Proc. of *The Physics and Chemistry of SiO_2 and Si- SiO_2 Interface*, vol.96-1, pp.525-537, The Electrochemical Society, 1996.
- [22] D.L.Griscom, "Hydrogen Model for Radiation-Induced Interface States in SiO_2 -on-Si Structures: A Review of the Evidence", *J.Electron.Mat.*, vol.21, no.7, pp.763-767, 1992.
- [23] Y.Wang, W.R.Fahrner and D.Bräunig, "Annealing of irradiation induced positive oxide charges in SiO_2 /Si-MOS struc-

- tures as described by hydrogen reactions", in Proc. of *Int. Conf. on Insul. Films on Sem. (INFOS)*, pp.223-226, 1993.
- [24] E.H.Nicollian and J.R.Brews, *MOS (Metal Oxide Semiconductor) Physics and Technology*, John Wiley & Sons, 1982.
- [25] J.R.Schwank, P.S.Winokur, P.J.McWhorter, F.W.Sexton, P.V.Dressendorfer and D.C.Turpin, "Physical mechanisms contributing to device 'rebound'", *IEEE Trans.Nuclear Science*, vol.31, no.6, pp.1434-1438, 1984.
- [26] A.Jakšić, G.Ristić and M.Pejović, "Effects of γ -irradiation and postirradiation thermal annealing in power VDMOSFETs", in Proc. of *MIEL Conf.*, Niš (YU), pp.241-246, 1995.
- [27] K.F.Galloway, M.Gaitan and T.J.Russell, "A simple model for separating interface and oxide charge effects in MOS device characteristics", *IEEE Trans.Nuclear Science*, vol.NS-31, no.6, pp.1497-1501, 1984.
- [28] S.Dimitrijev, S.Golubović, D.Župac, M.Pejović and N.Stojadinović, "Analysis of gamma-radiation induced instability mechanisms in CMOS transistors", *Solid-State Electronics*, vol.32, no.5, pp.349-353, 1989.
- [29] S.Dimitrijev and N.Stojadinović, "Analysis of CMOS transistor instabilities", *Solid-State Electronics*, vol.30, no.10, pp.991-1003, 1987.
- [30] R.J.van Overstraeten, G.Declerck and G.L.Broux, "Inadequacy of the classical theory of the MOS transistor operating in weak inversion", *IEEE Trans.Electron Devices*, vol.ED-20, no.12, pp.1150-1153, 1973.
- [31] J.-S.Lyu, K.-S.Nam and C.Lee, "Determination of the interface trap density in MOSFETs from the subthreshold slope measurements", in Proc. of *Conf. on Solid-State Dev.and Mat. (SSDM)*, Tsukuba (Japan), pp.167-169, 1992.
- [32] C.C.-H.Hsu and T.H.Ning, "Voltage and temperature dependence of interface trap generation by hot electrons in p- and n-poly gated MOSFETs", in Proc. of *VLSI Technology Symp.*, pp.17-18, 1991.
- [33] J.R.Schwank, D.M.Fleetwood, M.R.Shaneyfelt and P.S. Winokur, "A critical comparison of charge-pumping, dual-transistor and midgap measurement techniques", *IEEE Trans.Nuclear Science*, vol.40, no.6, pp.1666-1677, 1993.
- [34] D.M.Fleetwood, M.Shaneyfelt, J.Schwank, P.Winokur and F.Sexton, "Theory and application of dual-transistor charge separation analysis", *IEEE Trans.Nuclear Science*, vol.36, no.6, pp.1816-1824, 1989.
- [35] D.J.DiMaria and J.W.Stasiak, "Trap creation in silicon dioxide produced by hot electrons", *J.Appl.Phys.*, vol.65, no.6, pp.2342-2356, 1989.
- [36] E.H.Nicollian, "Electrical characterization of defects created in the Si-SiO₂ system by ionizing radiation", *J.Electron. Mat.*, vol.21, no.7, pp.721-729, 1992.
- [37] S.Manzini, "Effect of coulomb scattering in n-type silicon inversion layers", *J.Appl.Phys.*, vol.57, pp.411-414, 1985.
- [38] M.M.Heyns, D.K.Rao and R.F.De Keersmaecker, "Oxide field dependence of Si-SiO₂ interface state generation and charge trapping during electron injection", *Appl.Surf.Science*, vol.39, pp.327-338, 1989.
- [39] N.Yasuda, H.Nakamura, K.Taniguchi and C.Hamaguchi, "Interface state generation mechanism in n-mosfets", *Solid-State Electronics*, vol.32, no.12, pp.1579-1583, 1989.
- [40] N.Stojadinović, S.Djorić, S.Golubović and V.Davidović, "Separation of the irradiation induced gate oxide charge and interface traps effects in power VDMOSFETs", *Electron.Lett.*, vol.30, no.23, pp.1992-1993, 1995.
- [41] D.Župac, K.F.Galloway, R.D.Schrimpf and P.Augier, "Effects of radiation-induced oxide-trapped charge on inversion-layer hole mobility at 300 and 77K", *Appl.Phys.Lett.*, vol.60, no.25, pp.3156-3158, 1992.
- [42] R.J.van Overstraeten, G.Declerck and G.L.Broux, "The influence of surface potential fluctuations on the operation of the MOS transistor in weak inversion", *IEEE Trans.Electron Devices*, vol.ED-20, no.12, pp.1154-1158, 1973.
- [43] S.C.Sun and J.D.Plummer, "Electron mobility in inversion and accumulation layers on thermally oxidized silicon surfaces", *IEEE Trans.Electron Devices*, vol.ED-27, no.8, pp.1497-1508, 1980.
- [44] C.T.Sah, T.H.Ning and L.L.Tschopp, "The scattering of electrons by surface oxide charges and by lattice vibrations at the silicon-silicon dioxide interface", *Surface Science*, vol.32, pp.561-575, 1972.
- [45] F.Gámiz, J.A.López-Villanueva, J.Banqueri and J.E. Carrasco, "Influence of the oxide-charge distribution profile on electron mobility in MOSFET's", *IEEE Trans.Electron Devices*, vol.42, no.5, pp.999-1004, 1995.
- [46] N.Stojadinović, M.Pejović, S.Golubović, G.Ristić, V. Davidović and S.Dimitrijev, "Effect of radiation-induced oxide-trapped charge on mobility in p-channel MOSFETs", *Electron.Lett.*, vol.31, no.6, pp.497-498, 1995.
- [47] S.Djorić and V.Davidović, "Analysis of Gamma-Irradiation Induced Oxide Charge and Interface Trap Effects in Power VDMOSFETs", in Proc. of *MIEL Conf.*, Niš (YU), pp.259-262, 1995.
- [48] P.Habaš, "Split C-V characteristics of VDMOS transistors and their application in study of gate oxide degradation", in preparation.
- [49] J.S.Brugler and P.G.A.Jespers, "Charge pumping in MOS devices", *IEEE Trans.Electron Devices*, vol.ED-16, no.3, pp.297-302, 1969.
- [50] G.Groeseneken, H.E.Maes, N.Beltra'n and R.F.De Keersmaecker, "A reliable approach to charge-pumping measurements in MOS transistors", *IEEE Trans.Electron Devices*, vol.ED-31, no.1, pp.42-53, 1984.
- [51] P.Habaš, Z.Prijić and D.Pantić, "The application of charge-pumping technique to characterize the Si/SiO₂ interface in power VDMOSFETs", in Proc. of *Int.Conf.on Insul.Films on Sem. (INFOS)*, Grenoble (F), pp.171-174, June 1995.
- [52] P.Habaš, "The application of the charge-pumping technique in reliability analysis of MOS devices", in Proc. of *RELETRONIC*, Budapest (Hungary), pp.319-328, Oct. 1995.
- [53] A.Jakšić and P.Igić, "Use of charge pumping for characterising interface traps during thermal annealing of irradiated power VDMOSFETs", *Electronics Lett.*, vol.32, no.23, pp.2183-2184, 1996.
- [54] S.C.Witzak, K.Galloway, R.Schrimpf, J.Titus, J.R.Brews and G.Prevost, "The Determination of Si-SiO₂ Interface Trap Density in Irradiated four-terminal VDMOSFETs using Charge Pumping", *IEEE Trans.Nuclear Science*, vol.43, no.6, pp.2558-2564, 1996.
- [55] P.Habaš, *Analysis of Physical Effects in Small Silicon MOS Devices*, Technical Univ. Vienna (A), 1993.
- [56] G.Prevost, P.Augier and J.-M.Palau, "The use of charge-pumping for characterizing irradiated power MOSFETs", in Proc. of *RADECS*, Oct. 1995.
- [57] Group of authors, *MINIMOS 6 - User's Guide*, Institute for Microelectronics, Technical University Vienna (A), 1995.
- [58] P.Habaš, "Qualitative Analysis and Analytical Model of the Charge Pumping Characteristics of MOS Structure", in Proc. of *MIEL Conf.*, Niš (YU), pp.605-610, 1997.
- [59] P.Habaš, D.Pantić, Z.Prijić and N.Stojadinović, "Technology CAD of low-voltage power VDMOSFET", in Proc. of *CAS*, Sinaia (R), pp.501-510, Oct. 1994.

MODELING & SIMULATION OF AC/DC CONVERTERS IN MODERN ELECTRIC DRIVES

Vladimir Katić and Dušan Graovac

UNIVERSITY OF NOVI SAD
FACULTY OF ENGINEERING

Institute for Power, Electronics & Telecommunication Engineering
21000 Novi Sad, Fruškogorska 11
YUGOSLAVIA

E-mail: katav@uns.ns.ac.yu, dusangr@Eunet.yu

Abstract: Modern electric drives are characterised with application of digitally controlled power electronics converters. For proper design of control and power electronic converter circuit, a computer simulation is necessary. Usually, the simulation model consists of power electronic converter model with its control circuit and model of the electric machine with a load. A variety of models are available for each part. In this paper, the review and discussion of different AC/DC converter models are presented. In the first part, the models of power electronics converters are selected for different application. Then, the models of the particular electric machine type and control circuit are shown. At the end, examples of DC motor drive supplied from the current type of AC/DC converter and AC motor drive that apply voltage AC/DC converter with PWM control are shown. The simulation scheme, voltage and current waveforms are given.

Keywords: Mathematical modeling, Power electronics converters, Drives

List of symbols:

- | | |
|--|---|
| C - capacitance of input filter. | PF - power factor. |
| C_d - capacitance of DC link filter. | R - dumping resistance of the filter. |
| $\cos\Phi_1$ - displacement power factor (DPF). | R_d - DC motor resistance, armature resistance. |
| E_d - e.m.f. of DC motor. | R_e - overall resistance at the AC input of converter added to on-state resistance of power semiconductors. |
| $F_\omega(s)$ - transfer function of the control circuit. | S - apparent power. |
| h - harmonic order. | s - Laplace transform plane. |
| HDI - individual harmonic distortion of input current. | [T] - Transfer function matrix. |
| $[i_{ac}(\omega t)]$ - input current matrix. | T_a and T_m - armature and mechanical time constants. |
| $I_{acF}(s)$ - Laplace presentation of the current at input terminals of LC filter. | T_d - load time constant. |
| $[i_{ach}(\omega t)]$ - input current h-th harmonic matrix. | THDI - total harmonic distortion of input current. |
| $I_{ac}(s)$ - Laplace presentation of the current at input terminals of the rectifier. | [T_n] - Negative sequence transfer function matrix. |
| i_{ach} - h-th harmonic of the current at input terminals of rectifier. | [T_p] - Positive sequence transfer function matrix. |
| I_{acFh} - h-th harmonic of the current at input terminals of LC filter. | T_{pi} - time delay of current sensor. |
| $i_{ac1}, i_{ac2}, i_{ac3}$ - line currents in phases 1,2,3. | $T_{p\omega}$ - time delay of speed sensor. |
| I_d - DC motor current. | T_s - switching period. |
| I_n - rated DC motor current. | T_T - time delay of rectifier. |
| i_0, i_d, i_q - zero, d and q component of AC current. | T_ω - time delay of speed regulator. |
| J - moment of inertia. | U_{ac} - supply voltage. |
| k_{pi} - gain of current sensor. | $[u_{ac}(\omega t)]$ - input voltage matrix. |
| $k_{p\omega}$ - gain of speed sensor. | $[u_{ach}(\omega t)]$ - h-th harmonic input voltage matrix. |
| k_ω - gain of speed regulator. | $u_{ac1}, u_{ac2}, u_{ac3}$ - balanced phase voltages of phases 1,2,3. |
| L - the input filter inductance. | $u_{ac1h}, u_{ac2h}, u_{ac3h}$ - the h-th harmonics voltages of phases 1,2,3. |
| L_d - DC motor inductance, armature inductance. | |
| L_n - supply inductance. | |
| m_L and m_b - load and base torque. | |
| P - active power. | |

$U_d(\omega)$ - DC motor or DC side voltage.
 U_{d0} - average value of DC voltage.
 U_{dh} - value of the DC voltage h-th harmonics.
 U_n - rated DC motor voltage.
 $[u_{sh}(\omega)]$ - supply voltage matrix.
 U_1, U_2, U_3 - maximum values of phase voltages 1,2,3.
 U_{1h}, U_{2h}, U_{3h} - maximum values of the h-th harmonics of phase voltages 1,2,3.
 X_C - rectifier transformer or commutation inductance.
 X_n - network inductance.

X_C and X_L - input filter inductances
 $[X_{Nh}]$ - the h-th harmonic line inductance matrix.
 Z_{dh} - load impedance at harmonic h.
 Ψ_f - flux.
 Ψ_{fn} - normalized nominal flux.
 ϕ_h - phase angle of DC current h-th harmonics.
 Φ_1 - displacement power factor (DPF) angle.
 ω - angular frequency of supply.
 $\omega_a, \omega_b, \omega_n$ - actual, base and nominal angular speed.

1. INTRODUCTION

An electrical energy converter in a modern variable speed electric motor drives, consists of power electronic converter (single or combined), control circuitry and electrical motor (electrical to mechanical energy converter) with its load torque. For proper analysis and design of drive, it is necessary to develop models for all mentioned integral parts.

Models of electrical machines are well known [1,2]. General electric machine model can be represented by a set of equations representing electromagnetic and mechanical properties [1]. Such approach is very complex and assumes complicated mathematical apparatus - linear transformations are used. The transformed models are developed for each type of electric machines in form of differential non-linear equations with time invariant coefficients.

Drives, control strategy and control circuitry are also well described [2,3]. In the last decade, switch mode control techniques, such as pulse width modulation (PWM) have prevailed over phase controlled ones. However, such converters require fast switching components, capable of operating on high frequencies and special consideration during converter design.

Modelling power electronics converters is a broad subject, which can be considered as modelling AC/DC converters, DC/AC converters, DC/DC converters and AC/AC converters. The aim of modelling is to provide transfer function of converter in a form suitable for further connection to other blocks of a drive.

The general form of a power electronics converter is a nine-switch AC/AC converter called matrix converter [4]. All other types are special cases of it. It is developed for application in variable speed AC motor drives, which are rapidly replacing existing DC motor drives. However, it requires bilateral (four-quadrant) type of switch, so it is still not adopted from manufacturers. Present, solution for AC drives consists of AC/DC converter at supply end and

DC/AC converter at motor end. Such converters are performing the same conversion, in two steps. The converters themselves have the same configuration, while the flow of power is in inverse direction. Therefore, they have the same transfer function, i.e.; they can be modelled in a same way.

For power electronic converters modelling, two general approaches have been presented: modelling in the area of large signals and in the area of small signals. The first group of models is applied in analysis of power electronic converter input and output characteristics, while the second in obtaining linearized converter and control circuit transfer function for use mainly in DC/DC power supplies. In this paper, large signal modelling will be treated and discussed.

The model of power converter can be in form of macro model or micro model, depending on a way the power switch has been modelled. For the process of micromodeling, it is necessary to know a large number of physical parameters of switch as well as the semiconductors physics. Such approach is used in program SPICE. Although the micromodeling is very useful in semiconductor industry, for study of power electronic converter in a drive or other application macro model is quite adequate. Furthermore, considering the computer time and the need for joining model of converter, machine, power supply and control circuitry together, macromodeling shows better results than micromodeling. The most simple macro model of power switch is the ideal switch with the zero resistance in on state and infinitive resistance in off state.

The most common converter in industry is AC/DC one, whether it works in a DC drive or together with inverter in an AC drive. The customary approach in AC/DC converter modelling is to use steady state conditions and undistorted power supply.

Three-phase line-commutated, uncontrolled (diode bridge) rectifiers are usually applied in AC motor adjustable speed drives or in DC servo

motor drives. They are easy to model, as they are line commutated. Due to smoothing capacitor in DC link, discontinuous conduction of the diode rectifier occurs resulting in high input current total harmonic distortion.

Three-phase line-commutated, phase-controlled AC/DC converter, supplying DC motor drives is one of the most applied types. Models of such a converter differ in complexity to fulfil different tasks, so idealized, quasi-real model and real model of converter are recognized [5]. Models in generalized form, which can be quasi-real or real, are based on transfer matrix and considered in this paper.

However, above mentioned AC/DC converters are acting as sources of voltage and current harmonics. They also have progressively poorer power factor with decreasing of output voltage. Disadvantages of three-phase line commutated converters can be improved if pulse width modulation (PWM) control and forced commutation are applied [6]. Such PWM controlled AC/DC converters, known as PWM rectifiers, have found application in DC motor drives, PWM rectifier-inverter frequency changers etc. A much better power factor - close to 1, is achieved, but application of a low size AC filter for input current and voltage harmonic minimization is still necessary.

Further two types of AC/DC converter - current or voltage exists. Continuous or constant DC current achieved by DC link inductance characterizes current one. Voltage AC/DC converters can be recognized by DC side capacitance, i.e. continuous or constant DC voltage. As duality of both types exists, it is sufficient to examine only one [6].

In this paper, modeling of both types is described in detail, while all results can be easily applied to both current and voltage DC/AC converters as well. The authors developed models for two classes of current AC/DC converters - phase controlled one and one controlled by means of PWM using the MATLAB 4.2 software [7], especially SIMULINK toolbox. That software has been used because of a large number of different simulation blocks (linear and non-linear) and because of quality algorithms available for simulation. Models can be used for reliable estimating of converters behaviour in cases of unbalance in supply network or distorted power supply in both transient and steady states of drive.

At the end, complete model of DC motor drive supplied by a PWM rectifier and two models of AC drives supplied by AC/DC/AC converters are presented as examples. The models are applied for analysis of transient and steady state behaviour of converter, for investigation of line

current harmonics and characteristics of control circuitry.

2. MATHEMATICAL MODEL OF AC/DC CONVERTER

Fig. 1 displays the basic configuration of the power part of the system consisting of: three phase current source AC/DC converter which supplies the DC load that can be either the accumulator charging system or the DC motor drive. Switches P1-P6 are thyristors in case of phase-controlled converter. In case of PWM controlled converter, they are formed by the serial connection of power transistor and diode. On the AC side of the converter a LC filter is connected in order to minimize the supply harmonics. Filter capacitance also prevents voltage stresses on semiconductor devices and therefore serves as the snubber.

By the change of state of power switches during the converter operation configuration of circuit is constantly changing. Such behaviour is very difficult to model. In circuit that consists of n switches, possible number of states is 2^n . Large number of possible states is the main problem in formulating the equations that explains dynamic performance of the converter circuit.

One of the approaches in converter modelling is based on the fact that circuit is moving through the working states. Each of the states is defined by different equations and pass from one state to another is defined by certain criterion. Such criterion can be: Change of sign of one state variable, decrementing of state variable until zero level etc. State variables calculated at the end of one interval are used in another and such an operation is performed cyclically.

Models of AC/DC converters are needed for different purposes with various level of complexity. Idealized, quasi-real and real models can be distinguished, depending on level of real parameters approximation. Each of these models can be further divided into sub-groups, so following classification can be proposed:

- models that represent an AC/DC converter as a simple current source (idealized model). Application - for rough harmonic analysis in power networks, or harmonic power flow etc.
- models with idealized input voltage, output current and converter parameters, which use transfer matrix (idealized model). Application - for education purposes, quick (brief) engineering analysis of converter.
- models with inclusion of line and load inductance (quasi-real models). Application - modeling and line harmonics analysis.
- models with complete set of equations, (real analysis). Application - for full analysis,

- control circuit parameters calculation, transient and steady state analysis.
- models in generalised form (real analysis). Application - research of the effects of unbalance, network harmonic distortion, errors in switching impulses, e.t.c.

Covering all these models will result in lengthy paper. Therefore, only models that use transfer matrix, either as idealized or as real models, will be presented.

2.1 Model which use transfer matrix (idealized model)

Transfer function matrix [T] connects directly input and output current and voltage.

$$[i_{ac}(\omega t)] = \begin{bmatrix} i_{ac1}(\omega t) \\ i_{ac2}(\omega t) \\ i_{ac3}(\omega t) \end{bmatrix} = [T]^T \cdot I_d(\omega t) \quad (1)$$

$$\begin{aligned} U_d(\omega t) &= [T] \cdot [u_{ac}(\omega t)] = [T] \cdot \begin{bmatrix} u_{ac1}(\omega t) \\ u_{ac2}(\omega t) \\ u_{ac3}(\omega t) \end{bmatrix} = \\ &= [T] \cdot \begin{bmatrix} U_1 \sin(\omega t) \\ U_2 \sin(\omega t - 2\pi/3) \\ U_3 \sin(\omega t + 2\pi/3) \end{bmatrix} \end{aligned} \quad (2)$$

Transfer function matrix is defined as a set of time dependent switching functions of converter

legs (T_1 to T_3) or converter switches (SW_1 to SW_6):

$$[T] = \begin{bmatrix} T_1 & T_2 & T_3 \end{bmatrix} = \begin{bmatrix} SW_1 & SW_3 & SW_5 \\ SW_2 & SW_4 & SW_6 \end{bmatrix} \quad (3)$$

Switching functions of switches SW_1 to SW_6 have value 1 when switch is ON and 0 when switch is OFF. The characteristic of current controlled or DC current link converters is that Boolean sum of upper or lower switches values must be always 1:

$$\begin{aligned} SW_1 + SW_3 + SW_5 &= 1 \\ SW_2 + SW_4 + SW_6 &= 1 \end{aligned} \quad (4)$$

Transfer matrix model can be applied to both types of current controlled AC/DC converters, line commutated and PWM rectifier (fig.1). In the case of the line commutated rectifier, switching function has only one pulse of width $2\pi/3$, while for PWM rectifier it has NP pulses of different width, depending on carrier frequency, modulation index and type of PWM technique [8].

In both cases, process of commutation is neglected, which is good enough for PWM rectifier modelling, but not for line-commutated rectifier. For line-commutated rectifier, the transfer function can be corrected with additional amplitude level of value 1/2, which represents commutation process. Other solutions are also possible, but without application of transfer matrix - quasi-real models [5].

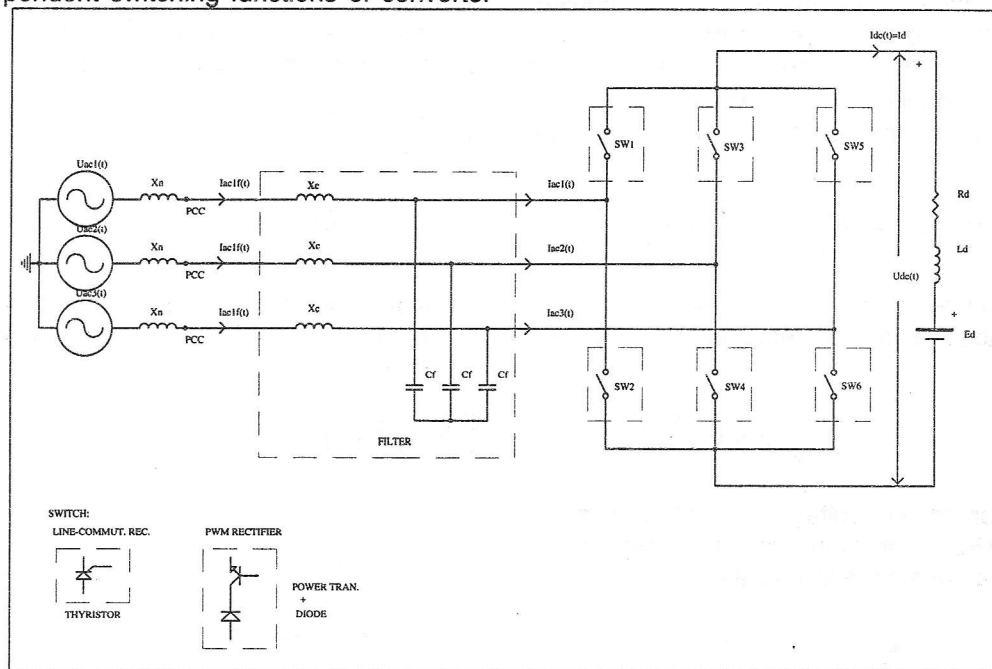


Fig. 1 - A general scheme of AC/DC converter.

2.2 Generalised model with transfer matrix (real models)

A general model using transfer matrix consists of four general equations [9]:

$$U_d(\omega t) = [\mathbf{T}] \cdot \sum_{h=1}^{\infty} [\mathbf{u}_{ach}(\omega t)] = [\mathbf{T}] \cdot \sum_{h=1}^{\infty} \begin{bmatrix} u_{ac1h} \\ u_{ac2h} \\ u_{ac3h} \end{bmatrix} = [\mathbf{T}] \cdot \sum_{h=1}^{\infty} \begin{bmatrix} U_{1h} \sin(h\omega t - \phi_{1h}) \\ U_{2h} \sin(h\omega t - \phi_{2h}) \\ U_{3h} \sin(h\omega t - \phi_{3h}) \end{bmatrix} \quad (5)$$

In the case of unbalance and switching function errors, similarly to [8], transfer and input voltage matrix can be represented with two

$$U_d(\omega t) = \left\{ [\mathbf{T}_p] + [\mathbf{T}_n] \right\} \cdot \left\{ [\mathbf{u}_{ac1p}(\omega t)] + [\mathbf{u}_{ac1n}(\omega t)] + \sum_{h=3}^{\infty} [\mathbf{u}_{achp}(\omega t)] + \sum_{h=3}^{\infty} [\mathbf{u}_{achn}(\omega t)] \right\} \quad (6)$$

In this way, the influence of network voltage harmonics, supply voltage unbalance and

balanced matrices - positive (index p) and negative (index n) ones:

switching function errors can be easily explained:

$$\begin{aligned} U_d(\omega t) = & [\mathbf{T}_p] \cdot [\mathbf{u}_{ac1p}] + [\mathbf{T}_p] \cdot [\mathbf{u}_{ac1n}] + [\mathbf{T}_n] \cdot [\mathbf{u}_{ac1p}] + [\mathbf{T}_n] \cdot [\mathbf{u}_{ac1n}] + \\ & + [\mathbf{T}_p] \cdot \sum_{h=3}^{\infty} [\mathbf{u}_{achp}] + [\mathbf{T}_p] \cdot \sum_{h=3}^{\infty} [\mathbf{u}_{achn}] + [\mathbf{T}_n] \cdot \sum_{h=3}^{\infty} [\mathbf{u}_{achp}] + [\mathbf{T}_n] \cdot \sum_{h=3}^{\infty} [\mathbf{u}_{achn}] \end{aligned} \quad (7)$$

The first four addends represent effect of unbalance and switching function errors in case of "clean" network, while the others effects of unbalance and switching function errors in case of existing network "pollution". The products of positive component of the transfer matrix with positive component of the input voltage matrix and also negative component of the transfer matrix with negative component of the input voltage matrix (the first, the fourth, the fifth and the eight addend in (7)) yield to the DC component of the output voltage and the

characteristic harmonics such as 6,12,18 etc. The cross products between respective positive and negative sequence components of the transfer matrix and the input voltage matrix yield to the DC voltage's uncharacteristic harmonics, such as 2,4,8,10, etc. For idealized case (balanced and error free operation on "clean" network) respective negative sequence components are zero and higher harmonics i.e. uncharacteristic harmonics are also zero.

2. Equation for DC current, which include the effect of DC current ripple:

$$I_d(\omega t) = (U_{d0} - E_d)/R_d + \sum_{h=2}^{\infty} [(U_{dh}/Z_{dh}) \cdot \sin(h\omega t + \phi_h)] \quad (8)$$

The presence of DC current harmonics (the second addend in (8)) represents DC current ripple.

3. Equation for AC current in which the effects of all above mentioned phenomena are included indirectly:

$$[\mathbf{i}_{ac}(\omega t)] = [\mathbf{T}^T \cdot I_d(\omega t)] = \sum_{h=1}^{\infty} [\mathbf{i}_{ach}(\omega t)] \quad (9)$$

4. Equation for AC voltage at point of common coupling (PCC) (fig.1) in which the effect of line inductance unbalance is included:

$$\sum_{h=1}^{\infty} [\mathbf{u}_{ach}(\omega t)] = \sum_{h=1}^{\infty} \left\{ [\mathbf{u}_{sh}(\omega t)] - [\mathbf{X}_{Nh}] \cdot \frac{d[\mathbf{i}_{ach}(\omega t)]}{d(\omega t)} \right\} \quad (10)$$

The matrix of line inductance $[X_{Nh}]$ includes network inductance X_n and rectifier transformer or commutation inductance X_C .

3. MATHEMATICAL MODEL OF THE DC MOTOR

The basic mathematical model of DC electric machine describes its electromagnetic and mechanical subsystem [1]. It is very complex and not suitable for engineering calculation.

$$T_d \cdot \frac{dI_d}{dt} = \frac{1}{R_d} (U_d - \psi_f \omega_a) - I_d, \quad T_d = L_d / R_d \quad (11)$$

$$T_m \cdot \frac{d\omega_a}{dt} = \psi_f I_d - m_L, \quad T_m = \frac{J\omega_b}{m_b}, \quad \omega_b = \omega_n, \quad m_b = \frac{U_n I_n}{\omega_n} \quad (12)$$

4. AC FILTER TRANSFER FUNCTION

AC side filter (Fig.1) can be modelled in per-phase manner:

$$\begin{aligned} I_{acF}(s) &= \frac{1+sRC}{s^2LC+sRC+1} I_{ac}(s) + \\ &+ \frac{sC}{s^2LC+sRC+1} U_{ac}(s) \end{aligned} \quad (13)$$

If the damping resistance is neglected the standard form of Fourier domain equations for AC filter analysis can be obtained [6]:

$$\begin{aligned} I_{acFh} &= \frac{I_{ach}}{1-h^2w^2} \\ I_{acF1} &= \frac{I_{ac1}}{1-w^2} \sqrt{1-w^4-(1/X_c^N)^2} \end{aligned} \quad (14)$$

$$\begin{aligned} w^2 &= \frac{X_L^N}{X_C^N}; \quad X_L^N = X_L \frac{I_{ac1}}{U_{ac}} \\ X_C^N &= X_C \frac{I_{ac1}}{U_{ac}} \end{aligned} \quad (15)$$

THDI, HDI and power factor (PF) can be found from (2) and (3) in the following manner:

$$F_\omega(s) = \frac{(k_\omega / k_{pi}) \cdot \psi_{fn} \cdot (1+sT_\omega)}{s^2 T_\omega T_m \cdot (1+sT_e) + (k_{pw} k_\omega / k_{pi}) \psi_{fn} (1+sT_\omega)}, \quad T_e'' = 2(T_T + T_{pi}) + T_{p\omega} \quad (20)$$

6. MODERN DC DRIVES

Modern DC drives consists of fully controlled AC/DC converter supplying DC motor loaded

Therefore, linear transformations are used and models are developed for each machine type.

A model of separately excited DC motor with adjustable armature voltage presents DC machine modeling. DC motor is represented with voltage and torque equations including load torque. Armature current is only considered, with flux as a parameter. The equations are normalised with DC motor rated values (U_n , I_n , ω_n):

$$HDL_{acFh} = HDL_{ach} \frac{1-w^2}{1-h^2w^2} \left[1-w^4 - \left(\frac{1}{X_C^N} \right)^2 \right]^{1/2} \quad (16)$$

$$THDI_{acF} = \sqrt{\sum_{h=2}^{\infty} HDI_{acFh}^2} \quad (17)$$

$$PF = \frac{P}{S} \approx \frac{\cos \Phi_1}{\sqrt{1+THDI_{acF}^2}} \quad (18)$$

The displacement power factor (DPF) angle Φ_1 can be derived as:

$$\Phi_1 = \text{atan} \left(\frac{U_{ac}}{I_{ac} X_c} \right) - \text{atan} \left(\frac{X_L I_{ac}}{U_{ac} (1-X_L/X_c)} \right) \quad (19)$$

By observing the equation (7) one can notice that Φ_1 (and DPF) strongly depends on the modulation index (through the I_{ac}). Therefore, by the use of the classical off-line control method it is not possible to obtain the unity power factor through the transient states of the drive.

5. CONTROL CIRCUIT MODEL

Control circuit is represented by its transfer function $F_\omega(s)$ [10]:

with mechanical load. The converter is connected to the power supply via input inductance X_C , representing the sum of rectifier

transformer leakage inductance and parasite inductance of cables, or the sum of commutation inductance and parasite inductance of cables. As a method for harmonic reduction, three-phase capacitor battery was considered at the converter's input, forming with input inductance a simple LC filter. Fig. 2 shows block diagram of complete drive together with details of the load and control circuit.

The mathematical model of the complete DC drive have been developed and used in analysis, i.e., the models of the DC motor, AC/DC converter, closed-loop control circuit and power supply. For easier model solving MATLAB software have been used [7]. A block scheme of complete drive, represented in MATLAB notation is shown on fig. 3.

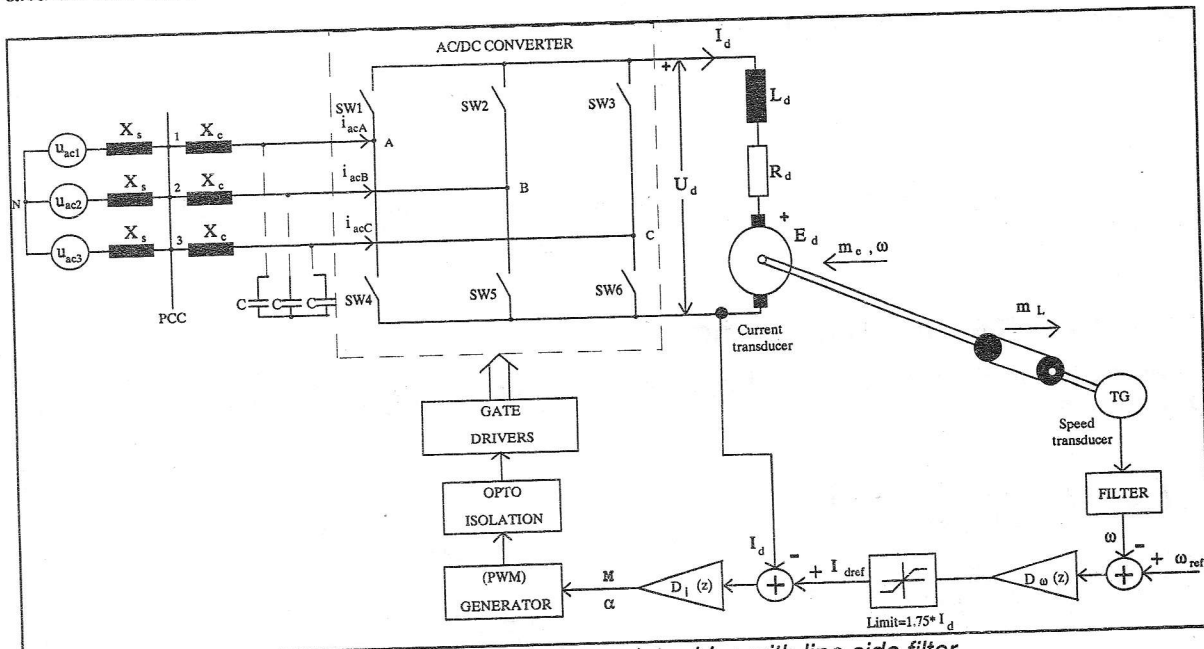


Fig.2 – Block diagram of complete drive with line side filter.

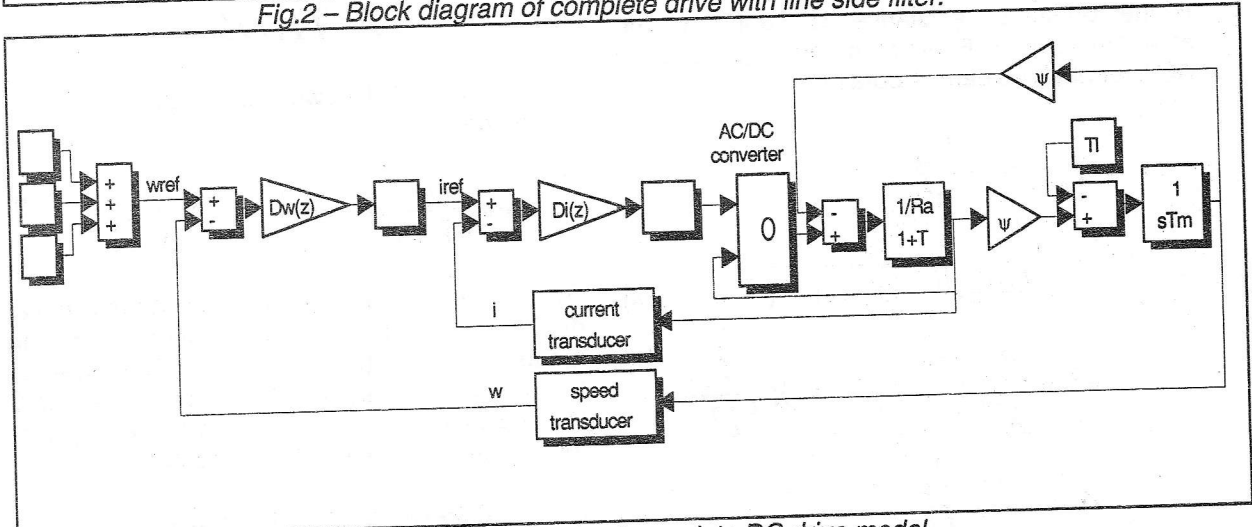


Fig.3 – MATLAB diagram of complete DC drive model.

Block named "AC/DC converter" represent either line-commutated, phase controlled or PWM controlled rectifier. Their MATLAB models are developed separately according to previously described methods.

6.1 Line-commutated rectifier supplied DC drive modelling

Fig. 4 represents MATLAB diagram of line-commutated phase-controlled rectifier. As an

example of model application, output (DC) and input (AC) voltage and current wave shapes of during steady state are given on Figs. 5 and 6, respectively. Such model was also applied for step response analysis and control circuit optimization. Fig.7 shows the resulting current and speed referring to nominal ones. The oscillatory variations of input current during the first half of start up can be observed. This indicates that some actions must be taken in optimization of control circuit parameters.

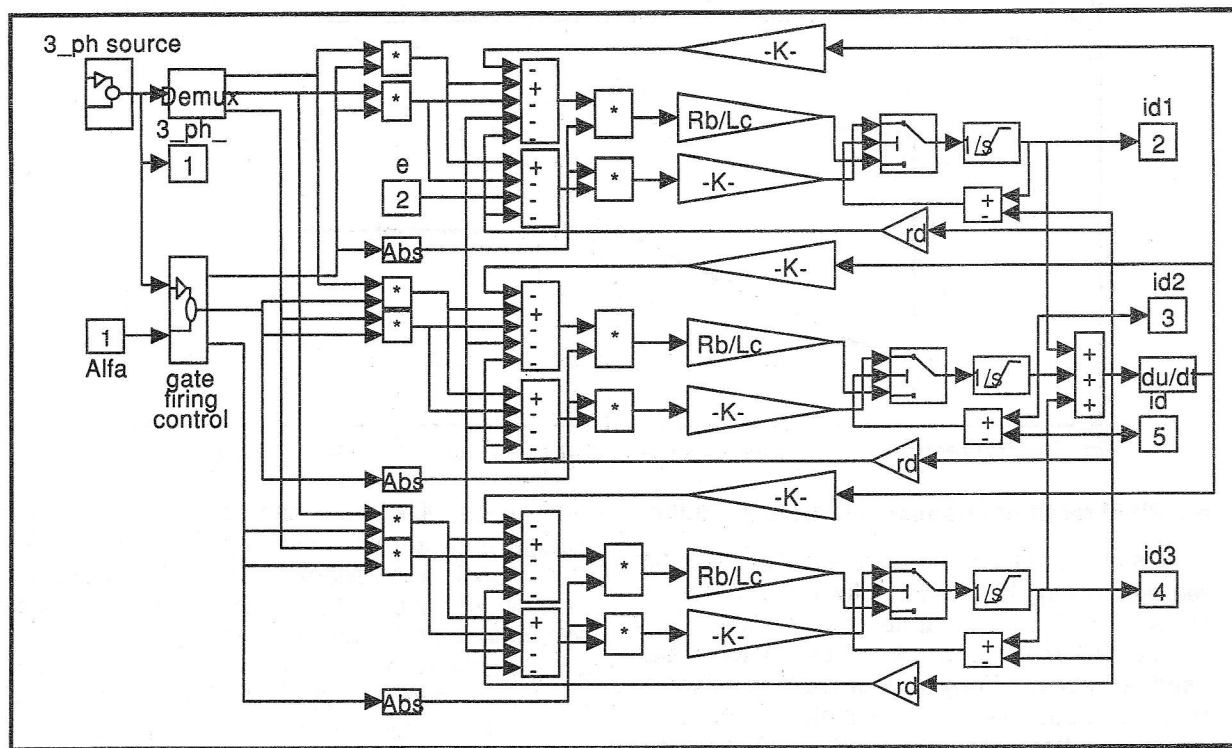


Fig.4 - MATLAB diagram of phase controlled line commutated rectifier.

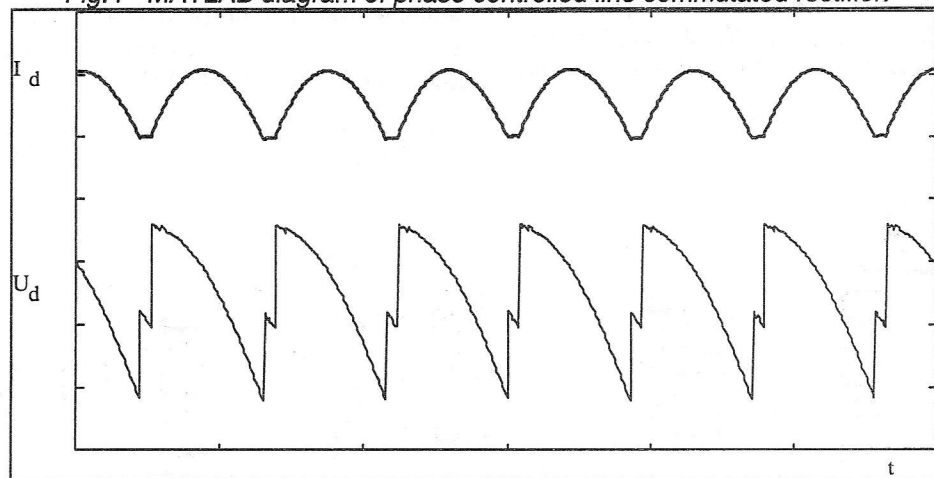


Fig. 5 – Line-commutated rectifier output (DC) current and voltage wave forms.

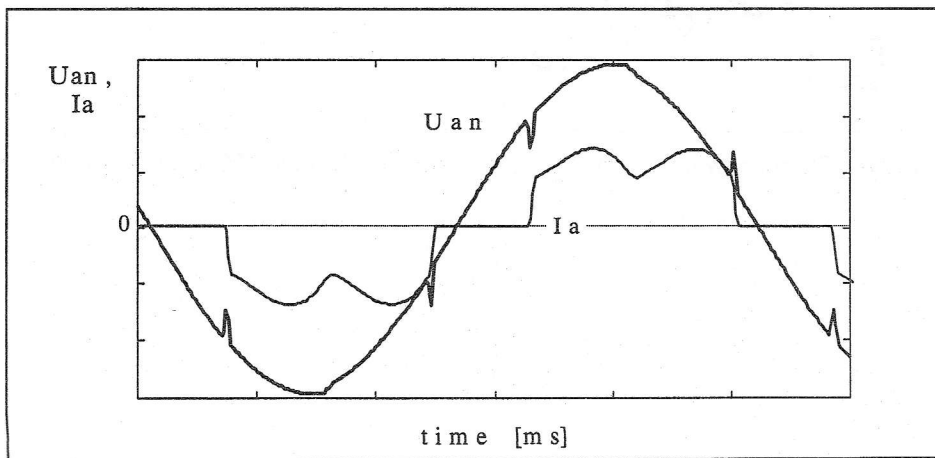


Fig.6 - Line-commutated rectifier input (AC) voltage and current wave forms.

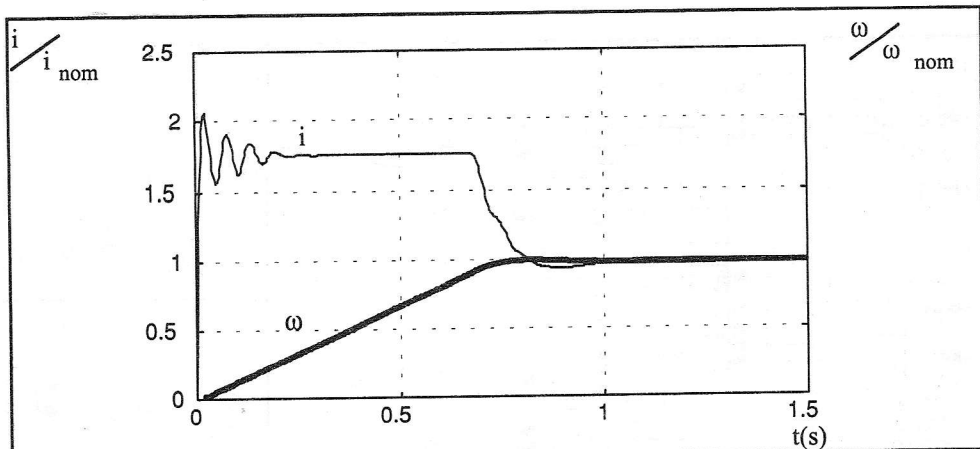


Fig. 7 - Step response of motors speed and current in case of phase controlled rectifier

6.2 PWM rectifier supplied DC drive modelling

A model of DC motor drive supplied by PWM rectifier using MATLAB software notation is shown on fig.8. Separate models for power supply, DC motor and control circuit were also used as above. They are brought together to form a model of the complete drive. Such approach offers accurate results, but it is very complex - real model. It requires special software configuration and consumption of computer time.

The results of model application are current and voltage waveforms at the both ends of PWM

rectifier i.e. line side and load (motor) side voltage and current. They are shown on fig.9. The model also enables complete harmonic analysis of injected harmonic distortion, during both steady and transient states. Fig.10 shows an example of model application for the input current harmonic analysis. Individual harmonic distortion time function (HD $i(t)$) during DC motor drive start-up and speed change with constant load torque has been regarded. Such analysis enables optimization of size and performance of input AC filter for harmonics elimination and power factor correction [11].

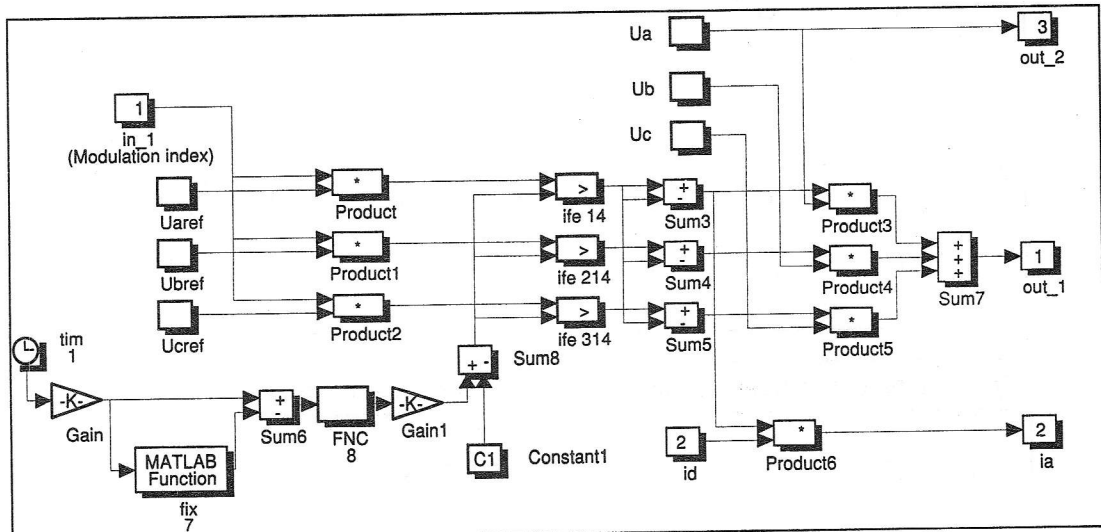


Fig.8 - Block scheme of PWM rectifier model realised in MATLAB software.

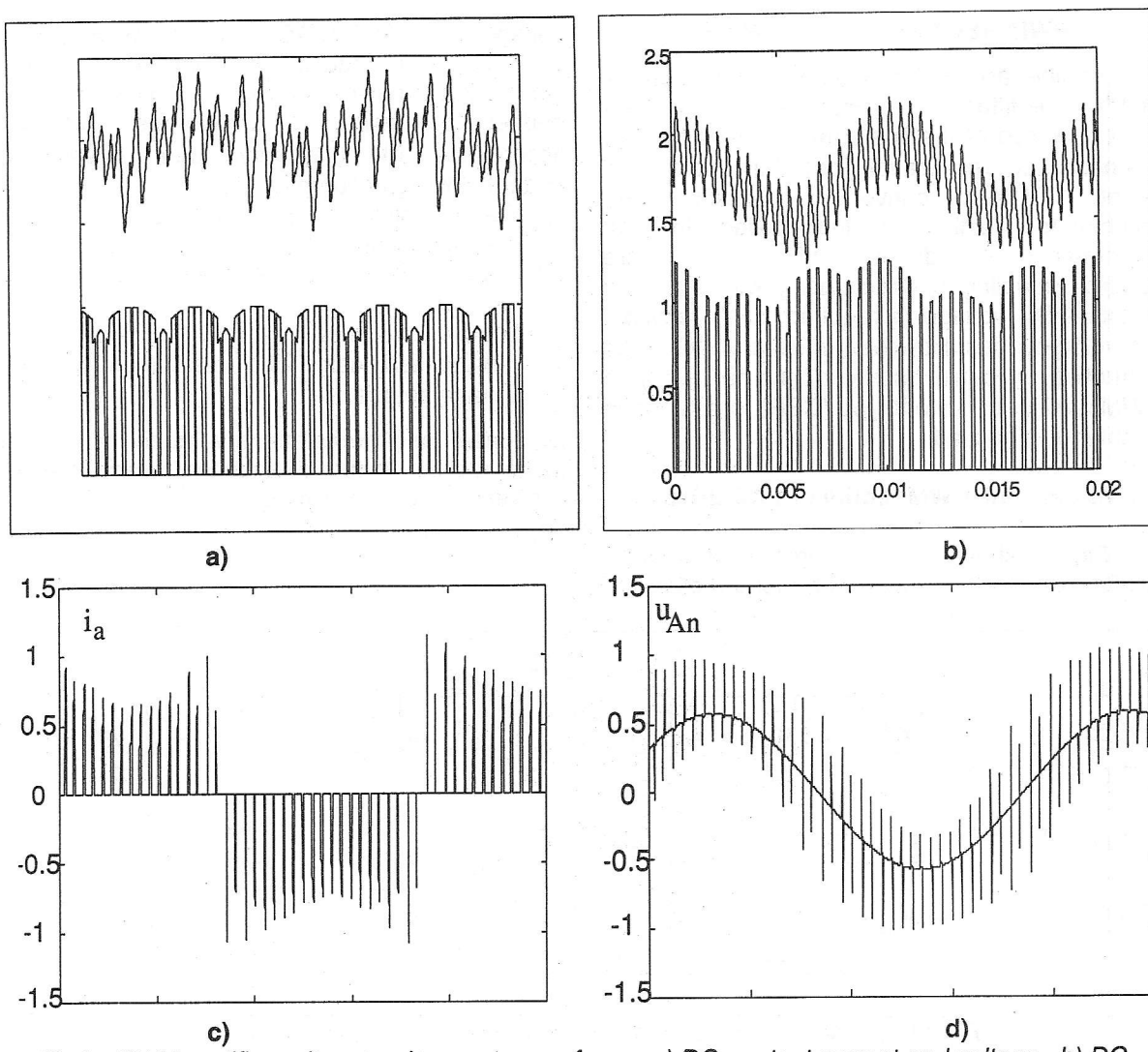


Fig.9 - PWM rectifier voltage and current wave forms: a) DC - output current and voltage, b) DC - output current and voltage during start-up, c) AC - input current, d) AC - input voltage.

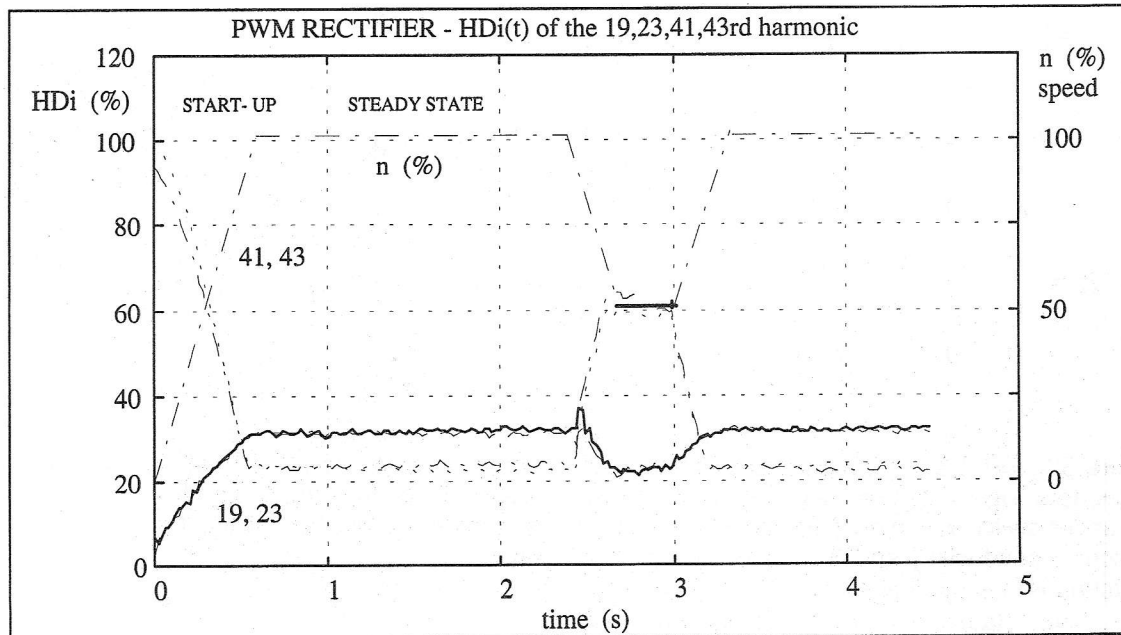


Fig.10 - PWM rectifier input current harmonic distortion during start-up and speed change of DC motor drive.

7. PWM RECTIFIER IN AC DRIVE

Another application of both line-commutated or PWM rectifier is in modern AC drives. They are connected at the line side terminals forming the necessary rectification for DC link voltage to supply DC/AC converter. Usually, line commutated rectifier is uncontrolled. In high performance AC drives PWM rectifiers are applied, enabling bi-directional power flow. As constant DC voltage is required, such rectifiers are voltage types. However, in case of AC motor controlled by current-sourced inverter (CSI), a PWM rectifier of current type (CSR), presented in chapter 6, is applied.

7.1 Voltage link PWM rectifier in AC drives

Fig.11 shows block diagram of voltage AC/DC converter (PWM switch mode rectifier) in

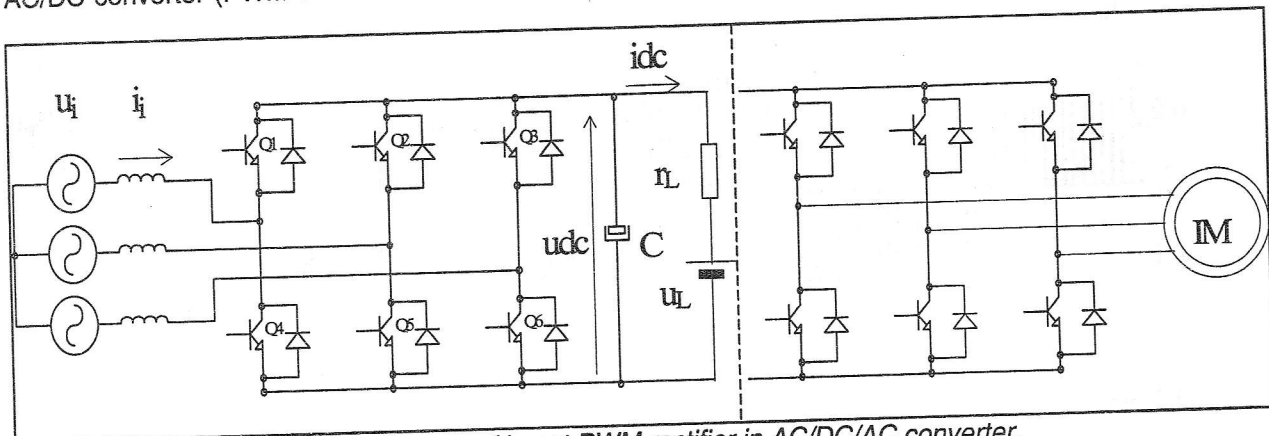


Fig.11 - Block diagram of boost PWM rectifier in AC/DC/AC converter.

$$\dot{x} = E^{-1}Ax + Bu \quad (21)$$

$$x = [i_{ac1} \ i_{ac2} \ i_{ac3} \ U_{dc}]^T \quad (22)$$

$$u = [u_{ac1} \ u_{ac2} \ u_{ac3} \ u_L]^T \quad (23)$$

$$E = \begin{bmatrix} L_n & 0 & 0 & 0 \\ 0 & L_n & 0 & 0 \\ 0 & 0 & L_n & 0 \\ 0 & 0 & 0 & C_d \end{bmatrix} \quad (24)$$

where SW_i , $i=1,2,3$ are the switching functions of converters legs with following meaning: $SW_i=1 \Rightarrow$ upper switch is conducting, $SW_i=-1 \Rightarrow$ lower switch is conducting and $SW_i=0 \Rightarrow$ none of the switches is on. Such system can be transferred to steady-state equations using the dq

voltage linked AC/DC/AC converter implemented in U/f control of induction machine. Anti parallel connection of power transistor and diode forms a bi-directional switch Q_i . Converters model in accordance with [12] have been developed under following assumptions:

1. Supply voltages (u_i , $i=1,2,3$) are balanced and sinusoidal
2. Supply inductance are linear, saturation is neglected
3. Load, i.e. load current i_{dc} , can be represented using the resistance r_L and voltage source u_L

Non-linear and non-stationary model of switch mode rectifier in the state-space representation is given by the following equations:

$$A = \begin{bmatrix} -R_e & 0 & 0 & -\left(SW_1 - \frac{1}{3}\sum_{i=1}^3 SW_i\right) \\ 0 & -R_e & 0 & -\left(SW_2 - \frac{1}{3}\sum_{i=1}^3 SW_i\right) \\ 0 & 0 & -R_e & -\left(SW_3 - \frac{1}{3}\sum_{i=1}^3 SW_i\right) \\ SW_1 & SW_2 & SW_3 & -\frac{1}{r_L} \end{bmatrix} \quad (25)$$

$$B = \begin{bmatrix} 1 & 0 & 0 & 0 \\ 0 & 1 & 0 & 0 \\ 0 & 0 & 1 & 0 \\ 0 & 0 & 0 & \frac{1}{r_L} \end{bmatrix} \quad (26)$$

transformation, which is well known from the theory of electrical machines [1]. Transformation is defined by the use of the transform matrix T and T^{-1} :

$$T = \frac{1}{\sqrt{3}} \begin{bmatrix} 1 & e^{-j\alpha x} & e^{j\alpha x} & 0 \\ 1 & e^{-j(\alpha - \frac{2\pi}{3})} & e^{j(\alpha - \frac{2\pi}{3})} & 0 \\ 1 & e^{-j(\alpha + \frac{2\pi}{3})} & e^{j(\alpha + \frac{2\pi}{3})} & 0 \\ 0 & 0 & 0 & \sqrt{3} \end{bmatrix} \quad T^{-1} = \frac{1}{\sqrt{3}} \begin{bmatrix} 1 & 1 & 1 & 0 \\ e^{j\alpha x} & e^{j(\alpha - \frac{2\pi}{3})} & e^{j(\alpha + \frac{2\pi}{3})} & 0 \\ e^{-j\alpha x} & e^{-j(\alpha - \frac{2\pi}{3})} & e^{-j(\alpha + \frac{2\pi}{3})} & 0 \\ 0 & 0 & 0 & \sqrt{3} \end{bmatrix} \quad (27)$$

$$\dot{x}_{dq} = [i_0 \ i_d \ i_q \ U_{dc}]^T = T^{-1}x; \quad x = T \dot{x}_{dq} \quad (28)$$

If the system is balance, zero components do not exist.

In addition, if fast and accurate control of input current is obtained (for instance by the use

$$\begin{bmatrix} L\dot{i}_d \\ L\dot{i}_q \\ Cu_{dc} \end{bmatrix} = \begin{bmatrix} j\omega L - \frac{L}{T_s} & 0 & 0 \\ 0 & j\omega L - \frac{L}{T_s} & 0 \\ a_{31} & a_{32} & -\frac{1}{r_L} \end{bmatrix} \begin{bmatrix} \dot{i}_d \\ \dot{i}_q \\ u_{dc} \end{bmatrix} + \begin{bmatrix} \frac{\sqrt{3}L}{2T_s} i_{ref} \\ \frac{\sqrt{3}L}{2T_s} i_{ref} \\ \frac{U_L}{r_L} \end{bmatrix} \quad (29)$$

$$a_{31} = \left(\frac{\sqrt{3}\sqrt{2}U}{2} - \left(R - \frac{L}{T_s} \right) i_d - \frac{\sqrt{3}L i_{ref}}{2T_s} \right) \quad a_{32} = \left(\frac{\sqrt{3}\sqrt{2}U}{2} - \left(R - \frac{L}{T_s} \right) i_q - \frac{\sqrt{3}L i_{ref}}{2T_s} \right) \quad (30)$$

If the PWM rectifier is controlled in such a way that switching frequency is nearly constant it is possible [12] to use the well-known state space averaging method to get a linearised transfer function.

The above described model was used to test and compare a novel approach in control circuit realization (adaptive regulation) aiming to improve overall dynamic characteristics of drive and to decrease line current pollution [13]. The complete drive has been modelled (including: PWM AC/DC converter, DC link, inverter and U/f controlled induction machine) using the SIMULINK toolbox of the MATLAB. Fig.12 shows waveform of reference (i_{1ref}) and actual phase

of hysteresis regulators) it is possible to simplify the model with only one command value and that is reference of the phase current (i_{ref}):

current (i_1). It can be seen that real current follows reference inside the hysteresis band and that the first harmonic components of AC side current and voltage are in phase i.e. that unity displacement factor is obtained. The obtained spectrum of phase current is presented on Fig.13.

Time response of DC voltage to situation of loading and unloading of induction machine with $\pm 50\%$ of nominal load is shown on figs. 14 and 15. In the case of adaptive regulation (fig.15), response is significantly faster, which is a consequence of possibility of better DC voltage regulator construction comparing to classical hysteresis current controller.

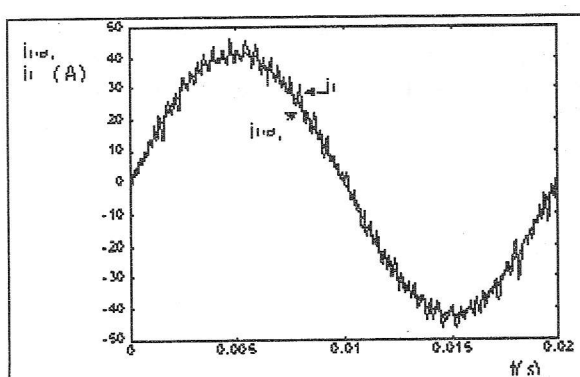


Fig.12 - Reference and actual phase current

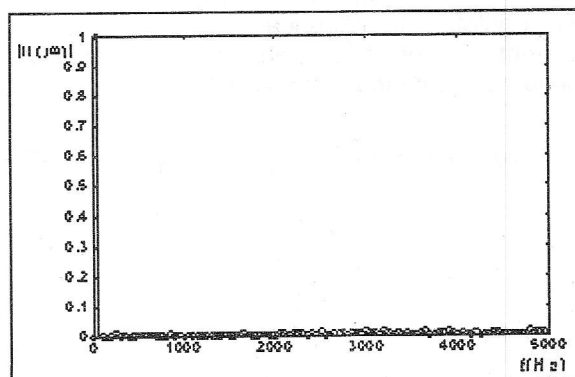


Fig.13 - Frequency spectrum of input current

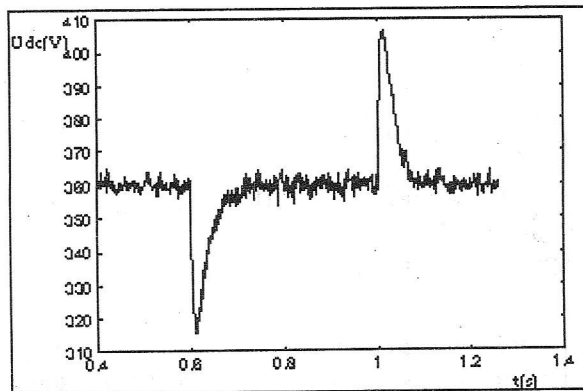


Fig. 14 - DC voltage - classical regulator

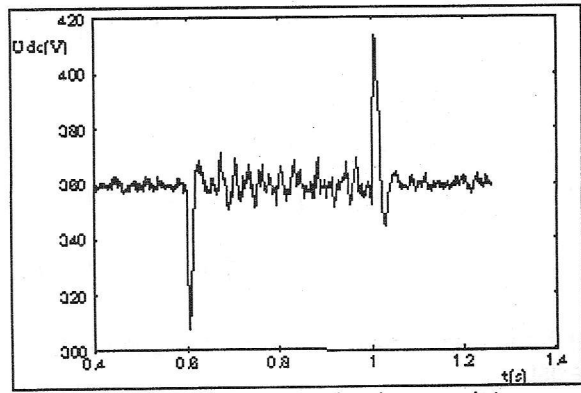


Fig. 15 - DC voltage - adaptive regulator.

7.2 Current link PWM rectifier in AC drives

Fig. 16 shows the AC drive where the CSI supply the AC machine with the variable frequency currents. The current magnitude is set by the appropriate AC/DC converter control. The PWM pattern is implemented for the converter control purposes. The characteristic of such configuration is appearance of interharmonics (harmonics that exist at the frequencies that are not related to the supply frequency). The interharmonics appear as the consequence of the fact that both the rectifier output voltage as well as the input inverter voltage (rectified voltage from the machine terminals) form the DC link current. Thus, AC supply currents consist of the characteristic rectifier harmonics modulated by the harmonics of the inverters output (machine input) harmonics.

Elimination of the interharmonics is very difficult, because the supply harmonic components vary with the angular velocity of the motor (or the CSI output frequency) that is changing. Therefore, use of passive filters is not possible, since the danger of the resonance. The above-described model has been also used for testing of a new control strategy to eliminate the interharmonics [14]. Fig. 17 shows the proposed on-line regulation method for active current type rectifier. The magnitude of the AC current reference is formed by the output of DC current PI regulator. If influence of the no-load line current can be neglected, then the reference supply current magnitude equals:

$$\hat{I}_{a,b,c_ref} = \sqrt{2} I_{a,b,c_ref} = \sqrt{\frac{2}{3}} I_{dref} \quad (31)$$

The sinusoidal templates, in phase with supply voltages formed by the synchronization signals, multiply those reference magnitudes. Reference signals are compared with actual line currents and their difference is fed to hysteresis band current controller. Output from the hysteresis controller forms bi-level switching signals SB necessary for the rectifier control. From the bi-level signal ($SB_i, i=1, \dots, 3$), a tri-level signal ($ST_i, i=1, \dots, 3$), necessary for proper operation of AC/DC converter is derived: $ST_1 = SB_1 - SB_2$. For the inductive type loads it is necessary to ensure the existence of the DC current path that must be obtained within the converter. Since only two of the switches conduct at the same time - one in the upper and one in the lower part of the bridge, then the gating signals ($SW_i, i=1, \dots, 6$) can be derived from the tri-level signals in the following manner (example is given for the SW_1):

$$SW_1 = ST_1 \vee (\overline{ST_1} \wedge \overline{ST_2} \wedge \overline{ST_3} \wedge ST_4) \quad (32)$$

This means that the switch SW_i should be gated when its tri-level function is active or when its complementary transistor conducts and none of the switches in the same bridge leg (upper or lower) conduct. The complete system including the AC supply, different rectifiers, DC link, inverter, AC machine and the control circuitry was modeled and simulated using the SIMULINK toolbox of MATLAB. Converters were modeled using real macro models based on non-linear transfer function approach described in chapter 2, while the AC machine was modeled using the dq domain theory with inclusion of the saturation effects [2].

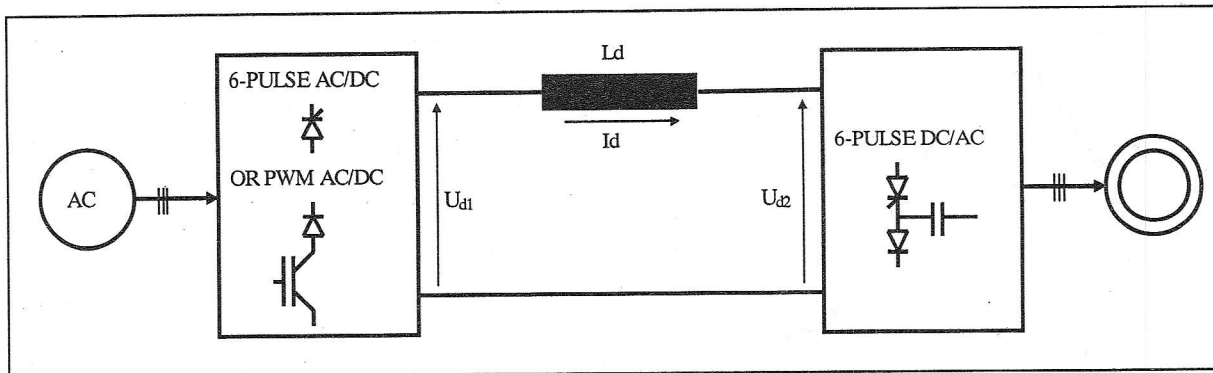


Fig. 16 - Block diagram of the CSR-CSI fed AC drive.

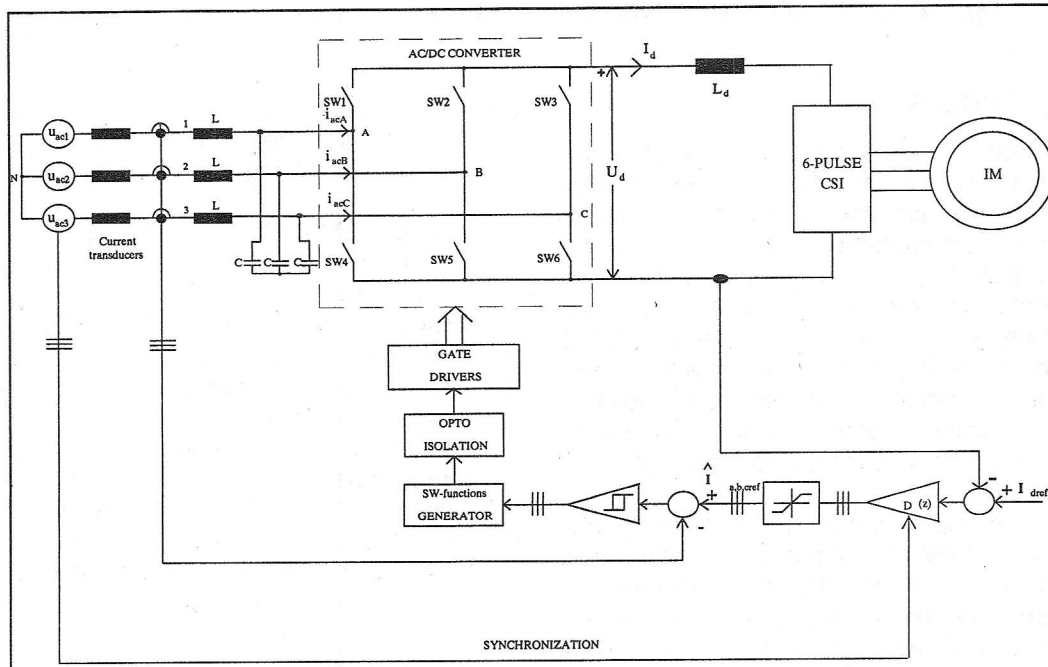
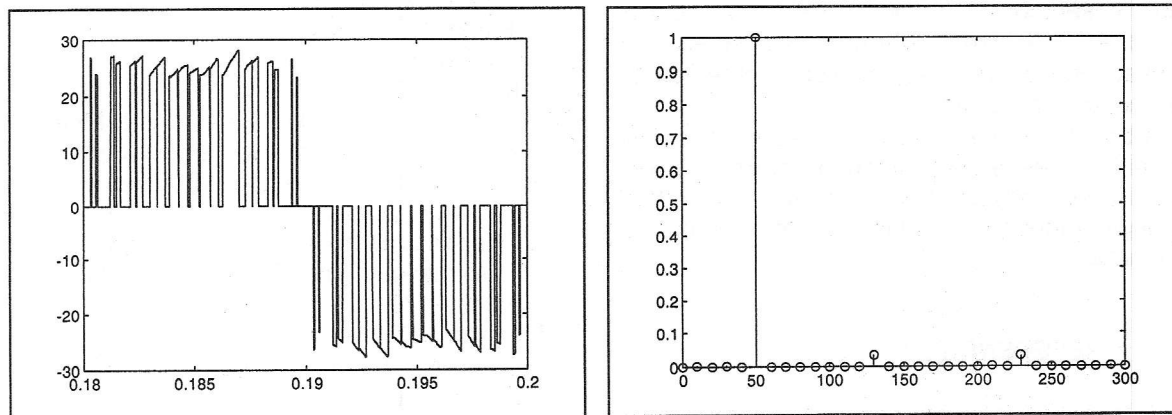


Fig. 17 - AC/DC converter with proposed on-line control.

Figures 18 and 19 show the results of simulation, the AC current wave forms and their spectrums in case of standard PWM and on-line controlled PWM rectifiers. It can be seen that in

the first case interharmonics are reduced, while in the second case they are fully eliminated by the proposed control method.

Fig. 18 – Standard PWM rectifier: $f_e=30\text{Hz}$, reduced interharmonics at $f=|50\text{Hz}\pm6*30\text{Hz}|=130\text{Hz}$, 230Hz

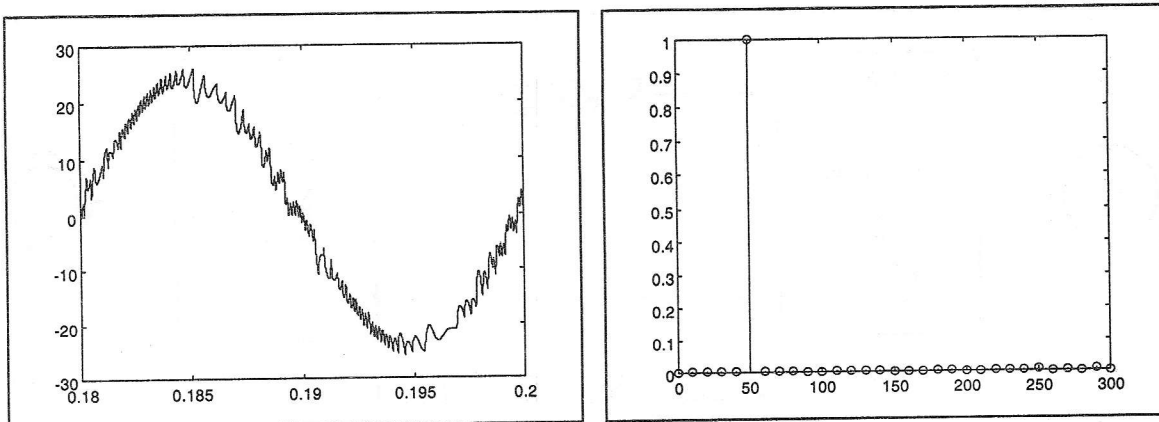


Fig. 19 - On-line controlled PWM rectifier: $f_e=30\text{Hz}$ – eliminated interharmonics.

10. CONCLUSION

The paper summarised different approaches in energy converters modelling. Special attention is paid on power electronic converters modelling for both line-commutated phase controlled and PWM controlled AC/DC converters. For research of contemporary electric drives, a model that uses transfer function is proposed. AC/DC converter modelling is given in details for two kinds of converters – current and voltage. Electric machine, control circuit and power network modelling is presented on the most universal form.

As an example of energy converter models application, a brief description of DC motor drive supplied by current AC/DC converter is presented. The model includes a closed-loop control circuit. Results show voltage and current waveforms. The model is used for investigation of line current harmonics. It proved to be very useful, as it enables both transient and steady state investigations.

Another example shows application of voltage type AC/DC converter, controlled by PWM, in modern high performance induction drive control. The model of complete AC drive is developed and presented, including closed-loop control circuit, AC machine model and load variation. It is used and proved very useful in research of new control strategies.

A transfer function model is also successfully applied for research of interharmonics in CSR-CSI fed AC drives. The resulting new control strategy proved suitable for interharmonics elimination.

11. REFERENCES

- [1] V.Vučković, "Theory of Electrical Machines", Nauka, Beograd, 1992, (in Serbian).
- [2] V.Vučković, "Electric Drives", Elektrotehnički fakultet, Beograd, 1997, (in Serbian).

- [3] J.Kassakian, M.Schlecht, G.Verghese, "Principles of Power Electronics", Addison-Wesley Publishing Comp., Reading (MA), 1991.
- [4] L.Huber, D.Borojević, N.Buranj, "Analysis, design and implementation of the space-vector modulator for forced-commutated cycloconverters", IEE PROCEEDINGS - Part B, Vol.139, No.2, pp.103-113, March 1992.
- [5] V.Katić, "A New Method of Three-Phase Bridge Rectifier Current and Voltage Harmonics Determination", IASTED - International Journal of Power and Energy Systems, Vol.14, No.1, 1994, pp.44-48.
- [6] J.Kolar, H.Ertl, F.Zach, "Analysis of the Duality of Three Phase PWM Converter With DC Voltage Link and DC Current Link", Conf. Record of the 24th IAS Annual Meeting, San Diego (USA), Oct.1989, pp.724-737.
- [7] Mathworks, "MATLAB-Users Guide", 1994.
- [8] P.Enjeti, P.Ziogas, M.Ehsani, "Unbalanced PWM Converter Analysis and Corrective Measures", Conference Record of the 24th IAS Annual Meeting, San Diego (USA), Oct.1989, pp.861-870.
- [9] V.Katić, D.Graovac: "A Method of Real Analysis of AC/DC Converter Line Side Harmonics", Facta Universitatis - Series: Electronics and Energetics, Vol.10, No.1, 1997, pp.107-123.
- [10] V.Katić, V.Vasić, D.Graovac: "The Methods of Electrical Energy Converters Modeling", Monograph, Contemporary Problems in Power Engineering, Faculty of Technical Sciences / School of Technology, Novi Sad (Yugoslavia) / Thessaloniki (Greece), 1995, pp.169-179.
- [11] V.Katić, D.Graovac: "Unbalanced AC/DC Converter AC Filter Design in Transient and Steady State", IEEE Int. Symposium on Industrial Electronics ISIE'96, Warsaw (Poland), June 1996, pp.778-783.

- [12] R. Wu, S. B. Dewan, G. R. Slemon "Analysis of a PWM AC to DC voltage source converter under the predicted current control with a fixed switching frequency", *IEEE Trans. on Industry Applications*, vol.27, no.4, July/August 1991, pp.756-764
- [13] D.Graovac, V.Katić: "A Method of PWM Rectifier Control in Voltage Linked AC/DC/AC Converter", IX IEEE MELECON '98, Tel-Aviv (Israel), May 1998, pp.1032-1036.
- [14] D.Graovac, V.Katić, Đ. Oros, M. Zubić, V. Vasić: "A Simulation Study For Prediction And Elimination Of Supply Interharmonic Components In CSI Fed AC Drive", 6-th Inter. Conf. on Modelling and Simulation of Electric Machines, Converters & Systems - ELECTRIMACS'99, Lisboa (Portugal), Sep.1999.

SMART SENSOR CHANNEL MODELING ACCORDING TO IEEE P1451 STANDARD

Authors: Saša Ristić, Mile Stojčev, Faculty of Electronic Engineering, Niš

Abstract: A model is an abstract description of a system or a process. It provides a simplified representation that promotes understanding and enables simulation of many complex electronic systems such as smart sensors. One convenient procedure for the generation of smart sensor channel model is described in this paper. The basic idea is based on the following fact: The smart sensor operation is considered as a form of channel signal processing. We adopted IEEE Std. 1451 as a set of rules for presentation of the smart sensor channel model. Accordingly, we have decomposed the channel processing structure into several hierarchically organized modules-blocks. The proposed model was verified during the process of functional simulation. For model presentation HDL description was used. This approach enable us to simulate the smart sensor behavior in the earlier phases of its design, and avoid late-stage physical design surprises.

1. INTRODUCTION

In nowadays industrial and scientific measuring-information and control systems numerous different transducer types are evident. For example, the system for monitoring complex power plant consists of several thousands different sensors for process parameter sensing, as well as a couple of hundreds different actuators for process control. Similarly, in a smart building system, including subsystems for lighting, air condition, security, transport, communication, etc., there is several hundreds of sensors and actuators. Huge amount of installation of these devices leads to their massive fabrication. Such quantitative trend is followed by an increased requirement concerning functionality, performance and reliability for smart transducers. According to this, higher operation autonomy and complete automatization are attained. It can be said that in such processes the direct control by a man is reduced, although his more sophisticated functions are fully emancipated.

As a consequence of the above mentioned trends, the design of measuring-information and control systems (MICS) becomes more and more demanding for designers. During the design process, two crucial groups of requirements are evident: The first one relates to more powerful developing tools, and the second one to efficient models of the system and its components. In general, a global system model resolves different system aspects: hierarchy, topology, communication protocols, implementation issues, etc. From the other side, the component modeling primarily relates to its architecture and functional description. Both of model types should be specified by a standard. In last few years several standards concerning measuring-information and control systems were appeared. World leading companies and standard associations have formed special committees and working groups for standard specification. In the field of MICS standardization, efforts of the NIST's

and IEEE's working group for *Smart Transducer Standard* development have been pronounced.

Namely, four working groups were formed by these organizations. The objectives of these groups were to propose four standards: (a) P1451.1 - *Network Capable Application Processor - Information Model* [1]; (b) P1451.2 - *Transducer to Microprocessor Communication Protocols and Transducer Electronic Data Sheet* [2]; (c) P1451.3 - *Digital Communication and Transducer Electronic Data Sheet (TEDS) Formats for Distributed Multidrop Systems* [3]; and (d) P1451.4 - *Mixed-mode Communication Protocols and Interface - Transducer Electronic data Sheets (TEDS) Formats* [4]. During 1997, recommendation of IEEE Std. 1451.2 have been approved. [5].

Objective of this paper relates to functional decomposition of the smart transducer, i.e. smart sensor, according to specified behavioral description and related standard settings. The main part of this paper relates to a procedure for smart sensor model developing, as well as the process of functional simulation as a part of the verification process.

2. BASIC SPECIFICATION CONCEPTS OF IEEE Std. 1451

We define a smart transducer as a unit which provides the following functions [6,9]: (a) sensing of a physical quantity; (b) converting a physical quantity into electrical signal; (c) electrical signal conditioning; (d) converting the conditioned signal into digital domain; (e) digital signal processing; (f) communicating with other MICS's constituents; (g) interfacing with the process in the control loop; (h) converting the electrical signal into physical quantity; (i) self-calibration, influence of offset voltage/current elimination, auto-zero adjustment, and self-testing. Functions (a) to (f) and (i) typifies sensors. While functions from (e) - (i) are reserved for actuators.

According to this standard, a MICS is a distributed one. It could be seen as a network of nodes (sensors and actuators) that communicate each-other on client-server or publisher-subscriber principle, as well as a set of monitoring and control nodes for users. From a user point of view, full transparency of other system's aspects (such as interconnection issues, topology, communication protocols, conversion type, data formats, etc.) is achieved. This important feature results from the implemented concept of interoperability. Interoperability means the ability of

different types and categories system objects to interact in the aim of doing the common job or the global function. This feature is realized by organizing the system functions and services according to some model of networking, such as ISO's OSI layers organization [8].

The smart transducer structure derived according to P1451 standard is shown in Fig. 2. As it can be seen, a smart transducer is a device including four functional modules:

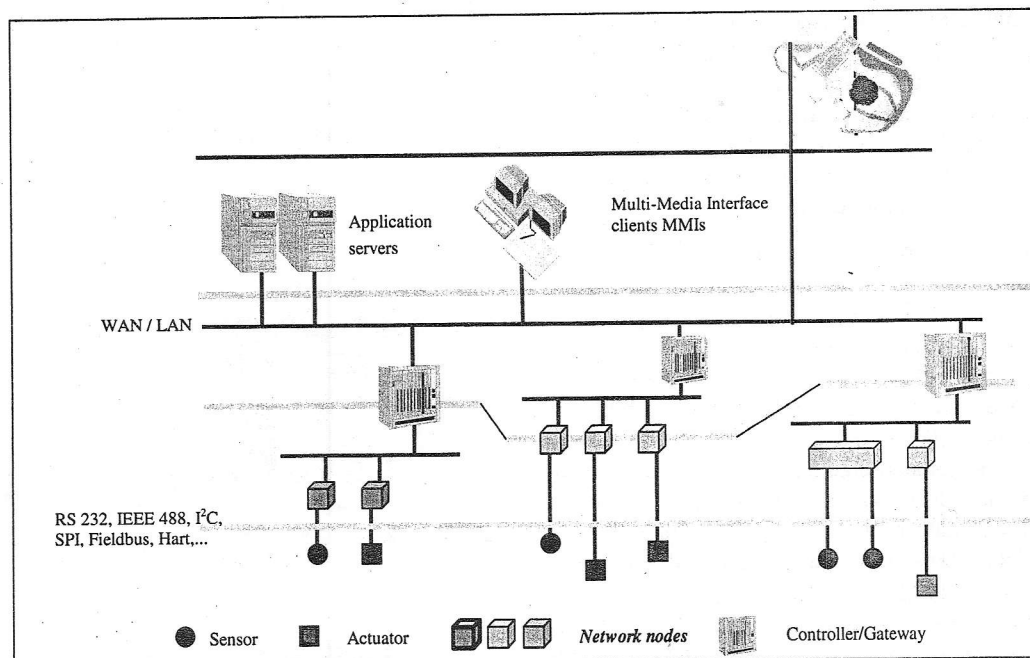


Fig. 1. Global view of the system for automatic measurement, processing, management and administration

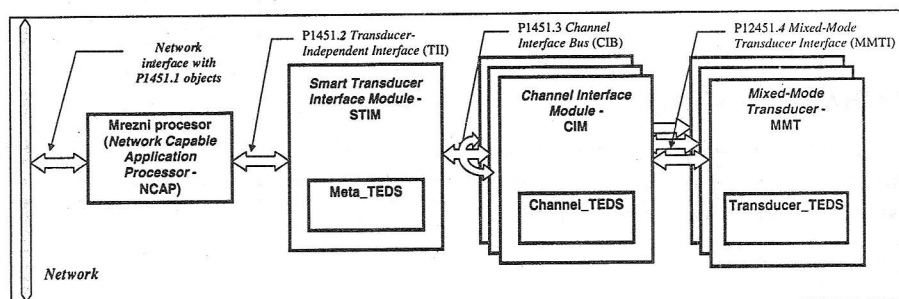


Fig. 2. Block-structure of a smart transducer according to P1451 standard

Network Capable Application Processor - NCAP, Smart Transducer Interface Module - STIM, Channel Interface Module - CIM, and Mixed-mode Transducer - MMT. In this moment, P1451.1 and P1451.2 standards define the functionality of the NCAP and STIM, respectively. The other two modules, the CIM and MMT, are defined by the P1451.3 and P1451.4 drafts of the IEEE Standard Board, respectively. Functions performed by the NCAP are the following:

- (i) Network services support: at physical level, it provides an interface with a standard network, while

at the logical level, a support to corresponding protocol. One typical MICS representative based on installing smart-transducers is organized into four-layers, and is pictured in Fig. 1; (ii) Application program running - from aspect of application, the program (built-in firmware) interprets commands, and undertakes series of activities (actions) defined for each command or event; (iii) Providing the correct interface - according to P1451.2, NCAP is coupled with hierarchically lower module.

The STIM provides support for coupling with the NCAP, performs processing, and carries out a coupling with hierarchically lower CIM module. The module CIM provides coupling with the STIM, performs processing, and supports coupling with the hierarchically lower MMT module.

The MMT's activities are the following: (i) providing correct coupling with CIM - the interface specification is defined by P1451.4; (ii) accepting and interpreting commands concerning setting of operation mode (self-test, self-calibration, normal operation), and setting optional running condition from the metrological point of view (the elimination of voltage/current offset influence); (iii) performing an inter/intra-domain transformation of the measured quantity or action, and normalization of the magnitude of the electrical signal (in a case of sensor), or accepting the electrical signal and transforming it into the action (in a case of actuator).

It is significant to point out that, concerning the IEEE Std. 1451, the above-mentioned modules correspond only to sets of functions that are hierarchically organized. The standard does not suggest how the physical implementation should be done. Having this in mind, we can say that STIM performs his own functions as well as the functions of transparent blocks of concatenated channels- (CIMs), and mixed-mode modules (MMTs). Implementing this concept, the smart transducer channel is characterized by a channel data, status information, type of units, etc. The Std. 1451 suggests seven types of transducer channels: (a) sensor, (b) actuator, (c) buffered sensor, (d) data sequence sensor, (e) buffered data sequence sensor, (f) event sequence sensor, and (g) general transducer [2]. In the sequel, the basic channel building blocks will be described.

3. SENSOR CHANNEL MODEL

Our basic idea was the following: Using functional and architectural decomposition we can identify each constituent of NCAP, STIM, CIM, and MMT [10].

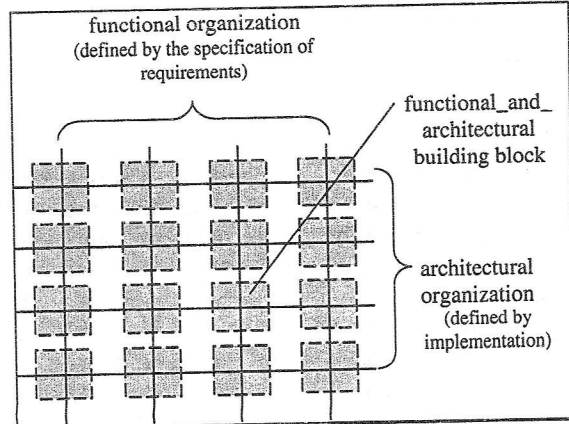


Fig. 4 Basic idea of the smart transducer modules decomposition

From the functional point of view, we have already specified the main functions for each module. Generally, we can say that each module consists of three functional units: *lower_level_interface*, *processing_unit*, and *upper_level_interface*. The first one provides correct interface with hierarchically lower module, the second one performs processing function, and the third one covers all activities concerning the interface with hierarchically upper module.

From an architectural point of view, the NCAP, STIM, CIM, and MMT are composed of: *xxx_Data_path*, *xxx_Control_unit* and *xxx_Driving_support* blocks (for more details see Fig. 5, 6, 7, and 8). For example, for the NCAP module the prefix *xxx_* should be substituted with *NCAP_*.

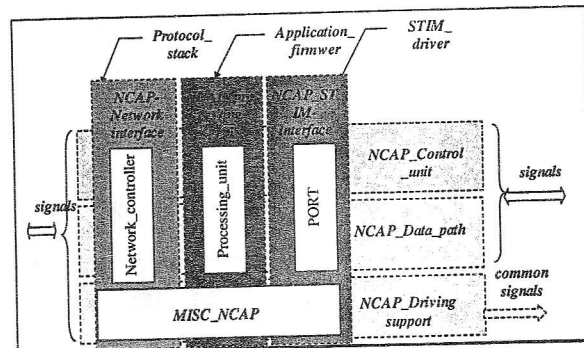


Fig. 5. NCAP module organization

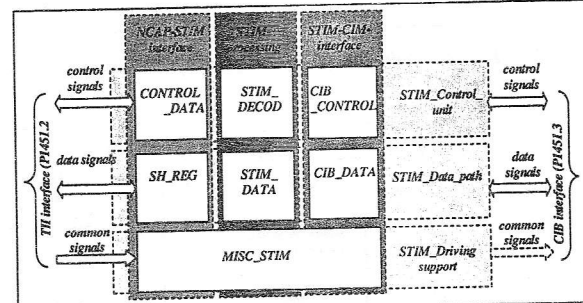


Fig. 6. Block-scheme of the STIM structure

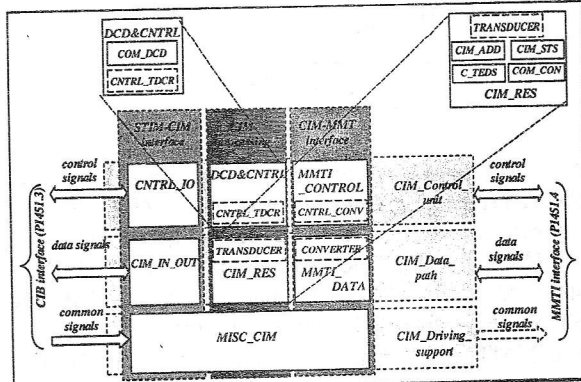


Fig. 7. The CIM structure on the level of block-scheme

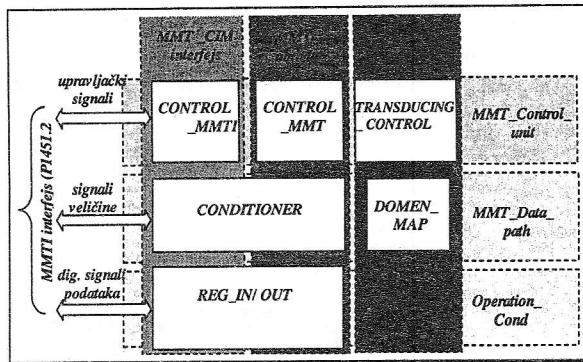


Fig. 7 The MMT structure on the level of block-scheme

The block *xxx_Data_path* provides resources during data buffering in data processing or data transfer. *xxx_Control_unit* provides control mechanisms for processing or transfer activities, while *xxx_Driving support* provides general services such as: distribution of power supply, clock signal distribution (uni-phase and/or poly-phase), generation of accurate time intervals, generation of referent calibration- and operating voltage or current signals, etc.

In cross-section area of functional and architectural blocks, we identify building block, depicted in figures 6, 7, and 8. From figures 6, 7, and 8, we identify basic building blocks of all modules, as well as specific building blocks characteristic for a transducer type, which belong to CIM or MMT modules [10]. In order to design the architecture of the smart transducer, for each building block, it is necessary: (a) to create a formal model, (b) to describe it, and (c) to implement it. In the following, the model of specific channel block CNTRL_CONV (Fig. 7) performing the control during the triggering process will be described.

4. SMART SENSOR FUNCTIONS AND ACTIVITIES

The *Processing_unit* of the NCAP runs an application program named *Application_firmware*. At the application layer, this program provides functions related to network messages interpreting. Application messages concerning smart transducer activities are divided into the following three categories: *IO_Read Massages*, *IO_Write Massages*, and *Event Massages*. Through the channel, a smart sensor looks like device that, on the request initiated by the NCAP application program, performs sensing, measurement or estimation of the physical value, and returns digital data representing this value, to the NCAP application. All activities of any STIM and MMT building blocks are grouped in two processes: (i) triggering, and (ii) data transfer.

As a response to the *IO_Read* or *IO_Write* message, the NCAP (*STIM_driver*) generates: (a) the *trigger signal*, for transducer data acquiring or actuating, and

(b) a NCAP-command concerning data transfer. For the smart sensor channel, this signal triggers the STIM activities related to the new process of acquiring data.

Triggering is realized through a handshake procedure between the NCAP and STIM modules. The NCAP initiates a trigger signal, then, the STIM responds with an acknowledgement signal. When the NCAP deactivates the trigger signal, the STIM will de-assert the acknowledgement signal. As it can be seen in Fig. 3 a), the operation of the STIM could be described as cooperation of two processes: (1) *Handshaking*, and (2) *Data_transfer*. The *Handshaking* is characterized by states: *Initialization*, *Quiescent*, and *Shaking*, while the process *Data_transfer* is characterized by its unique state - *Transfer*. During operation, some of the possible sequences are: *Quiescent->Transfer->Quiescent* - typical for triggering of an actuator, *Quiescent->Shaking->Quiescent->Transfer* - triggering of a sensor, or, *Quiescent->Transfer->Quiescent->Transfer* - reading/writing other data. Additionally, we have decomposed the state *Shaking* as shown in Fig. 3 b). Since the trigger signal has been, the current state of STIM operation is *Triggered*. The NCAP could reset the trigger signal before the triggered action is completed. In this case, the state *Break* becomes active. When the action finishes regularly (the signal *Action_completed*), the STIM activates the *ACK* signal (state *Acknow*), and, on trigger signal reset, it resets the acknowledgement signal (state *Ack_res*).

During the state *Triggered* the trigger signal is active and the STIM is waiting for action completion. For sensor channel, this action is related to acquiring and converting sensor data. Acquiring and converting activities could be initiated either by the trigger signal or by a trigger independent mechanism such as a continual periodical signal. Depending on this, all sensor channels could be divided into triggered, and sequential ones. In the sequel we will consider the triggered sensor channel, only. Channel specific logic includes two main parts: (a) data path, and (b) control unit. For the smart sensor channel logic design starts with describing the behavior during triggering. In Fig. 4 three global activities of the smart sensor channel are presented: *Acquiring_data*, *Data_conversion*, and *Data_valid*. Since the trigger signal has accepted, the activity *Acquiring_data* is performed. Duration of the *Acquiring_data* is defined by the STIM as multiple period of data sampling. At the end of sampling, the signal named *Action_completed* is generated, and processing continues with the state *Data_conversion*. Data becomes valid at the end of conversion. In Fig. 4, the activities of channel- and STIM-logic are presented concurrently.

Models of the STIM's and channel's logic, given in figures 3 and 4 are start points for formal description. Using the StateCAD tools [7], we will describe the logic of the smart sensor channel. In Fig. 5 a state

diagram for corresponding CNTRL_CONV building block is presented. The first two states in the state diagram, *WAIT_ACQ* and *ACQ_SMPL*, are derived from the state *Acquiring_data* given in Fig. 4. The

other two states are directly taken from the state diagram in Fig. 4. To obtain a valid data, it is necessary to complete conversion and to cancel the trigger signal.

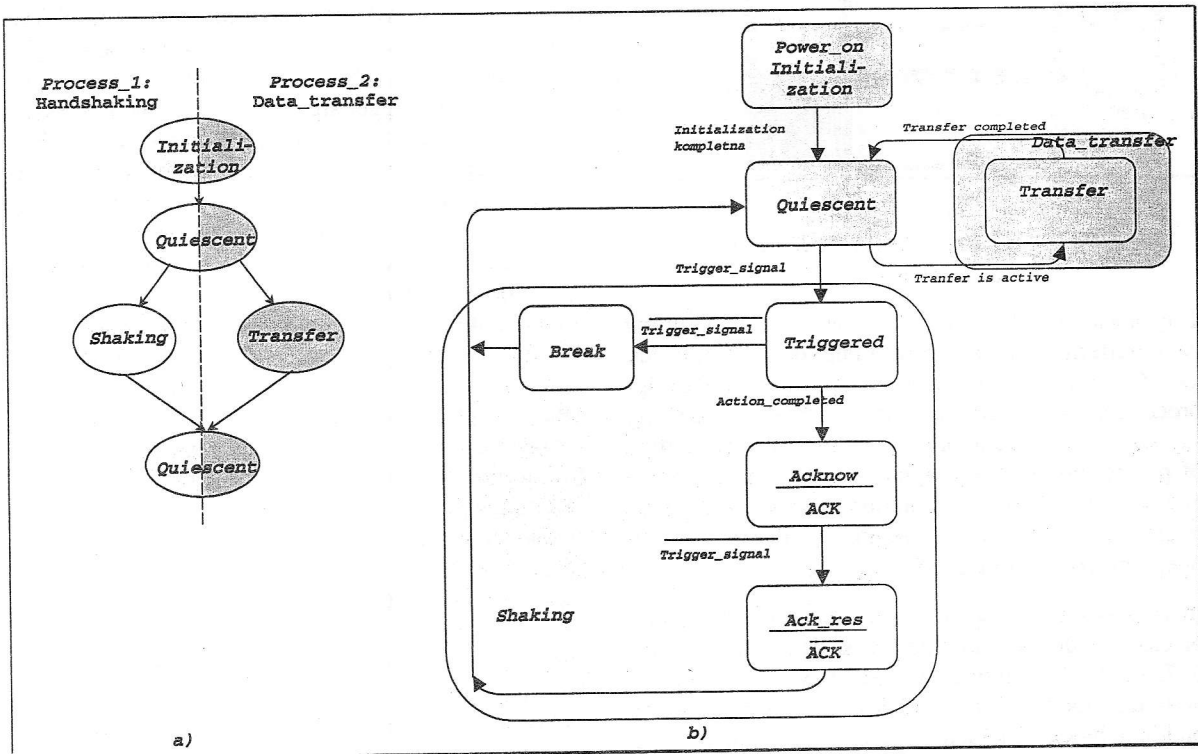


Fig 3. The STIM Behavioral model. a) Two concurrent processes; b) State diagram of the STIM

In this moment, the machine enters in state *DATA_VALID*. This state is characterized by a signal for latching the new value (*VALID*). As it can be seen in Fig 5, data is latched in a register named *BUFF*. This register is a channel data resource connected to a system bus.

The formal description of the sensor channel model is verified in a process of functional simulation performed by StateCAD tools. The resulting text file, shown in Fig 7, is a report of simulation process. In the first column, the simulator commands which involve input signal transitions (*RESET*, *NTRIG*, *END_SAMPLE*, and *CNV_CMP*), and the output signals checking (*BUFF[15..0]* and *VALID*) checks are given. The second- and the third column of this file represent current- and next state during the flow of simulation.

The model described by a state diagram (Fig. 5) could be easily transformed into a corresponding HDL description (ABEL or VHDL) by choosing one of the output options in StateCAD tools. On this way, it is possible to implement the description either as a FPGA circuit or, as an ASIC chip. The main advantage offered by StateCAD is an integrated

description of control- and data-path unit depicted in the same outline editor. The second advantage is that there is a possibility to generate different formal design entries at HDL description level.

5. CONCLUSION

A part of design process for a smart sensor interface module is described in this paper. The main goal of this description concerns modeling of smart sensor channel behavior and its functional simulation. The concept of smart sensor channel model is adopted from the specifications of IEEE Std. 1451. It is related to the key component of modern measuring-information and control systems designed as networks (i.e. control networks). The STIM module is an interface module placed between two other parts of smart transducer: network controller and transducer. The STIM could be implemented in one of three ways: by a micro-controller, as a FPGA circuit, or as an ASIC chip. Nevertheless, the process of modeling the smart transducer building blocks is crucial and unavoidable. Successfully obtained model of any smart transducer channel, supported and additionally processed by the powerful CAD tools, enables us to

quickly and efficiently realize the transducer as a network node.

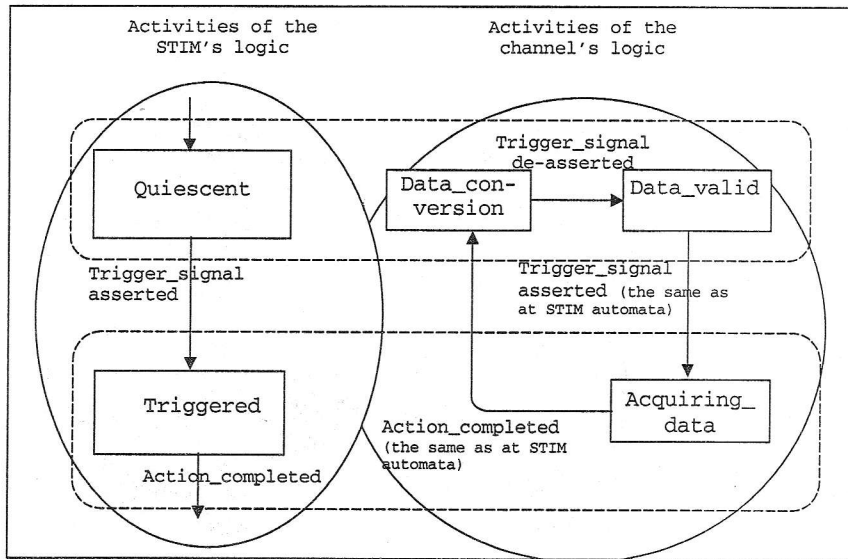


Fig 4. Activities of the smart sensor channel at triggering

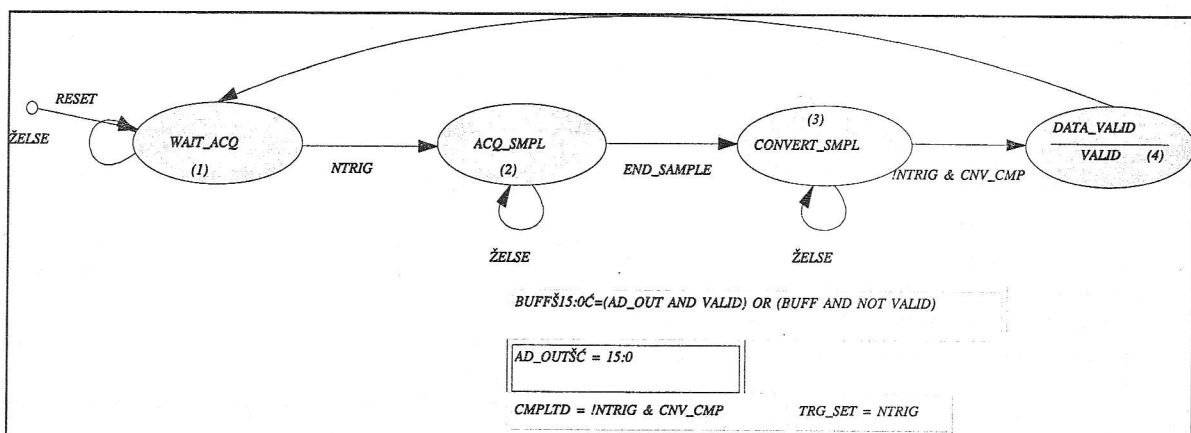


Fig 5. The model of the smart sensor channel as a StateCAD's state machine

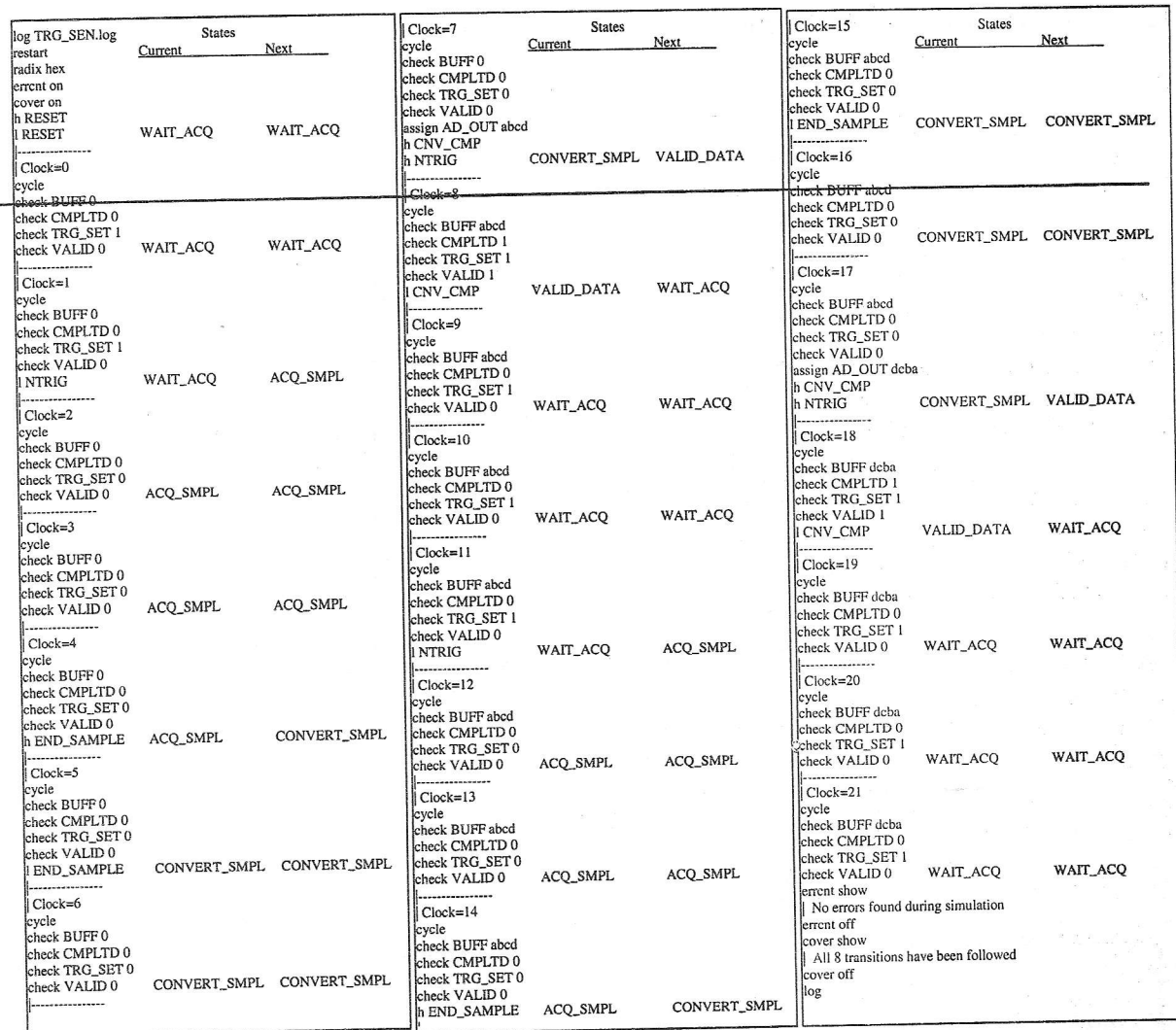


Fig 7 Test-sequence with the simulation report

6. REFERENCES

- [1] IEEE P1451.2 Standard for Smart Transducers Interface for Sensors and Actuators - Transducer to Microprocessor Communication Protocols and Transducer Electronic Data Sheet (TEDS) Formats, IEEE Standard Association, August, 1997
- [2] IEEE P1451.1 Network Capable Application Processor - Information Model, IEEE Standard Association, Draft 3.01, August, 1997
- [3] IEEE P1451.3 Standard for Smart Transducers Interface for Sensors and Actuators - Digital Communication and Transducer Electronic Data Sheet Formats for Distributed Multidrop Systems, <http://www.ic.ornl.gov/p1451/>
- [4] IEEE P1451.4 Standard for Smart Transducers Interface for Sensors and Actuators - Mixed-mode Communication Protocols and Transducer Electronic Data Sheet Formats, <http://www.ic.ornl.gov/p1451/>
- [5] Kang Lee, The Emerging IEEE-P1451 Standards for Smart Sensors and Actuators, IEEE Inst. and Measur. Soc. Newsletter, Summer 1997, No. 136, pp. 14-19.
- [6] Gert van der Horn, Johan Huijsing, Integrated Smart Sensors, Kluwer Academic Publishers, 1998
- [7] StateCAD User's Guide, Visual Software Solution Inc., 1998
- [8] Cook, C.S., A methodology for formulating measuring instrument specification, Measurement, Vol. 11, Elsevier Science Publ., 1993, pp.1-31
- [9] Nachtigal, C.L., Smart Sensor Intelligent Transducers and Transmitters, Ed. by Nachtigal, C.L., Instrumentation and Control, Fundamentals and Application, Wiley-Interscience Pub., 1990, pp.392-400
- [10] Mile K. Stojčev, Saša S. Ristić, Smart Transducer Architectural Organization Based on Standard IEEE P1451, Proc. on 4th Int. Conf. on Telecomm. in Modern Satellite, Cable and Broadcasting Services, TELSIKS'99, October 1999, pp. 484-494

SYMBOLIC ANALYSIS OF ELECTRONIC CIRCUITS – DEVELOPMENT AND APPLICATION

*Predrag Petković, Faculty of Electronic Engineering, Niš
Dejan Tošić, School of Electrical Engineering, Belgrade*

Abstract – *The most important characteristics of contemporary manufacturing are sophisticated tools and well trained employees. The electronic industry depends more than others on the tide connection between man's knowledge and machine complexity. Therefore it is expected from education of electrical engineers to create experts that should be able to quickly and reliably answer the question 'what should happen if...'. One of the most useful tools for prediction of circuit behavior is symbolic analysis (SA). This paper describes results of development and application of symbolic analysis computer programs at Faculty of Electronic Engineering, University of Niš, and School of Electrical Engineering, University of Belgrade.*

1. INTRODUCTION

This paper is motivated by the fact that we are at the end of the decade when a part of scientific community devoted research to the application of symbolic algebra for symbolic circuit design. Actually, this problem was established during the sixties when first attempts in using computers for manipulation with symbols were done. Unfortunately, the software tools were developed primarily to manage with numbers not with symbols. Therefore, all methods were based on numeric computation [1]. Simultaneously, the existing hardware could not support required complex computation and consequently, could provide efficient symbolic simulation only of small circuits. However, it was recognized that SA offers many benefits for circuit designers. [1]. Hence, as soon as the conditions allowed, at the eighties, the research in this area was continued.

Improving of hardware and software background inspired restoration of SA doctrine at the eighties. This was supported by increased interest for SA in two fields.

After fast development of digital ASIC during the seventies it was realized that the same design methodology might be useful for analog circuits, too. Besides, practical applications required integration of digital and analog circuits within the same chip. Although the analog part is usually much smaller, it appears that its design takes much more time. This disproportionality was caused by the lapse of development of appropriate supplies for analog circuit design. The main obstacle in evolution of these tools was lack of interconnection between functional and geometric description of analog design. However it was understood that symbolic circuit function can band the gap.

Secondly, the clock frequency of digital circuits is rapidly raised in last years. This caused that many parasite effects characterizing analog circuits become evident in digital circuits, too [2].

All of this stimulate the development of SA in the last decade. As result, several software packages for symbolic simulation of analog circuits were made [3, 4, 5].

Moreover, symbolic algebra find its place in other technical fields [6].

In our country two educational centers accepted the challenge to develop their own programs for SA.

Laboratory for Electronic Circuits Design Automation (LEDA) within Faculty of Electronic Engineering in Niš, continued research in this field that has been established by Professor Litovski in 1982 [7]. At School of Electrical Engineering (ETF) in Belgrade SA was the topic of Ph. D. thesis done by Mr. Tošić. Both researches started independently and took two directions. LEDA focused on development of algorithms for automatic generating circuit matrix determinant in symbolic form, while in ETF a program for SA was grown in environment of *Mathematica* program package.

The research of LEDA group resulted with two generations of program packages for SA. The first symbolic simulator, *SymSim*, is written in Lisp programming language, actually in *PC Scheme*, (a dialect produced by Texas Instruments) for PC 286 and MS DOS operating system. The detailed description of this package is given in the first M.S. thesis involved in SA in our country [8]. The second generation of this program, written in C programming language is named *SymSimC*, and run under Unix, and Linux operating systems.

The result of research in ETF is an original program package SALECAS that is described in the first Ph. D. thesis that treats SA in Yugoslavia [9].

The aim of this paper is to present different experiences in development and application of SA in our country. But first, in the next section we shall outline a brief definition of SA, its advantages and drawbacks. Besides we shall review novel methods for increasing its potentiality.

2. SYMBOLIC ANALYSIS

Traditionally, the education of electrical or electronic engineers starts with analysis of a simple circuit. Paper, pen and elementary algebra are sufficient for

deriving circuit function. Usually, circuit parameters and complex frequency are given in symbolic form. Therefore it is symbolic analysis. This method is irreplaceable for obtaining clear insight into the circuit behavior because it enables students to realize influence of particular parameters to the circuit response.

Unfortunately, this kind of analysis is not convenient for larger circuits. Hence, computer programs based on numerical mathematics were developed for circuit analysis. The most popular software package for this purpose is Spice.

The aim of circuit analysis is to give prediction about circuit behavior before it is produced. The obtained information may be considered from quantitative or qualitative aspects. It is obvious that numerical approach results with purely quantitative data. However, good insight into circuit behavior requires knowledge about qualitative dependence of circuit response to changes of relevant parameters. The most straight way to acquire this perception offers circuit function in symbolic form.

Whenever some problem overgrow possibilities of human mind to be solved quickly and correctly, man use computer. Of course, then a new problem arises: how to describe the problem to the machine and how to interpret its response. This emerges to the base objective of symbolic circuit analysis (SA).

So far, SA is effectively applicable only on linear circuits with complex frequency $x \in \{s, z\}$ as a variable. Generally, circuit function is a ratio of two polynomials in x :

$$H(x) = \frac{\sum_{i=0}^n a_i(p_1, \dots, p_k) x^i}{\sum_{i=0}^m b_i(p_1, \dots, p_k) x^i} \quad (1)$$

where coefficients a_i and b_i are terms in sum of product (SOP) form in respect to circuit parameters, p_k .

The best way to estimate the benefits of SA is to compare it with the alternate method for circuit analysis — classic analysis based on numerical mathematics, namely numerical analysis (NA). Actually, these are two complementary methods. In cases when one becomes inefficient, the other should be used. The advantages of SA are drawbacks of NA and vice versa.

The basic benefit of SA is good insight in circuit behavior. Besides, the result obtained by SA stays valuable as long as topology of the circuit is kept. In fact, the result is independent of parameter values.

Moreover, SA is immune to truncation errors typical for NA.

Finally, the result obtained by SA is very suitable for further post-processing. There are two different types of these activities.

Firstly, that are all applications that require finding circuit response on different values of parameters such are optimization [4], statistical analysis [10], tolerant analysis, fault analysis and fault modeling of analog and digital circuits [11, 12], etc.

Secondly, the result of SA given in form of (1) represents functional description of a circuit. As it corresponds to a known circuit topology, it is used in sophisticated software packages for automatic analog circuit design. As a matter of fact it helps in mapping from functional description to structural [4]. Thus, there are application of SA in automatic generating new topologies [3] and for parameter extraction [13].

Unfortunately, almost all good aspects of SA disappear when circuit complexity arise. Actually, algebraic expressions become cumbersome and effects of some parameters to the circuit response become hidden. Besides, the time needed for circuit function generating rises exponentially with the number of symbols. Therefore, a lot of effort is done to overcome or diminish these drawbacks. Depending on particular utilization of SA there are two strategies with this aim.

For applications that require repetitive evaluating of circuit function the solutions lay in development of algorithms for acceleration of circuit function generation [14] and optimal memorizing and manipulation with symbols [15].

Secondly, when the issue is good insight into circuit behavior, algorithms for symbolic approximation of algebraic expressions are implemented. Symbolic approximation is a method that automatically rejects all subdominant parameters from circuit function [16].

3. PRACTICAL EXPERIENCE

A. FACULTY OF ELECTRONIC ENGINEERING - NIŠ

At the beginning of the last decade we proceeded research of SA that initiated professor Litovski in 1982 [7]. At the time LEDA Laboratory possessed knowledge about numerical methods for circuit analysis. All algorithms needed for circuit analysis were implemented in several original software packages. All were based on modified nodal approach (MNA). Therefore, programming the matrix formulation part of symbolic simulator was not difficult task. However, there was no experience in *Lisp* programming language and appropriate data structures neither about principles for circuit determinant generating in symbolic form. Therefore we started with the algorithm described in [5]. Simultaneously we studied possibilities for upgrading

with the aim to improve its efficiency. Moreover we developed a new algorithm for factorization that considerably reduced time needed for circuit function generation [17]. Figure 1 shows the ratio of simulation acceleration in terms of circuit complexity. This example considers a ladder resistor network that is often used as a benchmark for this purposes. Solid line denotes case when all circuit elements take different symbolic values. Dashed line shows the case when all parameters in parallel and all in serial branches have same values.

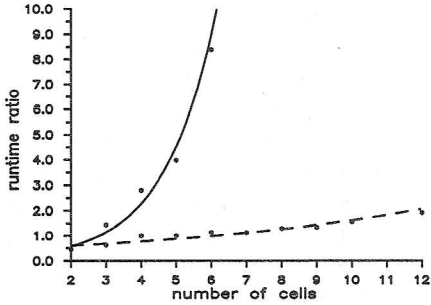


Fig. 1. Efficiency of algorithm for automatic factorization

Paper [18] approves that this algorithm is useful for factorization of already generated algebraic expressions.

Our original symbolic simulator, named *SymSim*, was successfully tested on many examples.

In the next, this paper will give a survey of applications and benefits of SA.

We start with one of practical examples that presents how good insight into circuit behavior can be achieved by SA. Filter presented in Figure 2. was developed by Ei EKOS factory within Ei – Holding Corporation in Niš, to separate different TV signals.

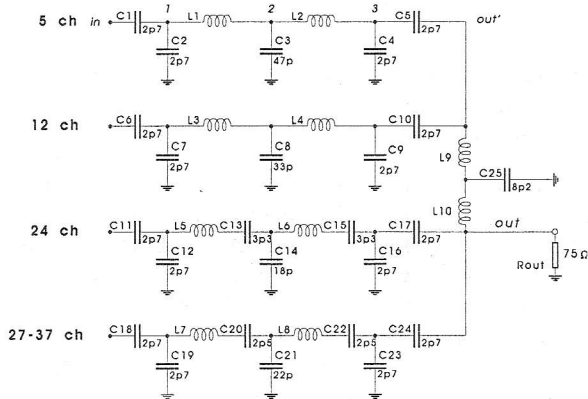


Fig. 2. Antenna filter

When circuit function in symbolic form is known, it is very easy to obtain 3D plot that shows magnitude in terms of frequency and one of the parameters. Figure

3 illustrates the influence of inductance $L_1=L_2=L$ on magnitude.

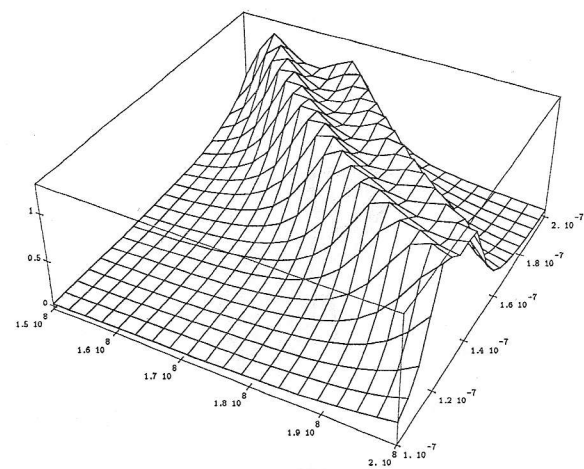


Fig. 3. Magnitude of output voltage of circuit presented in Fig.2 in terms of frequency and inductance L

An interesting application of SA is stability analysis. As an illustrative example let us consider feed-back amplifier presented in Figure 4a [19]. Simultaneously, Figure 4b shows the amplifier in a form of block diagram. This presentation is very suitable for SA of control systems. A specially convenience is possibility to define blocks in terms of their transfer function.

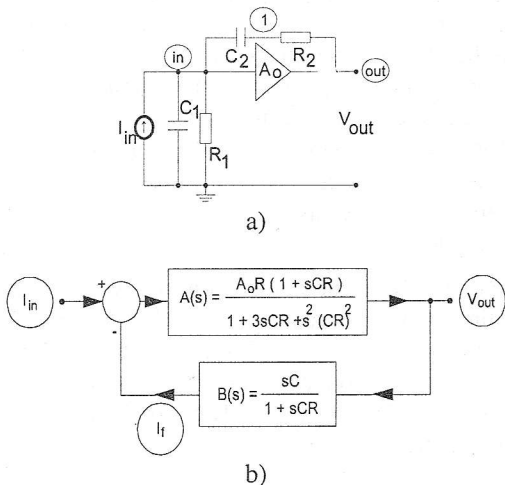


Fig. 4. a) Feed-back amplifier
b) Block representation of the feed-back amplifier

The best way to analyze stability of the amplifier is to inspect its circuit function. Therefore, appropriate Nyquist diagram is plotted in parametric form in Figure 5a, with amplification A_o as the parameter. Although this is common type of presentation that is suitable for stability analysis, more descriptive is the 3D presentation shown in Figure 5.b.

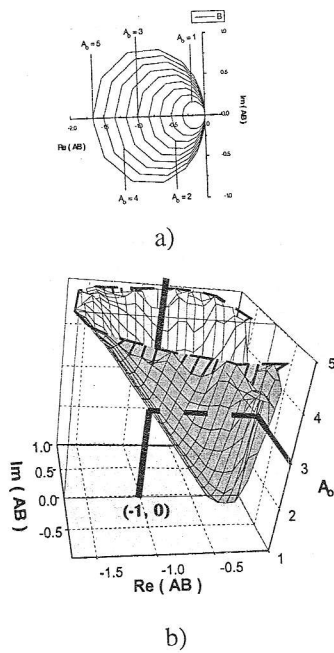


Fig. 5. a) Nyquist plot for feed-back amplifier
b) 3D plot of 5.a)

Program SymSim is adapted for automatic Y- and S-parameters extraction. Besides, it is accommodated to accept already generated parameters for next analysis. At this way hierarchical SA of complex circuits is enabled. [20-23]. Resulting expressions have nested form, that can be easily expanded into SOP form.

We have introduced SA in the field of ceramics material design, [24, 25]. Actually we used a circuit model of ceramics and generated appropriate symbolic circuit function. Assuming that relationship between technology parameters and parameters of the model are known, one can easily substitute them in the obtained expression. Then, it is obvious that it is possible to predict the influence of sintering temperature, for example, on characteristics of a ceramics device.

Our experience in the application of SA goes further than linear analog circuits. We used it for automatic test pattern generation and for defect modeling in digital circuits. Actually an original method was proposed in [26, 27] for CMOS combinational and sequential digital circuits.

Basic idea was to introduce logic *Transistor Logic Conductance Function*, TLCF). Its value shows if there exists a conductive path between an output and bias V_{dd} , or V_{ss} . Every transistor is treated as a controlled switch. Therefore it is replaced by a conductance controlled by a logic state. Then SA program can give an expression that represents equivalent conductance between output and bias in terms of particular conductance. However this is not sufficient to determine logic state at the output. Therefore, it is necessary to assign logic values 0 and 1 to the conductance to denote open transistor or

shorted transistor, respectively. Circuit function given in terms of these conductances makes TLCF. If there is at least one conductive path between output and V_{dd} the output takes high logic state, if there is a path towards V_{ss} , output is low. If there is no path neither to V_{dd} nor to V_{ss} , output is at high impedance. Oppositely, if both paths are conductive the output takes an unknown state. This method is suitable for fault modeling, even for modeling bridging or open faults, too. With that aim at every critical place in the circuit an extra conductance can be added. If it take value 0 the path is opened, if it takes value 1, it is closed.

So far we described SA in s-domain. However, the same efficiency SA shows in z-domain also. This option, is implemented in the latest version of program SymSimC. Actually, knowledge that already has existed in LEDA about numerical analysis of SC circuits [28] were expanded into symbolic domain. Differently to some other programs for SA of SC circuits, SymSimC uses MNA during matrix filling and is capable to treat operational amplifiers with final gain [29]. This option is illustrated in the example presented in Figure 6.

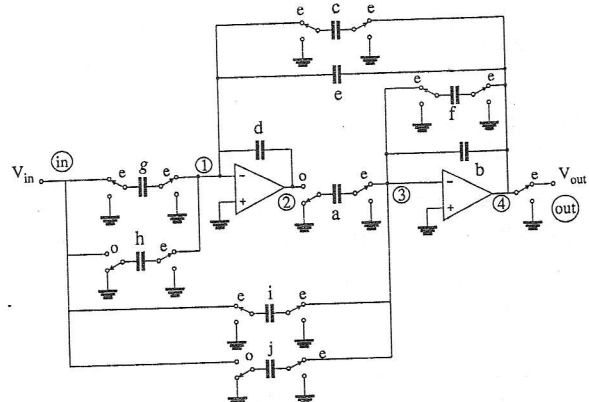


Fig. 6. LF Band-pass SC-filter

Figure 7 shows 3D plot where circuit function is presented in terms of frequency and final gain of operational amplifiers.

Simultaneously with research of different applications of SA we are proceeding to investigate methods for improvement possibilities of SA. Actually, we are working on few new algorithms for symbolic approximation and on a new algorithm for SA of complex circuits. We approach to the approximation at two levels. The goal of the first is to simplify already generated symbolic expression and to gain insight to influence of dominant parameters. The other is aimed to accelerate SA of complex circuits with neglecting unimportant circuit parameters in advance, at topological level, before generating circuit function [30]. From the former approach emerged an idea to split SA of a complex circuit to several analysis at

different frequency ranges. This presumes that at various frequencies, different parameters have dominant influence to circuit function. Therefore one gets reduced circuits for every frequency range. The obtained results have shown that considerable acceleration of SA can be obtained for some circuits [31].

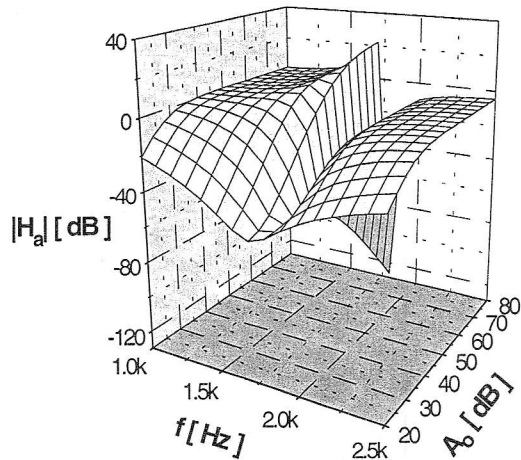


Fig. 7. Influence of final operational amplifier gain on circuit function for LF Band-pass SC filter.

B. SCHOOL OF ELECTRICAL ENGINEERING, BELGRADE

Symbolic analysis at the School of Electrical Engineering (ETF) in Belgrade has been directed towards the construction of algorithms that will be automated in *Mathematica*.

The underlining idea has been development of a unique framework for symbolic analysis and design of linear (and linearized) electrical circuits and systems. The review of principal research results follows.

Symbolic analysis of lumped linear time-invariant electric circuits [32] has been implemented in *Mathematica*; circuits whose graph is disconnected can be analyzed [33].

Symbolic synthesis of one class of second-order filters and amplitude equalizers [34] has been automated in SALECAS [9] and is carried out in the complex domain.

Symbolic simulator of linear time-invariant dynamic systems [35] performs analysis of continuous-time systems in the complex domain.

Symbolic analysis of DC load flow in electric power systems, i.e. symbolic derivation of average powers of

transmission lines in electric power systems [36,37] can analyze power systems up to 10-20 nodes.

Symbolic analysis of linear microwave circuits specified by scattering parameters is performed in the sinusoidal steady state, and complex wave signals are found symbolically [38].

Analysis and design of active filters is well suited for symbolic analysis if closed-form expressions exist for the filter parameters in terms of the transfer function coefficients [39]. For certain degrees the elliptic transfer function can be represented symbolically without the Jacobi functions [40, 41]. If we know the filter poles and zeros symbolically, we can compute the filter impulse and step response symbolically, too [42].

Combinational networks with acyclic directed graph has been analyzed symbolically [43], and all logical (Boolean) variables are treated as symbols.

Transfer functions of digital filters have been efficiently found symbolically [44]. Programmable digital filters can be symbolically analyzed in the complex *z*-domain [45]. Symbolic analysis and design has been successfully performed in the case of two-dimensional filters for image processing [46, 47].

Several algorithms for symbolic approximation have been proposed and automated in software [48, 49].

A concept of unified symbolic analysis of circuits and systems has been reported in [50].

The current research efforts are directed towards an automated symbolic simulator of linear circuits with a single feedback loop [51].

Symbolic analysis of large circuits has been approached with the hierarchical decomposition into blocks of known matrix parameters.

The future research directives are symbolic analysis of multidimensional digital filters, and algorithms for automated comparison and performance evaluation of digital filter realizations.

The software package SALECAS, developed in the doctoral dissertation of D. V. Tasic at ETF Belgrade [9], is based on the following decomposition.

Matrix approach to the analysis of linear electrical circuits and systems reveals a unique final form of the circuit/system equations — the matrix system of linear equations. What is specific for certain circuits and systems is the algorithm of forming required matrices and matrix equations, and identification of the circuit/system variables. The following text presents a new and unique concept and formulation of general symbolic analysis of linear electrical circuits and systems. The most general concept is proposed for: 1) representing linear circuits and systems, 2) representing the symbolic analysis knowledge, and 3)

formulating required matrices to solve a circuit or system.

The package SALECAS (Symbolic Analysis of Linear Circuits and Systems) has been developed in *Mathematica* to implement the above general concept of symbolic analysis.

In the text to follow the symbol CAS will be used as an acronym for "circuit and/or system."

At the highest level of abstraction, from the viewpoint of automated computer-aided symbolic analysis, a linear electric circuit or a linear system have identical representations in the form of a list: **system** = {"*class*", "*label*", *components*, *knowledge*}. The elements of the list are: *class* - the CAS sort/category, *label* - the CAS individual name unique for each instance of the CAS, *components* - the CAS constitutive elements or building blocks, *knowledge* - entities, rules and procedures for the CAS analysis. The following major CAS classes can be identified: **LEC** - time-invariant linear electric circuits, **MWC** - time-invariant linear microwave circuits, **CLS** - continuos-time dynamic stationary systems, **DLS** - discrete-time stationary systems, and **PS** - power systems. The CAS components represent ideal circuit elements, microwave network ports, functional blocks like integrators and differentiators, digital filter multipliers and delays, equivalent networks for modeling electronic devices, multiport networks whose matrix parameters are known, etc.

A CAS component is described by a list: **component** = {"*type*", "*name*", *connection*, *parameters*, *energy*}. The list items are: *type* - the component type/sort, *name* - the component's unique name, *connection* - the component's terminals or ports whose order of appearance includes the reference direction assumptions of associated variables, *parameters* - the component's parameters, *energy* - the initial conditions for capacitors, inductors and integrators.

The required knowledge to analyze a CAS is a list of the form: **knowledge** = {*library*, *variables*, *matrices*, *rules*, *procedures*, *presentation*}. The corresponding items are: *library* - the list of the component types and their definitions, *variables* -

voltages, currents, signals, average powers, etc. appearing in the analysis and requested as output quantities, *matrices* - matrices involved in the analysis, *rules* - rules to check the system description for syntax/semantics, to count variables, to determine the order of the system, to initialize the matrices, rules for reserved symbols (the complex frequencies *s* and *z* are special symbols), etc., *procedures* - are sets of actions and algorithms to formulate CAS equations, to reduce/compact this system of equation to solve it, to find the response or transfer functions, to approximate the result, etc., *presentation* - conventions of post-processing the result of the analysis to make it suitable for human inspection or machine further analysis.

A CAS library is a list of types: **library** = {*type1*, *type2*, *type3*, ...}. Each *type* is a list of the form: **type** = {*symbol*, *terminals*, *definition*, *stamp*}, whose items are: *symbol* - a graphical icon for schematic entry or displaying of a component, *terminals* - a list of terminals of a component, *definition* - constitutive equations of a component, *stamp* - rules for automated modification of the CAS matrices according to the component description.

The SALECAS entities and their interconnection is shown in Fig. 8.

SALECAS is a novel framework for general symbolic analysis of linear time-invariant circuits and systems, in which linear CAS are viewed as lists of items representing their identification, components and symbolic analysis knowledge. A consequent system of abstractions is developed to specify linear CAS and to provide encapsulation mechanisms of analysis procedures and entities. It can serve as a starting point for object-oriented decomposition in symbolic analysis (currently under research and development).

A unique conceptual engine is proposed for symbolic analysis of physically different systems. These systems are essentially different in appearance and physical background, but they have the same mathematical matrix formulation from the symbolic analysis viewpoint.

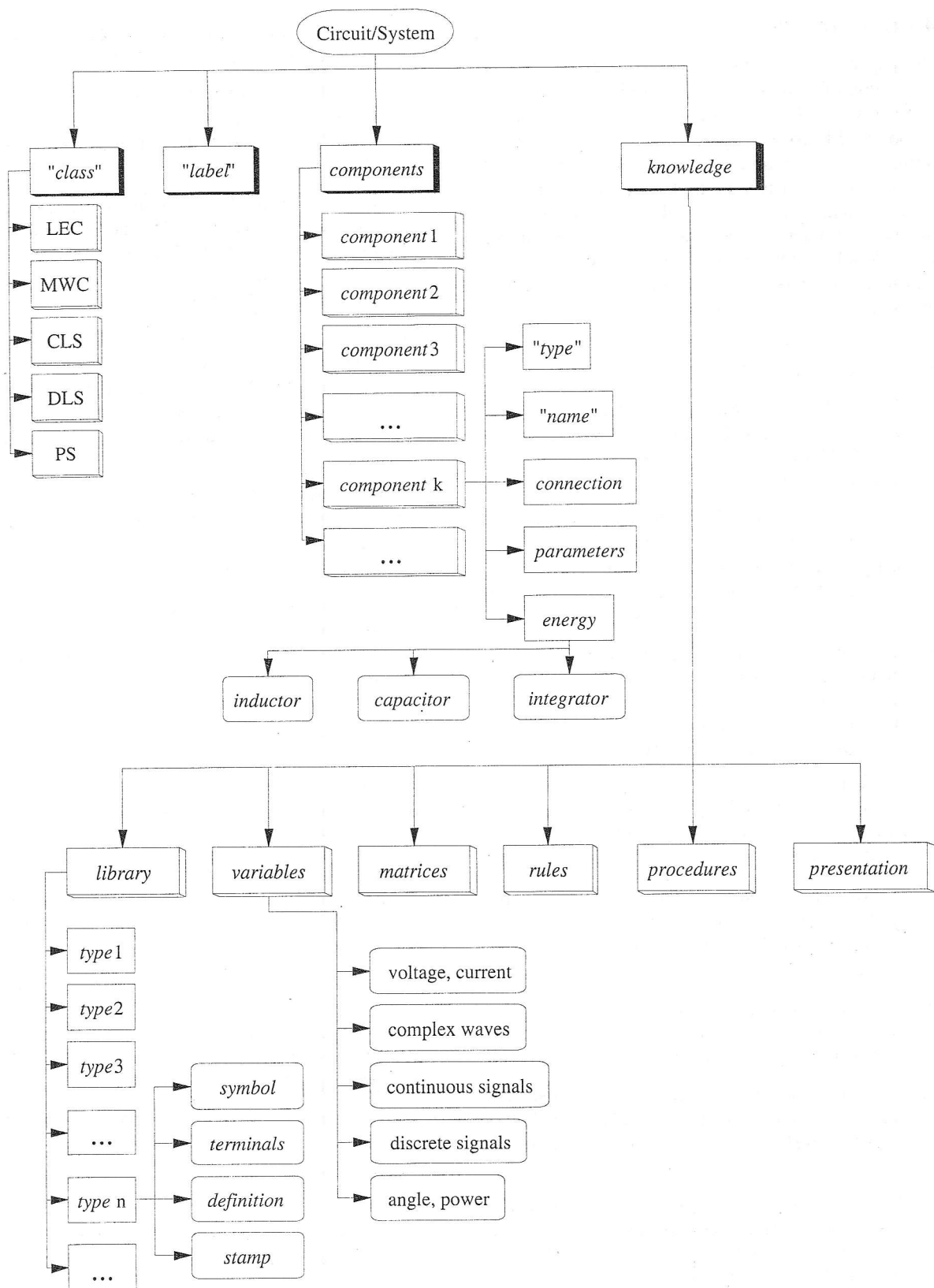


Fig. 8. The SALES CAS entities and their interconnection.

4. CONCLUSION

This paper summarized experiences in developing and application of symbolic analysis of electronic circuits at Faculty of Electronic Engineering in Niš and at School of Electrical Engineering in Belgrade. It is defined Symbolic simulation The definition of U radu su prikazana iskustva sa Elektronskog fakulteta u Nišu i Elektrotehničkog fakulteta u Beogradu u razvoju i primeni simboličke analize elektronskih kola. Pored definicije osnovnih pojmove koji se odnose na ovu oblast, istaknute su prednosti i mane u odnosu na numeričku analizu.

5. REFERENCES

- [1] P. M. Lin, "A Survey of Applications of Symbolic Network Functions", *IEEE Trans on Circuit Theory*, Vol. CT-20, No. 6, pp. 732-737, November 1973.
- [2] J. Shah, A. Younis, S. Saptnekar, M. Hassoun, "Symbolic analysis of power/ground networks using moment-matching methods", *Proc. ECCTD'97*, Budapest, pp. 1292-1297, September 1997.
- [3] A. Konczykowska, J. Mulawka, M. Bon, "Symbolic Simulation: A New Approach to Automated Electronic Circuit Design", *Int. Workshop on Artificial Intelligence for Industrial Applications*, Hitachi, May 1988.
- [4] G. Gielen, W. Sansen, "Symbolic Analysis for Automated Design of Analog Integrated Circuits", Kluwer Academic Publishers, Boston/London, 1991
- [5] S. Manetti, "New approach to automatic symbolic analysis of electric circuits", *IEE Proceedings-G*, Vol. 138, No. 1, pp. 22-28, February 1991.
- [6] K. Schlacher and R. Scheidl, "Modeling of Mechatronic Systems by Symbolic Computation", *EUROSIM'95*, pp. 657-662.
- [7] S. Stanojević, V. B. Litovski, "Simbolička analiza elektronskih kola", *Tehnika (Elektrotehnika)*, Vol. 31, No. 12, pp. 1985-1989, 1982.
- [8] R. Stevanović, Simbolička analiza linearnih elektronskih kola zasnovana na primeni simboličke algebre, Magistarska teza, Elektronski fakultet Niš, Jun, 1994.
- [9] D. Tošić, "Prilog algoritmima simboličke analize linearnih električnih kola i sistema pomoću računara", Doktorska disertacija, Elektrotehnički fakultet Beograd, 1996.
- [10] M. Styblinski and M. Qu, "Comparison of Symbolic Analysis, Approximation and Macromodeling Techniques for Statistical design of Quality of Analog Integrated Circuits", *Proc. ISCAS'97*, Seattle, pp. 2221-2224, April 1995.
- [11] Cho, R. Bryant, "Test Pattern Generation for Sequential MOS Circuits by Symbolic Fault Simulation", *Proc. 26th ACM/IEEE DAC*, pp. 418-423, 1989
- [12] Z. You, E. Sanchez-Sinencio and J. de Gyvez, "Analog System-Level Fault Diagnosis Based on a Symbolic Method in the Frequency Domain", *IEEE Tran. on Instrumentation and Measurement*, Vol. 44, No. 1, pp. 28-35, January 1995.
- [13] Zerounian, F. Aniel, N. Kauffman, R. Adde and A. Konczykowska, "Extraction Strategies of Semiconductor Device Parameters Using Symbolic Approach and Optimization Methods", *Proc. ECCTD'97*, Budapest, pp. 1298-1303, Sept. 1997.
- [14] E. Wehrhanh, "Symbolic Analysis of Large Linear Circuits with the Bilinear-Splitting Transformation", *Proc. ISCAS'95*, Seattle, pp. 2079-2082, April 1995.
- [15] M. Hassoun and P-M. Lin, "A Hierarchical Network Approach to Symbolic Analysis of Large-Scale Networks", *IEEE Tran. on Circuits and Systems-I*, Vol. 42, No. 4, pp. 201-211, April 1995.
- [16] F.V. Fernandez, A. Rodriguez-Vazquez J.D. Martin and J.L. Huertas, "Formula Approximation for Flat and Hierarchical Symbolic Analysis", *Analog Integrated Circuits and Signal Processing*, 3, pp. 43-58, 1993
- [17] P. Petković, S. Stojiljković and V. Litovski, "Factorization algorithm for symbolic circuit analysis" *IEE Electronic Letters*, Vol. 31, No. 13, pp. 1026-1027, June 1995.
- [18] M. Topa, P. Wambacq, G. Gielen, W. Sansen, E. Simion, "Postprocessing techniques for approximate symbolic network function of integrated building blocks", *Proc. of ECCTD'97*, Budapest, pp. 1464-1467, September 1997.
- [19] P. Petković, V. Marković and V. Litovski, "Application of symbolic simulator in the education process", *8th ISTET'95*, Thessaloniki, pp. 529-532, September 22-23, 1995.
- [20] P. Petković, V. Marković, R. Stevanović, D. Milovanović i V. Litovski, "Primena simboličke analize u projektovanju VF kola", *Proc. TELSIKS'93*, Niš, pp. 6.15-6.22, Oktobar 1993.
- [21] P. Petković and V. Marković, "Symbolic S-parameters analysis of microwave transistor models", *Proc. of the 17th Edition of Annual semiconductor Conference*, Sinaia, Romania, pp. 383-386, October 11-16, 1994.

- [22] P. Petković, V. Marković i V. Litovski, "Simbolička analiza mikrotalasnih kola u funkciji talasnih parametara", Proc. TELSIKS'95, Niš, pp. 477-480, Oktobar 1995.
- [23] V. Marković and P. Petković, "Symbolic approach to the microwave circuit design", Proc. 11th MIKON'96, Warsaw, Poland, pp. 541-545, May 27-30, 1996.
- [24] V. Mitić, P. Petković, S. Bogosavljević i M. Radmanović, "Simbolički metod za projektovanje električnih svojstava BaTiO₃-keramičkih materijala u funkciji parametara konsolidacije", Tehnika, god. 51., No. 7-8, pp. 6NM-10NM, 1996.
- [25] P. Petković, V. Mitić, and M. Radmanović, "Symbolic Approach in Prognoses of BaTiO₃-Ceramics Capacitive Behavior in Real Environment", Proc. MicroMat'97, Berlin, pp. 795-798, April 1997
- [26] P. Petković, D. Milovanović and V. Litovski, "Symbolic modeling of MOS combinational circuits", Microelectronics Reliability, Vol. 37, No. 1, pp. 137-157, 1997.
- [27] P. Petković, D. Milovanović and V. Litovski, "Symbolic Oriented Stuck Fault Modeling of CMOS Sequential Circuits", Proc. of 21st MIEL'97, Niš, pp. 783-786, September 1997.
- [28] D. Milovanović i V. Litovski, "Simulacija SC kola u frekventnom i vremenskom domenu primnom modifikovane metode čvorova", Zbornik ETAN'84, Split, pp. 109-116, Jun 1984.
- [29] V. Živković, P. Petković and D. Milovanović, "Automatic symbolic analysis of SC networks using a modified nodal approach", Microelectronics Journal 29 (1998), pp. 741-746.
- [30] P. Petković, V. Živković, "Symbolic Approximation in Analog Circuit Design", 18th International Spring Seminar on Semiconductor and Hybrid Technologies, Vol. 12, No. 1, Sozopol, Bulgaria, pp. 275-284, 1996.
- [31] P. Petković, V. Živković, "Segmented symbolic simulation", Proc. TELSIKS'97, Niš, pp. 130-133, Oktobar 1997.
- [32] Tošić and B. D. Reljin, "Symbolic analysis of electric circuits using the program SALEC", Proc. Third ELECTROSOFT '96, San Miniato, Italy, pp. 135-144, May 1996.
- [33] D. V. Tošić, B. D. Reljin, and I. S. Reljin, "Educational aspect in symbolic analysis of linear electric circuits", Proc. 8th ISTET'95, Thessaloniki, Greece, Sep. 1995, pp. 533-536.
- [34] D. V. Tošić, M. F. Hribsek, and B. D. Reljin, "Generation and design of new continuous-time second order gain equalizers using program SALEC," International Journal of Electronics and Communications (AEU - Archiv für Elektronik und Übertragungstechnik), vol. 50, no. 3, pp. 226-229, May 1996.
- [35] D. V. Tošić, B. D. Kovacevic, and B. D. Reljin, "Symbolic Analysis of Linear Dynamic Systems," Control and Computers, vol. 24, no. 2, pp. 54-59, 1996.
- [36] Skokljev and D. V. Tošić, "A new symbolic analysis approach to the DC load flow method," Electric Power System Research Journal, vol. 42, no. 2, pp. 127-138, 1997.
- [37] D. V. Tošić and I. A. Skokljev, "SALF - a tool for symbolic analysis of the DC load flow," Proc. 5th International Conference Tesla. III Millennium, Belgrade, 15-18 Oct. 1996, pp. III.19-III.26.
- [38] D. V. Tošić, A. R. Djordjevic, B. D. Reljin, "Symbolic Analysis of Microwave Circuits," Journal of Applied Electromagnetism, vol. 1, no. 1, pp. 37-45, 1997.
- [39] D. V. Tošić, M. D. Lutovac, B. L. Evans, I. M. Markoski, "A tool for symbolic analysis and design of analog active filters," 5th International Workshop on Symbolic Methods and Applications to Circuit Design (SMACD'98), Kaiserslautern, Germany, October 1998.
- [40] M. D. Lutovac, D. V. Tošić, I. M. Markoski, "Symbolic computation of elliptic rational functions," ibid.
- [41] M. D. Lutovac, D. V. Tošić, and B. L. Evans, "An algorithm for symbolic design of elliptic filters," Proc. 4th SMACD'96, Leuven, Belgium, Oct. 10-11, 1996, pp. 248-251.
- [42] D. V. Tošić, M. D. Lutovac, "Symbolic computation of impulse, step and sine response of linear time-invariant systems," Proc. SAUM'98, Niš, Serbia, Yugoslavia, September 28-30, 1998.
- [43] Dejan V. Tošić, Mirko Vujošević, "Symbolic Analysis of Systems Specified by Binary Boolean Functions," 4th BCOR'97, Thessaloniki, Greece, Oct. 20-23, 1997. (to appear in Proc. that will be published in 1998)
- [44] D. V. Tošić, M. D. Lutovac, and I. M. Markoski, "Symbolic derivation of transfer functions of discrete-time systems," Proc. 9th ISTET'97, Palermo, Italia, pp. 311-314, June 1997.
- [45] M. D. Lutovac, D. V. Tošić, and B. L. Evans, "Symbolic analysis of programmable digital filters," Proc. 21st MIEL'97, Niš, Serbia, Yugoslavia, 14-17 Sep. 1997, pp. 713-716.

- [46] D. V. *Tošić*, A. Mojsilovic, and M. Popovic, "Symbolic approach to 2D biorthogonal diamond-shaped filter design," *ibid*, pp. 709-712.
- [47] A. Mojsilovic, D. V. *Tošić*, and M. Popovic, "The design of 2D hexagonal filters based on transformations: The symbolic approach," *Proc., ECCTD'97*, Budapest, Hungary, 30.Sep.-3.Oct. 1997, pp. 890-895.
- [48] I. M. Markoski and D. V. *Tošić*, "Symbolic approximation of circuit response containing negative terms," *Proc. 21st MIEL'97*, Nis, Serbia, Yugoslavia, 14-17 Sep. 1997, pp. 705-708.
- [49] I. M. Markoski, D. V. *Tošić*, and B. D. Reljin, "A simple algorithm for formula approximation in symbolic analysis of linear circuits," *Proc. 9th ISTET'97*, Palermo, Italia, 9-11 June 1997, pp. 120-123.
- [50] D. V. *Tošić*, "SALECAS - a package for symbolic analysis of linear circuits and systems," *Proc. 4th SMACD'96*, Leuven, Belgium, Oct. 10-11, 1996, pp. 227-230.
- [51] B. Nikolić, D. V. *Tošić*, and S. Marjanovic, "Symbolic analysis of feedback amplifier circuits," *ibid*, pp. 244-247.

THE REAL-TIME SYSTEM IMPLIMENTATION OF THE CONTROL AND SUPERVISION UNIT FOR THE CIGARETTE PACKING MACHINE GD-X1

*Milun. S. Jevtić, Branimir Ž. Đorđević, Andrija S. Velimirović, Vladimir D. Živković
University of Niš, Faculty of Electronic Engineering, Niš*

Abstract - A realisation of the system for packing cigarettes process control and monitoring on GD-X1 machine is the point of this paper. Since it is based on the hard real-time system, the object-oriented realization of process visualisation is considered first. Some applied techniques for on-line built-in self-testing used for high security in machine control, are shown also.

1. INTRODUCTION

The visualization of a process (an industrial or chemical one) is the realization of possibility to easily recognize, in one place, the process state and to detect some change in it.

A graphic representation provides the easy noticing of relevant information from the huge information set, but it also demands the processing of the great data quantity due to its generation. Hence, the visualisation process involves a significant number of microcomputer hardware resources and processor time. By that way, the visualization in a system for control and supervision in the real-time with a rigid limits (Hard Real Time System - HRTS) demands the systematic and detailed realisation.

The software realizing the visualization has to support the time deadlines in HRTS [1] too. Besides that, it has to have the compact and correct code, the ability to control the exceptions, as well as the completely predictable behaviour.

Having in mind the more complex functionality of modern control units based on microcomputers, the demand for the predictable behaviour puts, in the first place, the consideration of the work safety. Therefore, besides carrying out the basic function, the microcomputer control system has to fulfill some other demands such as:

- high reliability - high probability of the continuing correct functioning in the given long time interval, and in the sense of the stable providing of the correct functioning of the system hardware and software resources;
- high stability - relatively low rate of repair time - reparation;
- minimal recovery time after the detected failure;
- extremely low level of failure in the short time interval;

- extremely high probability of transfer to the safety final state after the appearance of the wrong functioning;
- easy and timely diagnostics of the failure and defect;
- safety and protection - possibilities to protect the system from careless-wrong use or from malicious attempt of destroying the system function;
- responsibility - the system ability to continue functioning, eventually with smaller capacity, in the presence of failure, also without exceeding the period of critical processes.

Achieving these properties is closely related (connected) to introducing redundancy in the volume and time as basic resources of the system [2], [3]. Considering the compromise between the volume and time has the goal a profitable system, although the time usually plays the critical role. Especially in the control systems with the graphically supported interaction system-man, i.e. with the visualization of the process where it is handled (manipulated) with a great data quantity for generating the graphics representations.

By the realization of the system controlling the cigarette packing system on the machine GD-X1 tended (gravitated) toward the realization of all mentioned demands. Naturally, in that measure (rate) as it is appropriately. By a small redundancy in hardware and software, the goal is to achieve the timely failure detection and bringing the control processes - machine working in a safe state. The way this is achieved, i.e. the used technique of selftesting the control unit while it performs its basic function, will be presented in the following text. Also, the object oriented realization of graphic interaction for the visualization and conduction of dialogue in the system for control and supervision of the cigarette packing process.

2. GLOBAL SYSTEM DESCRIPTION

The system for controlling and supervision of the cigarette packing process (Fig. 1) will be examined here limited to the machine for making cigarette packages - GD-X1. It is realized as the two-hierarchical system with distributed control functions and the centralized supervising function in the process computer. Each control unit realized as HRTS competitively achieves activities of controlling,

following and memorizing the relevant working parameters, messages exchange with the process computer and selftesting.

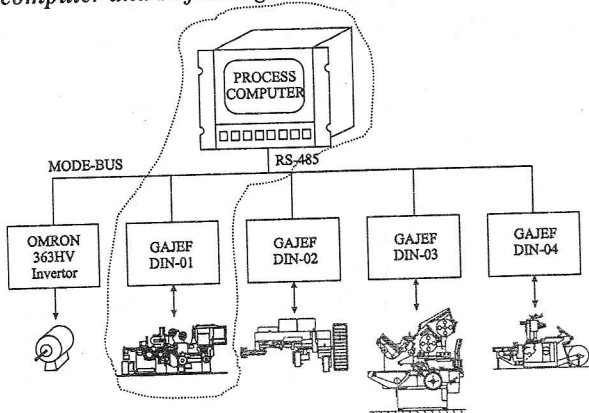


Fig. 1 Global structure of the control and supervision system

The process computer does not directly perform the control function, so it is realized as SRTS (Soft Real Time System). It has some additional activities, such as the supervision activity over the whole system, the activity of archiving the process parameters and events, the activity of generating reports and the activity of realizing the graphical interaction man-system.

The diagram of states of the system for packing cigarettes is given in Fig. 2. By turning on, the system is in an initial state (INIT), and, after the self-testing and checking the correctness of the machine state, it goes into the state of readiness (IDLE). States of readiness, work (RUN) and suspension (SUSP) makes the subset where the severe demands for the work in the real-time are given.

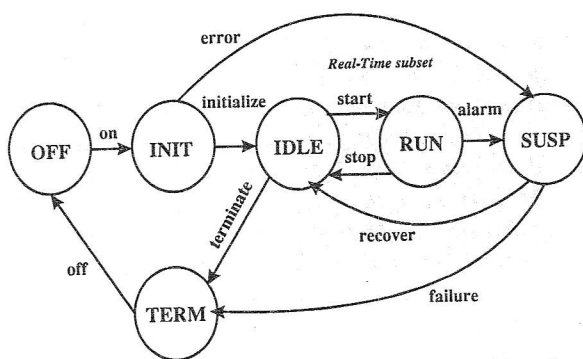


Fig. 2 State diagram of the system for packing the cigarettes

The total (whole) activity of the system can be recognized through the set of the following factors:

- operating and supervising activities of forming packages through machine;
- operating and supervising activities of feeding machine and safety circles of machine;

- regulation circle of the iron thermoregulator;
- regulation circle of the revolutions number of the machine engine;
- protocol of exchanging messages by the common asynchronous communication channel;
- processing of the package process parameters;
- processing of the excess events;
- generating reports on the system work;
- archiving of parameters and all relevant events in the system;
- generating the visual representation of the process state;
- interaction man-system;
- self-testing of the system.

Each factor [4] can be presented by one automat of the final states [5] - by the object which the certain ports are statically added on. Factors mutually communicate by the data exchange, and their working during the time is caused by the asynchronous external events, the real time clock and the interior sequence events.

3. "ON-LINE" ERRORS DETECTION

Different "on-line" errors detectors can be built in the microcomputer system. The basic principle of these detectors, which work while the system performs its basic function too, is the redundancy use in:

- devices (multiplying of hardwares),
- information (redundant codes),
- software, and/or
- time of performing.

Taking into consideration the working principles, mechanisms for the errors detection can be divided into three levels:

- circuit level
- system level (functional level), and
- application level.

All previously mentioned mechanisms of the errors detection are also applied to the realized microcomputer control unit of the cigarette packing machine GD-X1. In order to recognize the applied errors detectors in the control unit, first of all, the functioning of machine should be presented in brief.

The packaging operation (the cigarette package formation) is performed by the machine through 52 operations, i.e. 52 positions in the machine. The work of machine is by principle of pipeline. In each tact of the machine working, which corresponds to one revolution of the machine, at each position the corresponding operation over the potential cigarettes packages is done and their moving towards the next positions is performed. So, besides operating the current (course) of one revolution - cycle of the machine working, it is also

necessary to follow forming each package during all operations, i.e. during its passing through the machine (52 revolutions of machine). By that it is provided that the detection of some incorrectness on the package in some operation would be taken into consideration during the next operations over that potential package. For example, if the empty tip of some cigarette in the position for operation of this testing is detected, that heap of cigarettes should be thrown out (put out) at the later position for throwing out. After some tacts in the position for covering cigarettes for "empty package", the aluminium foil should not be pulled for covering cigarettes, then in the position for packing in the package wrapping, the wrapping should not be taken, and so on. Therefore, the marker m is joined to each potential package, and the marker "moves" together with it through the machine and influences the operation performance.

A number of the machine revolutions is also one sequence of tasks for the machine operating. It is realized as a sequence led by events. The synchronization between the tasks of operating and the phase angle of the machine is realized by the signals from the machine programmatic. It generates the set of digital signals called an operating vector, by which the operating sequence is defined - the sequence of performing the operating tasks in operating unit during one cycle of the machine working.

DETECTOR OF THE APPLICATION LEVEL

One sequence of operating, i.e. one cycle of the machine working, consists of the final number of allowed states. All transitional states, in which any operating task is not performed, are also included in the allowed states. These transitional states are results of an imperfectness of the mechanically adjustment of the machine, in other words differences that can appear from one machine to another and in their programmers.

By turning on the machine - starting the process of the machine operating, firstly on the basis of detecting two consecutive operating vectors in the operating unit, the phase is established - the mechanical position of the machine, and by that the operating process is put in the corresponding state.

On the basis of the described way of the machine working, the error detector on the level of application is realized. Namely, since the allowed sequence of the operating vector is defined, then each second sequence or unexpected vector value are treated as the failure in the operating process.

Transition (transfer) of the operating process from some state S_{i-1} into the next one S_i from the state sequence of the working machine cycle is presented in Fig. 3. The transition can be achieved

(realized) directly or across the transfer states SP_{ij} , which are less than two.

Only when the vector v_i is detected, during the transition into the state S_i the task z_i is activated. The functions values defining the state of relevant ON/OFF outputs are calculated in it on the basis of the immediate sensors states - u_{1-n} and memorized marker values - m_{1-32} joined to the potential packages. By setting the outputs, values of the corresponding markers are defined, and if it is necessary they are modified;

$$z_i : f_{ij}(U, M); \quad j = 1, \dots, k,$$

$$U = \{u_1, u_2, \dots, u_n\}, \quad M = \{m_1, m_2, \dots, m_{32}\},$$

k - number of outputs controlled by the task,

n - number of sensor outputs.

When the value of operating vector, different from all expected ones, is detected, the task of error ze is activated and it is transferred to the state "STOP MACHINE" and the error message is generated. It can be gone out from this state only by manual machine restarting - operating unit.

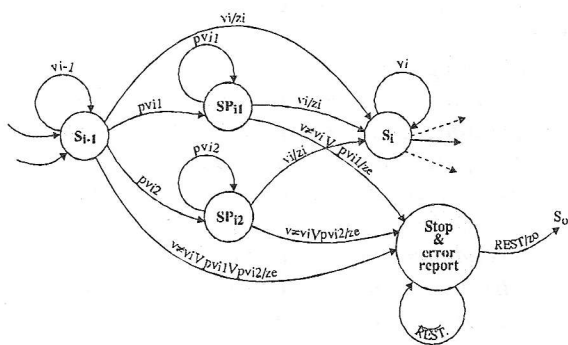


Fig. 3 Diagram of the operating process transition from the state S_{i-1} into the state S_i

DETECTORS OF THE SYSTEM LEVEL

On the system level, the greatest number of errors detectors is realized, because they are easily realized by software by the minimum additional hardware. Because of the possible place of the failure appearance in the operating system, independently of the used mechanism for the realization, errors detectors can be classified into:

- errors detectors in a microcomputer,
- errors detectors in sensors -on/off inputs and
- errors detectors in actuators -on/off outputs.

Errors Detection in Microcomputer:

For controlling the correctness of the programme code in the microcomputer memory, by which the operating algorithm is realized, a check sum (CS) for the programme code is calculated once in the cycle of the machine working (at the beginning of the cycle). If by checking the correctness CS the error is detected, the calculation

of CS is immediately repeated and the machine and operating unit are if the error is detected again.

The supervising timer for controlling the correct working of operating programme is built in the operating unit. But the build-in procedure of restarting the supervising timer in the programme code could not be done by the simple division (distribution) of the programme code into some segments. The problem is in the fact that the machine can work at the arbitrary speed from 0 to 300 revolutions in a minute. Also, it can be stopped (by the operator too) in any position, which results in the software loops (petlja) which duration can not be predicted in advance. For that reason, in the software loop, where the next event (the operating vector) is expected, the procedure for forming and checking CS for code segments making that loop is built in. If the correctness of CS is established, the procedure of restarting the supervising timer (WD) is activated. WD is initialized on the time which is defined on the basis of the time of performing the longest programme sequence of transferring the operating process from one into another state. That is clearly sequential series of instructions where there is no a condition (reason) or loop of the arbitrary long performing.

For the errors detection in data significant for operating (as the result of transferring error in the manipulation with data) the simple software technique of generating two data copies is applied. The first one as the real values of binary data, and the second one got by complementing the binary data. By using data for calculating the operation function, firstly the correctness of read data copies is checked. The calculation correctness can be checked using the complementary operation function. By detecting the error, the procedure of the detected error processing is started.

Errors Detection in on/off inputs:

Because of the increase of the reliability of gathered informations from sensors, the different ways of detection of sensors errors are realized. They are different because the significance and functioning of all sensors in the system are not the same. According to this, all sensors can be divided into three groups:

1. Sensors which generate the sequence for leading the machine operating - operating vectors;
2. Sensors that can have, during one cycle of the machine working, the change because of the testing;
3. Sensors that can not have one change in the cycle of the machine working at least.

For the first group of sensors (there are 8 of them in the machine), the error detector is practically already realized by the previously described detector on the application level. Each failure in some of these sensors will result in an incorrect operation vector , i.e. the incorrect

sequence of the operation vector. Which sensor has a failure can be easily established on the basis of vector values. The only left failure of these sensors is if all of them stop and permanently generate the zero vector from the moment when that vector is acceptable for the operating sequence. Practically, it can happen due to the break of sensors power supply and from the moment of turning on the machine. Detection of this failure is proved by the power supply line from the last sensor in the power supply series is connected to one ON/OFF input on a module which has the built-in selftesting function [6] and which is checked when the value of the operating vector is zero.

The second one, the greatest group of sensors in the machine, consists of sensors which, only in a certain (definite) moment - phase of the machine working, give the valid information. In some other moment - phase, their functionality can be examined (investigated) registering the correctness of the states sensors change in the moment of appearing the test position (Fig. 4). So, if they are without a failure, during one cycle of the machine working, they have to generate, at least once, the complementary state at the input while the test position is detecting. Naturally, the software test procedure in a microcomputer processes these changes.

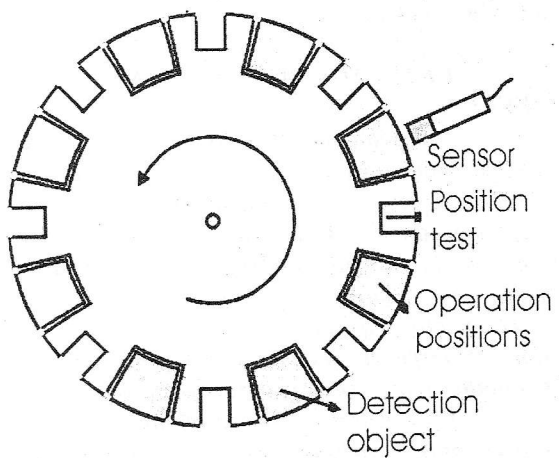


Fig. 4 Phases of testing and sensors working

The third group consists of sensors which continuously and during the greater number of the machine working cycles detect the same correct state. For example, detecting when the aluminium foil is used up on the roll (ring), or there are no cigarettes in the basket from where the cigarettes set of one package is formed, can be happened very rarely. That state can be detected on several hours, days, and even weeks. Since there is a need that this detection be reliable, on/off sensors with the built-in function of failure autodetection have to be used on these positions.

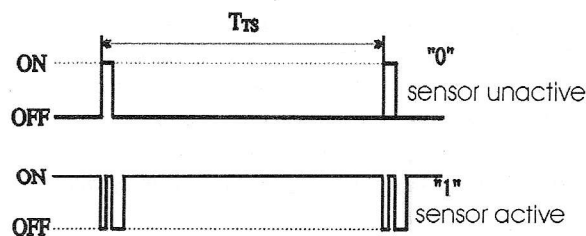


Fig. 5 Output signal of sensor with autodetection

These sensors generate the output signal of the shape presented in Fig. 5. In the case of any failure in sensor, the appropriate impulses of the constant period of testing T_{TS} are not generated in the output signal. The failure detector of these sensors is simply accomplished by the software procedure of testing - reading sensor states, which is built in as a periodic task activated from outside with the time limit for its activation.

Errors Detection in on/off outputs:

The most ON/OFF outputs, i.e. actuators, are not necessarily tested directly. The activities, which consequences are detected by the appropriate sensors, are accomplished by their activation/deactivation. For example, the deactivation of pulling blank coil (paper for the wrapping because in previous cycles - positions the uncorrectness for the package is detected) will be, after some angle move of the machine, detected by a sensor for detecting the blank coil presence. It is normal that the detection, that there is no blank coil, shouldn't initiate (provoke) the machine stopping. In other case, if the presence of blank coil is detected, and also when no presence of the blank coil is detected, the machine is stopped.

The correct state of the output of STOP MACHINE can be checking by detecting the change of the output current, as it is given in the module with the built-in selftesting [6]. The other possibility is that the state of the output itself be connected to one ON/OFF input, that has a sense if the output supply the actuator only by voltage. Besides all, the reliability of the output STOP MACHINE is increased using the doubling - paralleling. Two outputs, connected by the wire logic, are prompted by the same binary variable for STOP MACHINE.

Checking the ON/OFF outputs and actuators for signalization can be realized by an output with the built-in self-testing, as for the output STOP MACHINE. But with the further improvement of machine, the visualization of the machine working process is expected (so these outputs will not be necessary), checking the current signalization is realized at each machine starting by its short activation, or by activation at the demand of an operator in the procedure of the system maintenance.

DETECTORS OF CIRCUITS LEVEL

On the circuit level, the smallest number of errors detectors is realized because they mainly demand to be implemented even in the phase of circuits design. One detector of this level is built in the self-testing module ON/OFF input/output [6]. For its checking, the simple software procedure is built in the microcomputer. Taking the implemented errors detectors on higher level into consideration, this possibility of ON/OFF module is more important for the localization of failure which caused the detected error.

4. GRAPHIC INTERACTION

Although the wide-accepted "windows" interaction became a standard, it could not be applied to this concrete application. The reason for this are limits in the environment (the presence of dust, necessary simplicity, etc.), and because of them it is not possible to use "mouse" or classical keyboards. A foil keyboard with eight multifunctional buttons is used as the input device.

Graphic interaction is realized with the aim to have the following characteristics:

- user-friendly interface,
- unambiguity and clarity in the data presentation, and
- data presentation focus.

The unambiguity of data presentation comes from the need that the system always has to be in one unique state from the set of deterministic defined states. The clarity means many attributes, such as palette of colours, contrast, legibility, and so son.

Focusing means the need that the definite number of similar data is presented in the close part of presentation, i.e. classified according to its sense and time of appearance.

Since the graphic interaction is globally realized through two actors, CRT display is divided into two windows - two main areas: area in which the visualization process is realized, and a part where the dialogue man-system is realized. The visualization window serves for the graphic presentation of a process - machine and numerical presentations of the process parameters. This space is also used for the presentation of different reports and tables in the special tasks of the system working survey, its maintenance and servicing. The window for the dialogue contains a description of multifunctional buttons and command line. In that way, objects for visualization - Visual and dialogue - Dialogue. Each of them has an object responsible for presenting, an object which generates the shape and an object (document) which contains the characteristic data.

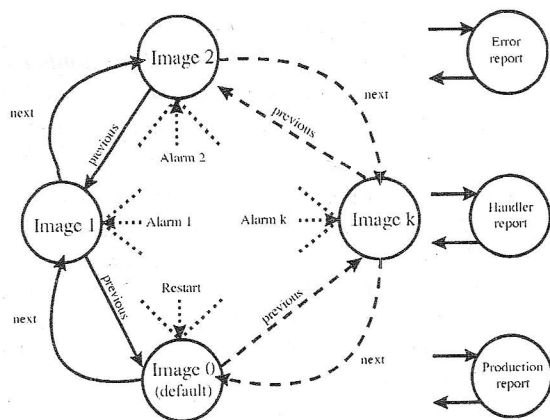


Fig. 6 The state diagram of a visual presentation

The object Dialogue is connected to the message M_KEY (accepted character for the keyboard). It can generate the message M_DRWTAST for the object DrawTastature, which designs the demanded keyboard and/or the command line. The following messages are generally joined to the object Visual: from the second of the real-time M_SECTIME, from asynchronous excess event M_AEXCEVENT, from the task of supervising and processing working parameters, and from Dialogue object. Objects DrawKeyboards (DrawTastature) and Visual use the chain Application - GDI - Device Driver - CRT Display.

5. ACTORS OF VISUALIZATION AND DIALOGUE

The factor of the visual presentation is described by finite state machine - FSM in Fig. 6. Each presentation image, besides the look of the machine or some detail - a part of the machine, contains the belonging sensors and actuators in which states they are indicated by the appropriate colours. The initial presentation is "Image 0", and the presentation change is a result of either "Alarm" or demands for the image changing ("previous", "next") from dialogue. Alarm is a result of one or more excessive events which are, in the appropriate image, noticed through sensors states and visual effects of warning. In the case of the simultaneous activation of many different alarms, we go to the figure which corresponds to the statically allocated alarm of the greatest priority. Automatic return to the previous - initial presentation will be done when the machine is restarted after the elimination of the stagnation (stoppage) reason. From Fig. 6, it can be also noticed that there is a possibility of transfers into the state of generating the report (about the production, stoppage, etc.) from any of presentation, on condition that the machine is not in the working regime, i.e. it is stopped.

With regard to jobs that some persons do in the system, the interaction can be divided into the interaction handler-system, operator-system, servicer-system and superuser-system. There are many (over 50) activities in each of these interactions. Besides the general common activities of reporting, cancellation and change of password, main dialogue activities of the operator are the imposition of production, the supervision of production and survey of the handler work. For the servicer, the most important dialogues are those for the support of the supervision of the machine working and the adjustment of the machine working. According to the technological demands of the process, the machine working is not possible in some states of interaction, i.e. there are limits in performing dialogues for different states of the process. The factor of the interaction man-system on the first levels of a dialogue is shown on Fig. 7. The unique visual object of the keyboard for describing the meaning of taster and the command line with the message and entry box, by which the dialogue man-system is performed, correspond to each state. Transfer from one state to the new one is possible on the basis of conjunctive condition of the prehistory (the interaction states) and demands made by a man in the dialogue. The demand is always the result of activating some taster - keyboard area, either by choosing the dialogue activities or commands, determining the end of input, or the single input of characters. So, besides the messages, pointers and markers are used for performing the function of low level. The most of states of the interaction in the figure, like Figs. 8 and 9, are the whole subobjects, i.e. automats. So, it is not appropriately to try (attempt) here with the detailed presentation of interaction. But one possible stream of interaction after the initialization of the system is presented in Fig. 8. Software for the realization of dialogue (and visual) is made as a set of functions - procedures. They are performed by transferring from one to other state of dialogue, which is the result of the message - the entry of characters from the keyboard, and sometimes messages from some other activities. Every procedure by its purely sequential structure, engages (involves) predictably and transitory the processing time , which is the prerequisite for the realization of RTS.

The operative states of the factor dialogue, which is started by the initialization of the whole system, point at its proceedings and engaging the processor shown in Fig. 9. The processor is engaged for dialogue only in the state RUNNING. The factor dialogue is in a system of a low priority, because it does not contain activities which relate to the system safety. The function STOP of the machine working in the dialogue is the regular stopping, and for the emergent -safety stop there are other factors distributed on all system components.

6. CONCLUSION

Realizing the operation system as RTS with the built-in selftesting in all levels, the reliability in the machine working by the minimal increase in hardware and acceptably increased the software complexity is significantly increased.

In the system, exploitation gave more than it is really expected. By detailed messages on detected stopping in the machine working directs to the defaults - unsuitability of mechanical machine

parts. Factors of visualization and dialogue are realized using Microsoft Visual C++ za PC hardware with AMD486 at 133 MHz. Each system function is performed through the defined set of instructions without loops which could provoke the unforeseeable times of performing. New versions of functions are developed, which, by messages, accept demands of interaction, and demands of factors of generating the visual presentation, and others.

STATES:

- s0 initialization;
- s1 logging - start session;
- s2 machine Handler active;
- s3 machine Operator active;
- s4 machine Servicer active;
- s5 session exit;
- s6 Operator or Servicer logging when Handler is already logged;
- s7 other Operator activities;
- s8 other Servicer activities;
- s9 Superuser active.

T_i ($i = 0, OM, 1, 2, \dots, 10$) - tastature;
 t_j ($j = 1, 2, 3, \dots, 8$) - tasters on appropriate tastature;
err - erroneous tastature input.

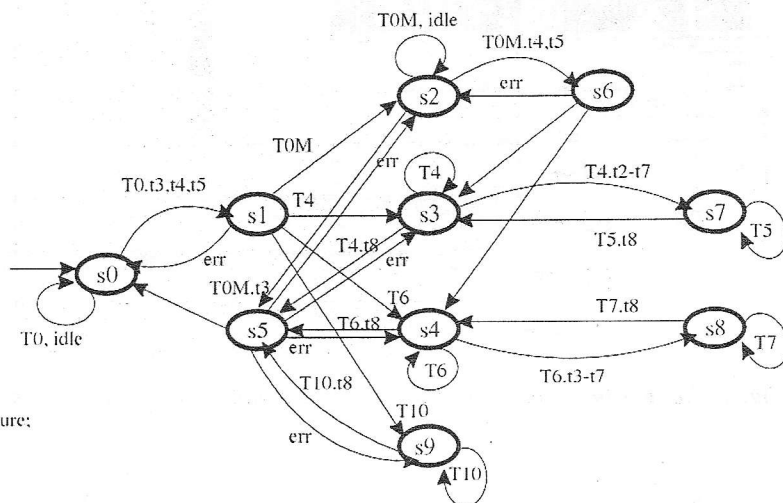


Fig. 7 Global diagram of changing the process states of the interaction man-system

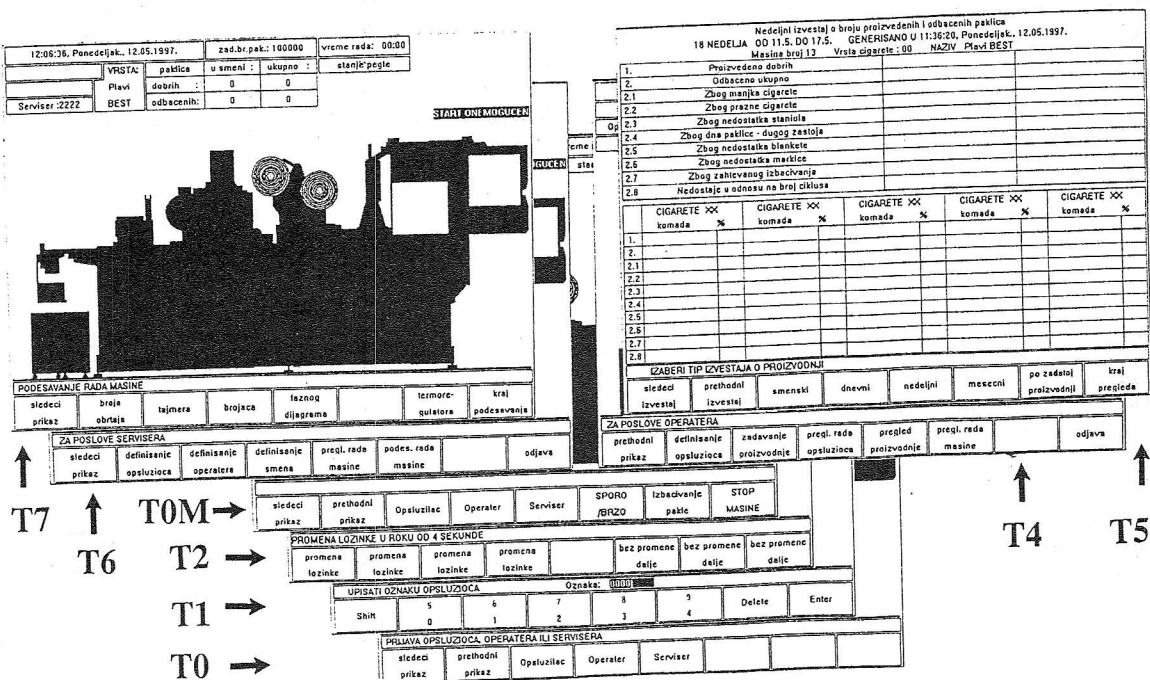


Fig. 8 Changes in the main window of visualization which supervise changes of the interaction man-system

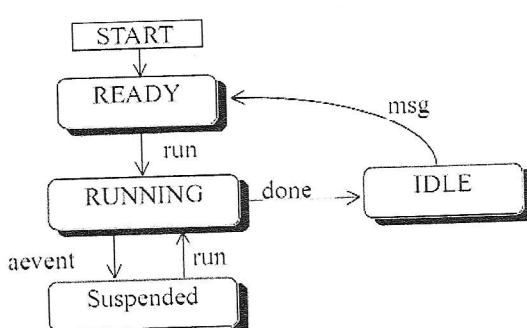


Fig. 9 Operative state of the factor dialogue

7. LITERATURE

- [1] J. Zhu, T. G. Lewis, W. Jackson, R. L. Wilson, "Scheduling in Hard Real-Time Applications", IEEE Software, Vol. 12, No. 3, May 1995, pp. 54-63.
- [2] M. Jevtić, M. Damnjanović, "Testing of Digital System in Real-Time Applications", Proc. 20th International Conference of Microelectronics, MIEL'95, Vol.2, pp. 835-840, Niš, Sept. 1995.
- [3] Vishwani D. Agrawal, Charles R. Kime, Kewal K. Saluja "A Tutorial on Built-In Self-Test, Part 2: Applications", IEEE Design & Test of Computers, Vol. 10, No. 2, pp. 69-77, June 1993.
- [4] Selic, B., Gullekson, G., Ward, P., *Real-Time Object-Oriented Modeling*, John Wiley & Sons, 1994.

- [5] J. Vučković, M. Jevtić, S. Vučković, "Modeling and Simulating Real-Time Systems" Proceedings of MIEL'95, Niš, Sept 1995. Vol. 2, pp. 867-870.
- [6] M. Jevtić, M. Damnjanović, G. Cvetković, "Modul ON/OFF ulaza-izlaza sa ugrađenim samotestiranjem", YU-INFO '95, Brezovica, April 1995.

BHATTACHARYYA DISTANCE IN EVALUATION OF THE FRAME-BASED NONSTATIONARY PATTERN RECOGNITION METHODS

Milan Marković, Milan Milosavljević, *Institute of Applied Mathematics and Electronics, Belgrade*
 Branko Kovačević, *Faculty of Electrical Engineering, University of Belgrade*

Abstract - We consider a possibility of evaluating frame-based nonstationary pattern recognition methods by using Bhattacharrya distance. Experimental part of the work refers to processing of natural speech, isolately spoken serbian vowels and digits, as the examples of nonstationary signal. Obtained results justify the use of the Bhattacharrya distance as the evaluation tool in the nonstationary pattern recognition systems.

1. INTRODUCTION

Bayes error is a very important performance index in pattern recognition, assessing the classifiability of data and measuring the discrimination capabilities of the features, even before considering what type of classifier should be designed. However, the calculation of the error probability is a very difficult task. Even when observation vectors have a normal distribution, we must resort to numerical techniques [1]. However, a closed-form expression for the Bayes error probability is the most desirable solution for a number of reasons. When we cannot obtain a closed-form expression, we may seek either a Bayes error estimate, or an upper bound of the Bayes error probability. As for the Bayes error estimation, very efficient estimation procedures based on k -NN approach are proposed in [1,2,3].

A situation is more complex in case of the nonstationary pattern recognition tasks. Namely, statistical pattern recognition methods are based on the assumption of stationarity of the processes to be recognized. There are many problems in applying these methods in the real-time recognition of data obtained from the nonstationary processes. The main problems are limited validity and size of the learning data set. One approach for solving these problems represents the frame-based pattern recognition methods. These methods are based on the idea that the nonstationary data process should be considered in

frames [4], and on using the unsupervised learning procedures for classifier design on the current frame of signal and its application as the initial classifier for the next frame. Based on the obtained initial partition of the next frame, the same unsupervised learning procedure gets started, and so on. As the unsupervised learning algorithm, the c-mean clustering algorithm or nearest mean reclassification rule is proposed in [4]. The iterative application of quadratic classifier, described by Fukunaga [1], as a more sophisticated and efficient unsupervised learning procedure is proposed, and justified in [5]. Additionally, in [6], a modification of the iterative quadratic classification procedure with the increased real-time application possibilities is given. It is shown in [6], that proposed modification has some robust characteristics to the inappropriateness of the assumed classification model.

This paper is dedicated to possible finding of a suitable criterion for evaluation the considered frame-based nonstationary pattern recognition methods: the c-mean clustering algorithm with Euclidean distance, the iterative quadratic classifications, and its real-time modification. Due to the fact that these methods are based on the unsupervised principle, the complex k -NN Bayes error estimation procedure, considered in [1,2,3], is not suitable for the nonstationary cases. Instead of this, we propose the use of the estimated upper bound trajectories of the Bayes error obtained by using Bhattacharrya distance. In the paper, the speech is used as a nonstationary signal and the comparative analysis is done through analyzing isolately spoken serbian vowels and digits. In fact, the considered methods are applied in a composed nonrobust/robust recursive AR speech analysis procedure, proposed in [6]. The procedure is based on an AR speech parameter estimation model, presented on Figure 1.

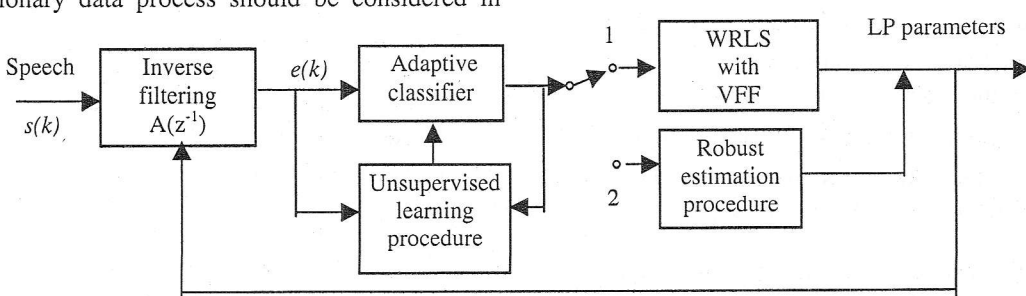


Figure 1: Block diagram of the proposed AR speech model identification system

The paper is organized as follows. Considered frame-based nonstationary pattern recognition methods are described in Section 2, and their possible applications in robust recursive AR speech parameter estimation in Section 3. Section 4 is dedicated to brief description of Bhattacharyya distance. Experimental analysis is presented in Section 5 while conclusion is given in Section 6.

2. FRAME-BASED NONSTATIONARY PATTERN RECOGNITION METHODS

The classical c-mean clustering algorithm could be described by the following. Assume that we want to classify N samples, X_1, \dots, X_N . Each sample is to be placed into one of L classes, $\omega_1, \dots, \omega_L$, where L is assumed to be given. The nearest mean reclassification rule has a form:

1. Choose an initial partition of given data set and calculate mean vectors: $M_1(0), \dots, M_L(0)$.
2. Having calculated mean vectors $M_1(l), \dots, M_L(l)$ at the l -th iteration, reclassify each X_i according to the nearest $M_j(l)$.
3. If the classification of any X_i is changed, calculate the new mean vectors $M_1(l+1), \dots, M_L(l+1)$ for the new class assignment, and repeat from Step (2). Otherwise, stop.

As well as the c-mean algorithm, the iterative quadratic classifications clustering algorithm is derived from the general clustering algorithms, described in [1]. The iterative quadratic classification clustering algorithm has a form:

1. Choose an initial partition of given data set and calculate: $P_i(0)$ (a priori class probability), $M_i(0)$, and $\Sigma_i(0)$ (a class covariance matrix) for $i=1, \dots, L$.
2. Having calculated a priori class probabilities, $P_i(l)$, mean vectors, $M_i(l)$, and covariance matrices, $\Sigma_i(l)$, at the l -th iteration, reclassify each X_j according to the smallest $(1/2)(X_j - M_i)^T \Sigma_i^{-1} (X_j - M_i) + (1/2)\ln|\Sigma_i| - \ln P_i$. The a priori class probability for ω_i is estimated by the number of ω_i -samples divided by the total number of samples.
3. If the classification of any X_j is changed, calculate the $P_i(l+1)$, $M_i(l+1)$, and $\Sigma_i(l+1)$ for the new class assignment, and repeat from Step (2). Otherwise, stop.

The application of the proposed algorithms for recognizing nonstationary data could be described by the following. The final quadratic classifier on

each frame of the signal is used as the initial quadratic classifier for the next frame to produce its initial partition. Based on that initial partition, the same iterative clustering procedure starts to produce the final quadratic classifier on that frame, and so on.

In order to assure the real-time application of the iterative quadratic classification algorithm, its modification is proposed in [6]. The modification consists of applying the given iterative clustering procedure only on the initial frame of the signal. For all subsequent frames, the algorithms stop at the first step of the procedure. In the other words, the final quadratic classifier on each frame of signal (except on the initial one) is obtained by using only the initial partition of that frame.

The convergence of the proposed algorithms depends on the following attributes of the initial classifier and the data: the error rate of the initial classifier, the size of the signal frames, and the validity of the model used to represent the class conditional probability densities.

3. APPLICATION IN ROBUST AR SPEECH PARAMETER ESTIMATION

The AR speech parameter estimation procedure (see Fig. 1) consists of estimation and classification part. As the estimation part, we use the weighted recursive least squares (WRLS) algorithm with variable forgetting factor (VFF), as in [5,6]. The classification part of the procedure consists of a classifier designed by using the above-mentioned unsupervised learning procedure [4,5,6]. In fact, in order to solve the problem of inappropriateness of AR modeling of speech production system, particularly on the voiced frames, a procedure for robustifying the WRLS algorithm with VFF based on the statistical nonstationary pattern recognition approach is proposed [5,6]. This procedure consists of the application of the statistical classifier with sliding training data set in the composed nonrobust/robust recursive AR speech analysis procedure. In this heuristic procedure, the classifier is used to classify the residual speech samples into the two classes. The first class consists of "small" residual samples and the second one consists of "large" residual samples [5,6]. The classification of the k -th residual sample selects either the nonrobust (first class) or the robust (second class) recursive AR procedure for LP parameter estimation at the k -time instance (see Fig. 1). This method is based on the assumption of the excitation for voiced speech as innovative process from mixture distribution, such that a large portion of the excitations are from a normal distribution with a very small variance while a small portion of the glottal excitations are also from the normal distribution with a much bigger variance [5,6]. In this case, the classifier is a very simple, one-dimensional, and mean vectors and covariance matrices are means and

variances, respectively. The classification consists of two steps: *initialization* and *adaptation*. On the initial frame of signal one has to determine the following: the starting LP parameters vector which is used as the initial condition for the proposed recursive procedure, the initial maximal residual value, and the initial partition of the frame. The initial classifier is obtained applying one of the iterative unsupervised learning procedures [4,5], based on the initial partition. The initial classifier is then applied in the classification of the residual speech samples obtained by the composed recursive AR speech analysis procedure. The result of k -th residual sample classification selects either the nonrobust recursive procedure or robust recursive procedure to estimate the vector of AR parameters in the k -time instance. The obtained vector is used to determine the $(k+1)$ residual sample and the procedure is continuing. In the considered frame-based adaptation procedures [4,5,6], the final quadratic classifier on each frame of signal is used as the initial quadratic classifier for the next frame to produce its initial partition. Based on that initial partition, the same iterative clustering procedure starts to produce the final quadratic classifier on that frame, and so on.

We assume that classification part of the procedure plays a dominant role in the parameter estimation accuracy. Following this assumption, in the experimental part of the paper we will try to evaluate the considered unsupervised learning procedures on the basis of the discrimination characteristics of the two classes of speech residual samples which are, in fact, products of the proposed AR speech parameter estimation procedure. Also, we will analyze how these results correspond with the comparative results referred to the efficiency in the estimation of AR speech model parameters.

4. BHATTACHARYYA DISTANCE

Bayesian classifier could be described by follows. Let us consider c classes of the training data set, ω_i , $i=1,\dots,c$; described by a posteriori probability functions $P(\omega_i|X)$. Bayes rule could be expressed as follows, [1]:

$$P(\omega_i|X) = \frac{P(\omega_i)p(X|\omega_i)}{p(X)} \quad (1)$$

where: $p(X)$ is a probability density function (pdf) of sample X , $p(X|\omega_i)$ is conditionally probability density function (cpdf), and $P(\omega_i)$ is a priori probability of the class ω_i . Bayesian classifiers is based on *Bayes decision rule* which is referred to the classification of sample X in that class ω satisfying:

$$P(\omega|X) = \max_{1 \leq i \leq c} \{P(\omega_i|X)\}. \quad (2)$$

The Bayes error is given by:

$$\begin{aligned} e &= 1 - \int_{R^n} \max_{1 \leq i \leq c} P(\omega_i|X)p(X)dx = \\ &= 1 - \int_{R^n} \max_{1 \leq i \leq c} P(\omega_i)p(X|\omega_i)dx. \end{aligned} \quad (3)$$

In a two-class case ($c=2$), the equation (3) could be rewritten as:

$$e = \int \min[P_1 p_1(X), P_2 p_2(X)]dX \quad (4)$$

where: P_1 , P_2 , and $p_1(X)$, $p_2(X)$ denote a posteriori probabilities and cpdfs of the first and second class, respectively. An upper bound of the integrand in (4) may be obtained by making use of the fact that:

$$\min[a,b] \leq a^s b^{1-s}, \quad 0 \leq s \leq 1, \quad \text{for } a,b \geq 0. \quad (5)$$

Using the inequality (5), e can be bounded by:

$$e_u = P_1^s P_2^{1-s} \int p_1^s(x) p_2^{1-s}(X)dX \quad \text{for } 0 \leq s \leq 1 \quad (6)$$

where e_u indicates an upper bound of e . This e_u is called the Chernoff bound [7]. The optimum s can be found by minimizing e_u . When two density functions are normal, $N_X(M_1, \Sigma_1)$ and $N_X(M_2, \Sigma_2)$, the integration (6) can be carried out to obtain a closed-form expression for e_u . That is:

$$\int p_1^s(X) p_2^{1-s}(X)dX = e^{-\mu(s)} \quad (7)$$

$$\begin{aligned} \mu(s) &= \frac{s(1-s)}{2} (M_2 - M_1)^T [\Sigma_1 + (1-s)\Sigma_2]^{-1} (M_2 - M_1) + \\ &+ \frac{1}{2} \ln \frac{|\Sigma_1 + (1-s)\Sigma_2|}{|\Sigma_1|^s |\Sigma_2|^{1-s}}. \end{aligned} \quad (8)$$

The expression (8) for $\mu(s)$ is called the Chernoff distance. For this case, the optimum s can be easily obtained by plotting $\mu(s)$ for various s with given M_i and Σ_i . The optimum s is the one which gives maximum value for $\mu(s)$.

In case that we do not insist on the optimum selection of s , we may obtain a less complicated upper bound. One of the possibilities is to select $s=1/2$. Then the upper bound is:

$$e_u = \sqrt{P_1 P_2} \int \sqrt{p_1(X) p_2(X)} dX = \sqrt{P_1 P_2} e^{-\mu(1/2)} \quad (9)$$

in general, and for normal distributions:

$$\begin{aligned} \mu(1/2) &= \frac{1}{8} (M_2 - M_1)^T \left[\frac{\Sigma_1 + \Sigma_2}{2} \right]^{-1} (M_2 - M_1) + \\ &+ \frac{1}{2} \ln \frac{|\frac{\Sigma_1 + \Sigma_2}{2}|}{\sqrt{|\Sigma_1||\Sigma_2|}} \end{aligned} \quad (10)$$

The term $\mu(1/2)$ is called the Bhattacharyya distance, and will be used as an important measure of the separability of two distribution [8]. In fact, the Bhattacharyya distance is the optimum Chernoff distance when $\Sigma_1=\Sigma_2$. As seen in (10), the Bhattacharyya distance consists of two terms. The first or second terms disappears when $M_1=M_2$ or $\Sigma_1=\Sigma_2$, respectively. Therefore, the first term gives the class separability due to the mean-difference, while the second term gives the class separability due to the covariance difference. It is important to know which term is dominant, because it determines what

type of a classifier must be designed for the given case.

5. EXPERIMENTAL ANALYSIS

The test signal consists of five isolately spoken vowels ("A", "E", "I", "O", "U") and ten isolately spoken digits ("1", "2", ..., "0") from one speaker. The signal is sampled with $f_s=10\text{kHz}$ and preemphasized with $q=1$. All experimental results are obtained by using AR model of 10th order. As the objective quality measure, the MAR (Mean Absolute Residual) criterion is used [6]:

$$J = 1/M \cdot \sum_{i=1}^M |s(i) - \hat{s}(i)| \quad (11)$$

where $s(i)$ is the speech sample at the i -th time instance, $\hat{s}(i)$ is its linear prediction, and M is total number of processed speech samples.

In this paper, we consider the nonrobust/robust recursive estimation procedure for parameter identification of nonstationary AR speech model based on the WRLS algorithm with VFF and unsupervised learning procedures for design of frame-based nonstationary pattern classifier. The main role of the classification part of the overall estimation scheme is selection of robust or nonrobust AR estimation procedure, for each incoming speech sample. Such approach is motivated by the fact that for some parts of speech signal (dominantly during open glottis) the robust estimation procedures are more suitable than conventional ones [9]. As we mentioned before, the following unsupervised learning methods: the c-mean clustering algorithm with Euclidean distance (denoted as CEUC) [4], the iterative quadratic classifications (CIQC) [5], and its real-time modification (RTQC) [6], are considered. As a comparative criteria of the considered methods (CEUC, CIQC, and RTQC algorithms), the upper bound trajectories of the Bayes error obtained by using Bhattacharyya distance [8] (which values are calculated at each time instances on the basis of the estimated corresponding classifier parameters) are used. The results of this evaluation are compared to the results obtained by parameter estimation efficiency evaluation of the considered methods [5,6].

The estimated upper bound trajectories of the Bayes error based on Bhattacharyya distance, obtained by using the CEUC, CIQC, and RTQC algorithms in analyzing the vowel "A" and digits "1", and "0" are presented on Fig. 2, 4 and 6. As the estimation efficiency comparative criteria, we use adaptiveness, sensitivity to the pitch impulses, bias, and variance of the obtained trajectories of the nonstationary AR speech model parameter estimates. Fig. 3, 5 and 7 show the estimated trajectories of the first AR parameter (AR_1) obtained by using the same frame-based procedures (frame length was 100 samples) in

analyzing the vowel "A" and digits "1", and "0", respectively, for the corresponding signal frames showed on Fig. 2, 4 and 6. In this case, we use reference parameter trajectories and comparative methodology, proposed in [9].

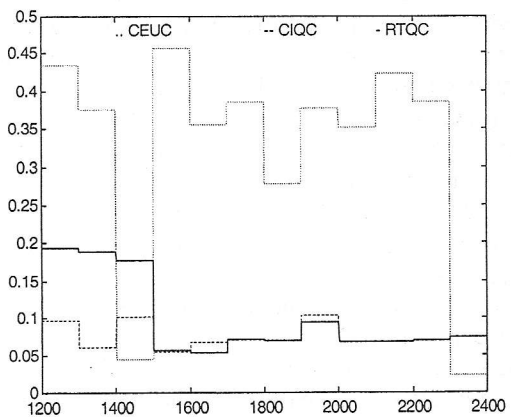


Figure 2: Upper bound trajectories of Bayes error obtained by using: CEUC, CIQC, and RTQC algorithms in analyzing the vowel "A" (frame length is $N=100$).

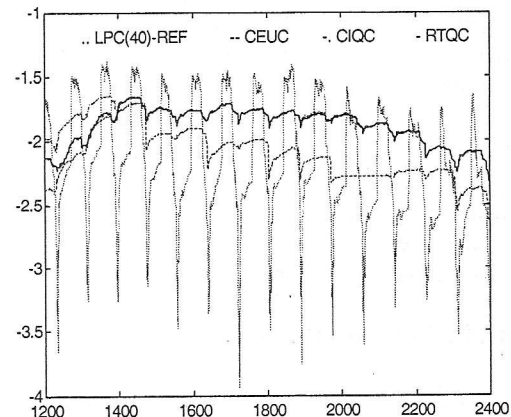


Figure 3: The AR_1 parameter trajectories obtained by using: LPC(40)-REF, CEUC, CIQC, and RTQC algorithms in analyzing the vowel "A" (frame length is $N=100$).

Mean values of the upper bound Bayes error trajectories obtained through analyzing of the all test data files are presented in Table 1. Also, to evaluate which term of the Bhattacharyya distance (10) is dominant, examples of trajectories of the first and second term of distance (10), obtained in analyzing the vowel "A" and digit "2", are given on Fig. 8 and 9, respectively.

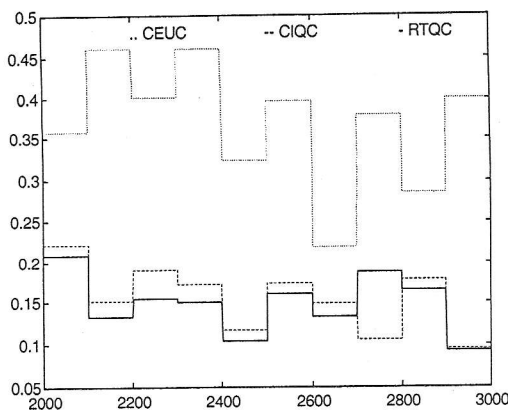


Figure 4: Upper bound trajectories of Bayes error obtained by using: CEUC, CIQC, and RTQC algorithms in analyzing the digit "1" (frame length is $N=100$).

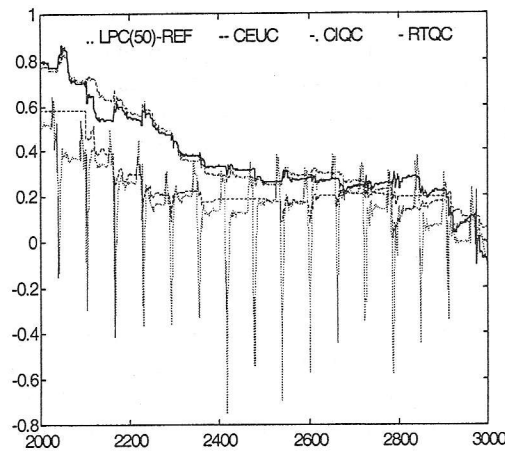


Figure 5: The AR₁ parameter trajectories obtained by using: LPC(50)-REF, CEUC, CIQC, and RTQC algorithms in analyzing the digit "1" (frame length is $N=100$).

Based on experimental results, presented in Table 1 and Fig. 2, 4 and 6, we could conclude that lower upper bounds of the Bayes error probability, i.e. better classification results for both vowels and digits analysis, are obtained by using the proposed robust recursive procedure with application of the unsupervised learning procedures for classifier design based on quadratic classifier (CIQC and RTQC algorithm). This corresponds well to the comparative results, presented on Fig. 3, 5 and 7, showing that the trajectories of AR₁ parameter estimates obtained by the robust recursive AR speech procedure with application of CIQC, and RTQC algorithms have lower bias, lower variance, more adaptiveness to the nonstationarity of the model parameters, and lower sensitivity to the pitch impulses than the same robust recursive procedure with application of CEUC

algorithm for classifier design. This also supports conclusion that classification part of the overall composed scheme places dominant role in ultimate estimation accuracy of nonstationary AR speech parameters.

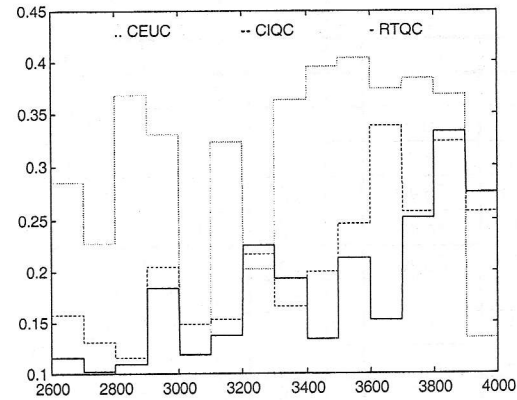


Figure 6: Upper bound trajectories of Bayes error obtained by using: CEUC, CIQC, and RTQC algorithms in analyzing the digit "0" (frame length is $N=100$).

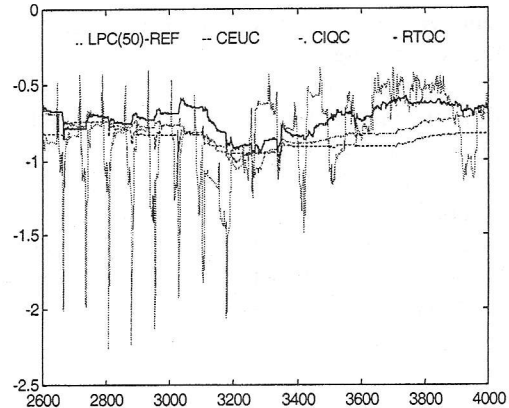


Figure 7: The AR₁ parameter trajectories obtained by using: LPC(50)-REF, CEUC, CIQC, and RTQC algorithms in analyzing the digit "0" (frame length is $N=100$).

The examples, presented on Fig. 8 and 9, show that the second term of the Bhattacharyya distance (10), is dominant meaning that some classifier with nonlinear discrimination function (such as quadratic one) should be used instead of classifier with linear discrimination function (such as c-mean algorithm with Euclidean distance). This conclusion is valid for both voiced speech segments (vowels, see Fig. 8) and mixed excitation ones (digits, see Fig. 9).

As for the comparative analysis of the CIQC and RTQC algorithm, the presented results show that both algorithms produce mostly similar results with slightly lower mean values of the upper bounds of the Bayes error obtained by using the CIQC algorithm (see Table 1). However, in some cases of digits

analysis (see the Fig. 6, and 7) better results, i.e. lower upper bound of the Bayes error as well as more accurate AR₁ parameter estimates are obtained by using the RTQC algorithm. An explanation of some differences in CIQC algorithm behavior when

Table 1: Mean values of the upper bounds of Bayes error; vowels and digits analysis.

| F | Length | CEUC | CIQC | RTQC |
|---|--------|-------|-------|-------|
| A | 3690 | 0.336 | 0.160 | 0.164 |
| E | 3690 | 0.335 | 0.150 | 0.143 |
| I | 3690 | 0.340 | 0.141 | 0.150 |
| O | 3690 | 0.332 | 0.140 | 0.191 |
| U | 3690 | 0.322 | 0.157 | 0.180 |
| 1 | 6690 | 0.325 | 0.194 | 0.230 |
| 2 | 6690 | 0.331 | 0.202 | 0.202 |
| 3 | 5690 | 0.332 | 0.211 | 0.232 |
| 4 | 6690 | 0.326 | 0.192 | 0.243 |
| 5 | 6690 | 0.338 | 0.202 | 0.245 |
| 6 | 7690 | 0.333 | 0.209 | 0.237 |
| 7 | 6690 | 0.321 | 0.198 | 0.228 |
| 8 | 7690 | 0.321 | 0.208 | 0.236 |
| 9 | 5690 | 0.325 | 0.225 | 0.218 |
| 0 | 5690 | 0.293 | 0.196 | 0.207 |

analyzing vowels and digits could be described by the fact that vowels are the examples of voiced speech, and digits are speech signals with the voiced and mixed excitation. In the latter case, the assumed two-class model of speech excitation is not completely appropriate, and this might be a reason why the results obtained by CIQC algorithm sometimes are not so good. In that case, the inherent robustness of RTQC algorithm, in the sense of its small sensitivity to deviations from the assumed excitation model, is clearly expressed (see Fig. 6, and 7).

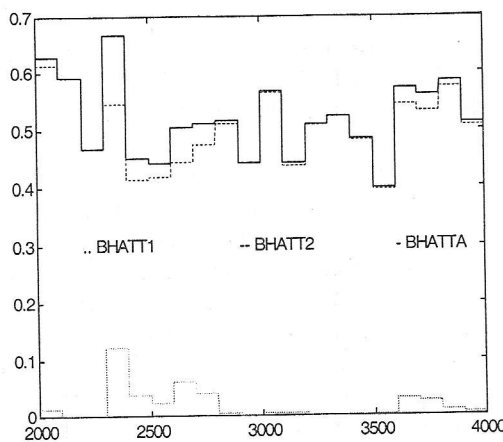


Figure 8: Bhattacharyya distance values obtained in analyzing the vowel "A"; BHATTA, BHATT1, and BHATT2 represent the Bhattacharyya distance, first term, and second term of the (10), respectively.

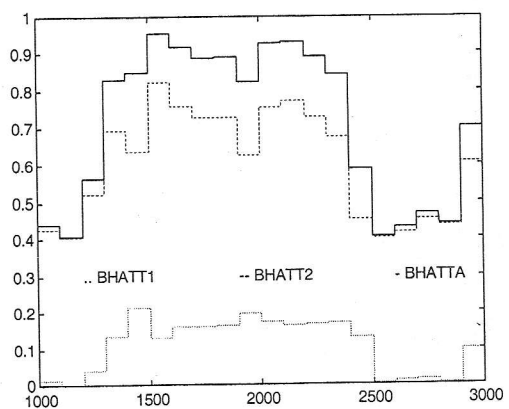


Figure 9: Bhattacharyya distance values obtained in analyzing the digit "2"; BHATTA, BHATT1, and BHATT2 represent the Bhattacharyya distance, first term, and second term of the (10), respectively.

Based on the entire experimental analysis, it could be concluded that the trajectories of the upper bound of Bayes error based on Bhattacharya distance could be used as an evaluation criterion for one-class of the frame-based nonstationary pattern recognition methods.

6. CONCLUSION

In this paper, we consider a possibility of evaluation of one-class of the frame-based nonstationary pattern recognition methods by using Bhattacharya distance. The nonstationary pattern recognition methods based on unsupervised learning procedures: c-mean clustering, iterative quadratic classifications, and its modification for real-time purposes, are considered. The considered methods are evaluated through their applications for design of nonstationary pattern classifier in composed nonrobust/robust AR speech parameter estimation procedure based on the weighted recursive least squares algorithm with variable forgetting factor. The comparative analysis is done through analyzing the natural speech, isolate spoken Serbian vowels and digits. Based on experimental results, we could conclude that lower upper bounds of the Bayes error probability, i.e. better results in both vowels and digits analysis, are obtained by using the proposed estimation procedure with the unsupervised learning procedure based on quadratic classifier, compared to the c-mean clustering algorithm. As for comparison between the two frame-based unsupervised learning procedure based on the quadratic classifier: iterative quadratic classifications and its real-time modification, we could conclude that the latter procedure produce globally better results due to its robustness to the two-class speech excitation model deviations which frequently happens in the case of

digits analysis. Based on the entire experimental analysis, it could be concluded that the trajectories of the upper bound of Bayes error based on Bhattacharrya distance could be used as an evaluation criterion for the frame-based nonstationary pattern recognition methods, due to the results correspond well to the comparative results based on the estimated parameter trajectories obtained by the considered robust recursive AR speech estimation procedure. Finally, our analysis led to conclusion that classification part of the composed nonrobust/robust AR speech estimation procedure has dominant influence on its accuracy.

REFERENCES

- [1] K. Fukunaga, *Introduction to Statistical Pattern Recognition*, ACADEMIC PRESS INC., 1990.
- [2] K. Fukunaga and D. Hummels, "Bayes Error Estimation Using Parzen and k -NN Procedures," *IEEE Trans. on PAMI*, vol. PAMI-9, pp. 634-643, 1987.
- [3] Lj. Buturović and M. Marković, "Improving k -Nearest Neighbor Bayes Error Estimates," in *Proc. of 11th IAPR International Conference on Pattern Recognition*, The Hague, The Netherlands, August 30-September 3, 1992.
- [4] D. Gutfinger and J. Sklansky, "Robust Classifiers by Mixed Adaptation," *IEEE Trans. on PAMI*, Vol. 13, No. 6, June 1991., pp. 552-567.
- [5] M. Marković, M. Milosavljević, B. Kovačević, "Clustering in Non-Stationary Pattern Recognition Systems," *SIGNAL PROCESSING VII: Theories and Applic.*, M. Holt, C. Cowan, P. Grant, W. Sandham (Eds.), 1994. European Association for Signal Processing (Proc. of EUSIPCO-94), Edinburgh, Scotland, 13-16 September, 1994.) pp. 1803-1806.
- [6] M. Marković, B. Kovačević, M. Milosavljević, "A Statistical Pattern Recognition Approach to Robust Recursive Identification of Non-Stationary AR Model of Speech Production System," *IEEE Trans. on Speech and Audio Processing*, Vol. 4, No. 6, November 1996, pp. 456-460.
- [7] H. Chernoff, "A measure of asymptotic efficiency for tests of a hypothesis based on the sum of observations," *Ann. Math. Stat.*, **23**, pp. 493-597, 1952.
- [8] A. Bhattacharyya, "On a measure of divergence between two statistical populations defined by their probability distributions," *Bull. Calcutta Math. Soc.*, **35**, pp. 99-110, 1943.
- [9] M. Veinović, B. Kovačević, M. Milosavljević, "Robust Non-recursive AR Speech Analysis," *Signal Processing*, Vol. 37, No. 2, May 1994., pp. 189-201.

ROBUST MODIFIED GENERALIZED LIKELIHOOD RATIO ALGORITHM FOR SPEECH ABRUPT CHANGE DETECTION

Mladen Veinović, Milan Milosavljević, Zoran Banjac, *Institut za primenjenu matematiku i elektroniku, Beograd*
 Branko Kovačević, *Elektrotehnicki fakultet, Beograd*

Abstract - A new robust modified generalized likelihood ratio algorithm, which enables the instants of abrupt changes in stationarity of a speech signal to be detected automatically, is proposed. The procedure is based on the calculation of discrimination function using robust least squares estimates of autoregressive speech residuals. The robust estimator differs from the conventional one by the insertion of nonlinear residual transformation, which has to cut off the spiky noise. The feasibility of the approach is demonstrated with experimental data concerning speech segmentation.

1. INTRODUCTION

Modeling and processing of the discrete signals, described as a quasistationary stochastic process with abruptly changing parameters, is a challenging theoretical problem and has great importance in a variety of applications, such as speech and biomedical signal processing, image analysis, failure detection in measurement and control, etc. The essential common problem in these applications is localization of the boundaries of stationary parts of a signal, or, equivalently, detecting the instants of abrupt changes of the signal stationarity [1]. There are many results which theoretically treat the change detection problem in different uncertainty conditions, assuming different stochastic models of a signal. In spite of these valuable achievements, building of a good algorithm for change detection within a given class of real signals still represents a difficult research task. Depending on the particular application, there may be different performance criteria which a detection scheme should be fulfilled. Despite of these differences, there are few common well established desirable properties of a good detection procedure: few false alarms; low detection delay, representing the delay between the estimated and actual change times; symmetrical detection, which means that the performances in the case of a change from a signal model A to a model B must be comparable to those when a change is from the model B to the model A; robustness in the sense of insensitivity of a detection algorithm to the changes of its parameters (window length, signal structure, thresholds, ...) under the signal variability; robustness with respect to the simplification of a signal model; ability for a quick and easy restart of the detection procedure.

In this paper we present a new robust algorithm for detecting the instants of abrupt changes in a discrete speech signal. The detection procedure is based on the modified generalized likelihood ratio (MGLR) algorithm [3], which calculate the so-called discrimination (D) function. The proposed scheme differs from the standard MGLR one by the procedure of D function calculation, which is based on the robust least squares (RLS) parameter estimation of the autoregressive (AR) model of a speech signal. The effect of RLS scheme is to assign less weight to a small portion of large residuals, so that the outliers, corresponding to the pitch pulses, will not greatly influence the final AR parameter estimates, as well as the efficiency of whole detection procedure.

2. STANDARD MGLR ALGORITHM

The standard MGLR algorithm uses three AR signal models of the same order, whose parameters have to be estimated on the fixed intervals, named windows, of a signal. Assume that the so-called reference and test windows both have the length I , while the third one is their union of the length $2I$. The reference, test and joint windows cover the intervals $[i-I+1, i]$, $[i+1, i+I]$ and $[i-I+1, i+I]$, respectively, and move one sample forward with each new sample of a signal, keeping the fixed length and relationship (Fig. 1).

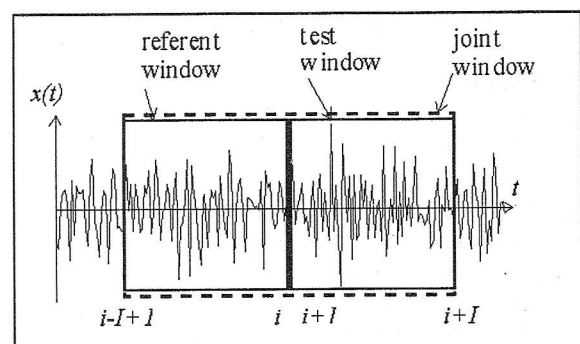


Figure 1: An analysis windows position in the MGLR algorithm

For given time instance i , we could consider two hypothesis: H_0 – no change is occurred at the i -th time instance, and H_1 – a change is occurred at the i -th time instance. Let us define a likelihood ratio between the hypothesis H_1 and H_0 , and denote it as the MGLR

discrimination function $D = \log \frac{P(H_1)}{P(H_0)}$. If we

assuming that a noise in the speech production model is zero mean white Gaussian process, and if we include a probability density function of the speech samples in the definition of the MGLR discrimination function we obtain the D function in the form

$$D(i, I) = L(i - I + 1, i + I) - L(i - I + 1, i) - L(i + 1, i + I) \quad (1)$$

where

$$L(c, d) = (d - c + 1) \ln \left(\frac{1}{d - c + 1} \sum_{j=c}^d \varepsilon_j^2 \right) \quad (2)$$

denotes the logarithmic likelihood function and ε_j is the residual of the estimated AR model at the interval (c, d) . It can be shown that (2) represent the general likelihood ratio (GLR) for the hypothesis that a change in the signal model is occurred at the instant i against the hypothesis that the signal remain unchanged on the interval $[i-I+1, i+I]$. The D function is not smooth, and its outstanding peaks provide a good indication for the most probable instants of signal changes. Two major factors influence the value of the D function: how quickly the signal is changed and how large the magnitude of a change is. Both these factors are recognizable in the short time trend of D function within the interval $[i-I/2+1, i+I/2]$, which covers I successive values of $D(i, I)$. If $[i_1, i_2]$ denotes the above interval, then $D(i, I)$ for $i \in [i_1, i_2]$ can be expressed in terms of the linear trend $t(i, I)$ as [2]

$$D(i, I) = t(i, I) + n(i, I) \quad (3)$$

where

$$t(i, I) = \alpha(i, I)k + \beta(i, I); \quad k = 1, \dots, I \quad (4)$$

with $n(i, I)$ being the noise component of D function. The parameters $\alpha(\cdot)$ and $\beta(\cdot)$ can be estimated using LS method, assuming that they are constant on the interval $[i_1, i_2]$. A local maximum of $\alpha(i, I)$ occurs at the instant $k=i_{\max}$ at which $D(i, I)$ increases the most rapidly within $[i_1, i_2]$. Similarly, $\alpha(i, I)$ attains its local minimum for $k=i_{\min}$ when $D(i, I)$ decreases the most rapidly on $[i_1, i_2]$. It is found heuristically that the parameter

$$\Delta\alpha = \Delta\alpha(i_{\max}, i_{\min}) = \alpha(i_{\max}, I) - \alpha(i_{\min}, I),$$

denoting the difference between two consecutive extremes of $\alpha(i, I)$, represents a good quantity for the decision whether the interval $[i_{\max}, i_{\min}]$ contains an instant of change in the signal stationarity. If $\Delta\alpha(i_{\max}, i_{\min}) < tr$ where tr denotes a properly

chosen threshold, as the most probable instant of change m within the interval $[i_{\max}, i_{\min}]$ we take the one at which the D function has the maximum value.

3. ROBUST MGLR ALGORITHM

The basic advantage of the MGLR algorithm, compared to the well known detection procedures in the literature [3], relates to the D function (1), which allow us to perform a posteriori analysis, since it appears in a closed form independent of the previously detected changes. The residuals ε_j , needed for the calculation of D function, we obtain from a robust LS (RLS) estimation of the AR parameters $a_i, i = 1, \dots, p$ of speech signal model [4]

$$s(j) + \sum_{i=1}^p a_i s(j-i) = e(j); \quad j = i - I + 1, \dots, i + I \quad (5)$$

where $s(j)$ is the derivative of the speech signal, or preemphasized speech signal, and the excitation $e(j)$ is the innovation random process of white-noise type for voiceless segments, while for voiced sounds $e(j)$ is a random process represented by a series of Dirac pulses with fundamental period, named the pitch period. The eq. (5) can be rewritten in the matrix linear regression form

$$S = X\theta + E \quad (6)$$

where S is the vector of signal segments of the length $2I$, θ is the vector of AR parameters, E is the vector of excitations and X is the $2I \times 2I$ dimensional observation matrix. In classical speech analysis, the parameter vector θ is determined by LS method, which minimizes the sum of squared residuals. This algorithm is optimal when the underlying observations are Gaussian. However, it is well known that the outliers corresponding to the pitch pulses have unusually large influence on the LS estimates [4]. Therefore, robust methods have been created to modify the LS estimates, in order to suppress the influence of outliers. Particularly, M-robust estimates [4] are defined as the minimization of the sum of weighted residuals

$$\sum_{i=1}^I \rho[\varepsilon_i(\theta)] \quad \varepsilon_i(\theta) = (s_i - x_i^T \theta) / d \quad (7)$$

where s_i is the i -th element of S , x_i is the i -th row of X , and d is an estimate of the scale of the distribution associated with E . Here $\rho(\cdot)$ is a robust score function which has to cut off the outliers. Since it is assumed that the speech excitation distribution has Gaussian-like middles and heavier tails, comparatively high efficiency at the Gaussian samples is also desired. Thus, $\rho(\cdot)$ should behave as quadratic function for

small arguments, but increases more slowly for large arguments. In this way, its first derivative $\psi(\cdot) = \rho'(\cdot)$ should be a saturation type nonlinearity, i.e. $\psi(z_i/d)d$ equals z_i if $z_i/d \leq \delta$, but is equal δd (i.e. $-\delta d$), where $\delta = 1.5$ is chosen to give the desired efficiency at the normal distribution [4]. Although ad-hoc, a popular robust estimate of scale is the median of absolute median deviations [4]

$$d = \frac{\text{median}|z_i - \text{median}(z_i)|}{0.6745} \quad (8)$$

Equating the first partial derivatives with respect to the elements of θ to zero, we see that this is equivalent to finding the solution associated with the p equations

$$\sum_{i=1}^I x_{ij} \psi(e_i(\theta)) = 0; \quad j = 1, \dots, p \quad (9)$$

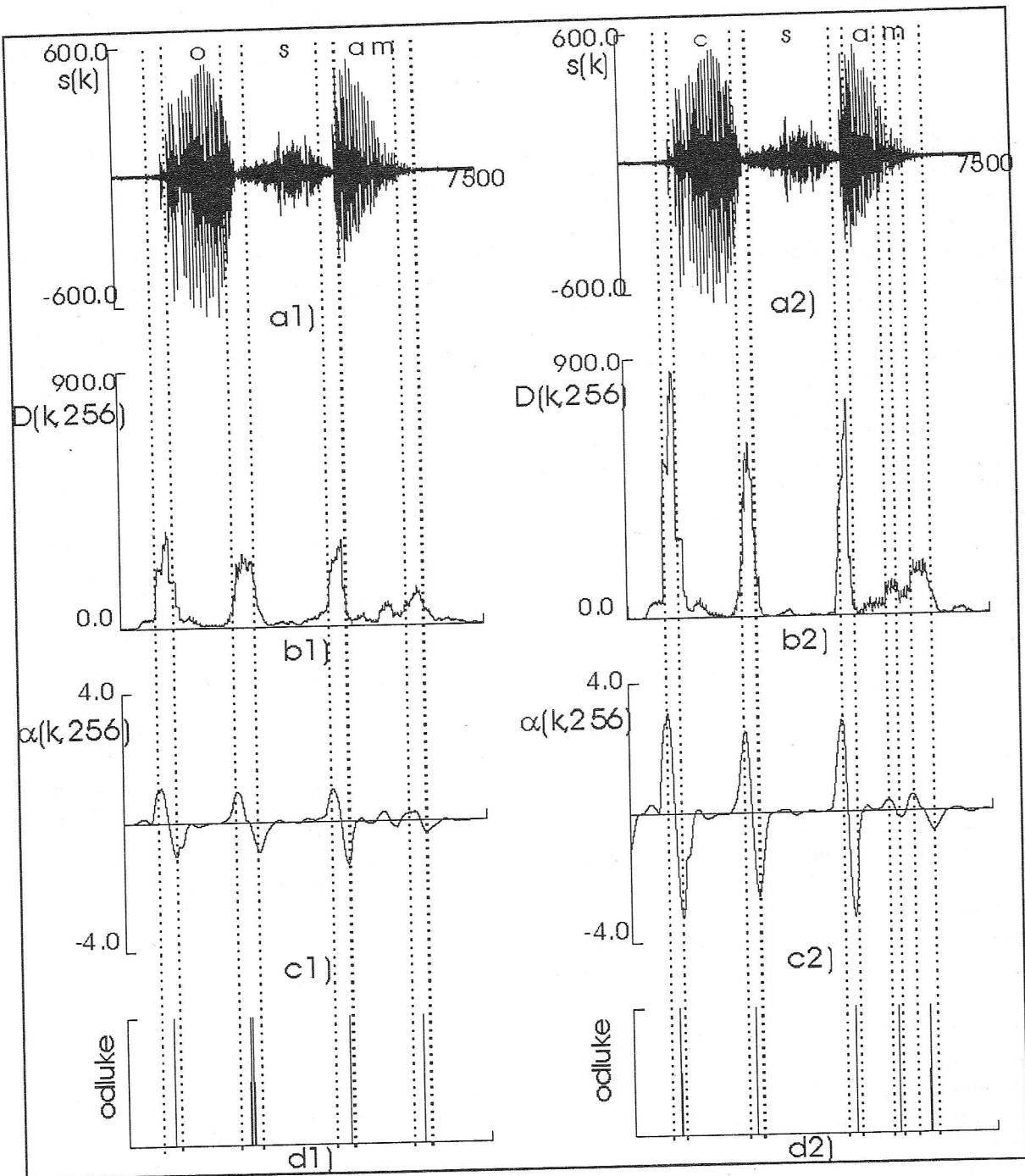


Fig. 2: Performance comparison for standard and robust MGLR algorithm on the natural speech:
 a1), a2) Isolate spoken Serbian digit "osam" ("8")
 b1) Estimated D function using standard MGLR;

- b2) Estimated D function using robust MGLR;
- c1) The slope of D function trend using standard MGLR;
- c2) The slope of D function trend using robust MGLR;
- d1) The instans of change obtained by standard MGLR;
- d2) The instans of change obtained by robust MGLR.

where x_{ij} is the element in the i -th row and j -th column of X . The solution of (9) becomes cumbersome, because of the fact that $\psi(\cdot)$ is nonlinear [4]. However, (9) can be expressed as a weighted least-squares approximation

$$\sum_{i=1}^I x_{ij} \varpi_{i0} (y_i - x_i^T \theta_0) \approx 0 \quad (10)$$

where

$$\varpi_{i0} = \begin{cases} \left[\psi[\varepsilon_i(\theta_0)] / \varepsilon_i(\theta_0) \right]; & \text{for } y_i \neq x_i^T \theta_0 \\ 1; & \text{for } y_i = x_i^T \theta_0 \end{cases} \quad (11)$$

with θ_0 being some initial parameter vector estimate. The estimate θ_0 can be obtained by using the classical LS algorithm. Thus, the one step solution is given by

$$\hat{\theta} = (X^T \Omega X)^{-1} X^T \Omega Y; \quad \Omega = \text{diag}\{\omega_{10}, \dots, \omega_{10}\} \quad (12)$$

4. EXPERIMENTAL EXAMPLE

To demonstrate the main features of the proposed detection procedure, we apply it to the natural human speech, that is ten isolately spoken Serbian digits ("1", "2", ..., "0") from one speaker. Fig.2. depicts the results of segmentation of Serbian isolately digit "osam" ('8') obtained by standard MGLR and robust MGLR, respectively. This results is characteristic for the algorithm behavior. The speech signal was low-pass filtered with an upper limit frequency of 4 kHz, and digitized by 12 bit A/D conversion with a sampling rate of 10 kHz. In addition, the preemphasis of the signal was also performed. Experimental results was obtained by using the 10th order AR model. In all experiments $I=256$ in the robust MGLR algorithm was adopted. Obviously, in the case of robust MGLR the shape of the D function, as well as the slope of its trend, better tracks the changes in signal stationarity.

5. CONCLUSION

In this paper a new algorithm for detecting the instants of abrupt changes in stationarity of a speech signal is presented. The algorithm differs from the standard MGLR scheme in that it uses a robust LS method for estimating the AR residuals of a signal, in order to calculate the discrimination function. The robust MGLR better tracks the changes in the signal stationarity than the standard one, and is proven to be an efficient procedure for speech signal segmentation. Finally, the robust MGLR algorithm fulfils all desirable properties which are imoprtant for practical efficiency of a change detection procedure.

REFERENCES

- [1] M.Basseville and A.Benveniste, *Detection of Abrupt Changes in Signals and Dynamical Systems*, Springer Verlag, New York, 1986.
- [2] M.Milosavljević, I.Konvalinka, "The modified generalized likelihood ratio algorithm (MGLR) for automatic detection of abrupt changes in stationarity of signals", *Proc. the 22-nd Annual Conf. Inform. Sci. Systems*, Princeton, NJ, 1988, pp.2369-2372.
- [3] U.Appel and A.V.Brandt, "A comparative study of three sequential time series segmentation algorithms", *Signal Processing*, Vol.6, No.1, 1984, pp.45-60.
- [4] M.Veinović, B.Kovacević, and M.Milosavljević, "Robust non-recursive AR speech analysis", *Signal Processing*, Vol.37, No.2, 1994, pp.189-201.
- [5] B.Kovačević, M.Veinović, M.Milosavljević, "Robust AR analysis of nonstationary discrete-time signals", *Proceedings of the third ICECS'96, Rodos, Greece, 13.10.-16.10. 1996.*, pp.980-983.

Nonlinear Activation Function and PDF for Nonlinear Prediction via Recurrent Neural Networks

Danilo P. Mandic

Abstract— We show that the area under the first derivative of the logistic nonlinear activation function of a neuron exhibits features of a Probability Density Function (PDF). Based upon that, a connection between the first derivative of a nonlinear activation function of a neuron in a Recurrent Neural Network (RNN), and a PDF of a nonstationary signal for a prediction application is provided, which leads to improved nonlinear prediction using RNNs.

I. INTRODUCTION

The Nonlinear Autoregressive Moving Average (NARMA) model can be written as [1]

$$x(k) = e(k) + h(x(k-1), \dots, x(k-p), e(k-1), \dots, e(k-q)) \quad (1)$$

where p denotes the order of the Autoregressive (AR) part, q denotes the order of the Moving Average (MA) part, with some nonlinear function $h(\cdot)$. Such a model is called a NARMA(p,q) model.

The NARMA scheme from (1), can be further approximated as [2]

$$\begin{aligned} y(k) &= \hat{x}(k) = \\ &= h(x(k-1), \dots, x(k-p), \hat{e}(k-1), \dots, \hat{e}(k-q)) = \\ &= H(x(k-1), \dots, x(k-p), y(k-1), \dots, y(k-q)) \end{aligned} \quad (2)$$

where H is some new, nonlinear smooth function. The last equation in (2) is now suitable for RNN implementation, with H becoming an activation function of the neuron, which is typically the logistic function denoted by

$$\Phi(v) = \frac{1}{1 + e^{-\beta v}} \quad (3)$$

and will be assumed in (2). For prediction applications based upon (2), it is important to choose properly the slope β in the nonlinear activation function Φ (3). So far, it has been done rather empirically [2], [3]. Recognising that the slope β is related to a step-size η in the learning process of the RNN [4], [5], it makes us question whether knowing the PDF of a nonlinear and nonstationary signal being predicted, a judgement about the size of β can be made, so that an RNN predictor has optimal parameters.

II. THE ROLE OF β IN THE LOGISTIC FUNCTION

In order to show the role of the slope β in the logistic function, let us consider a simple NARMA(1,1) predictor,

The author is with the Signal Processing Section of the Department of Electrical and Electronic Engineering, Imperial College of Science, Technology and Medicine, London, U.K. Telephone: +44 (171) 594 6313. Fax: +44 (171) 594 6234. E-mail: d.mandic@ic.ac.uk, http://www.dsp.ee.ic.ac.uk/~mandic .

realised by a recurrent neural network, i.e.

$$y(k) = \frac{1}{1 + e^{-\beta(w_1(k)y(k-1) + w_2(k)x(k-1) + w_3(k) \cdot 1)}} \quad (4)$$

It can be represented by a recurrent perceptron, given in Figure 1. The equations which describe the recurrent per-

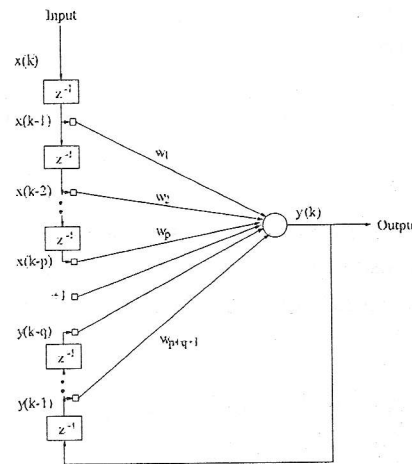


Fig. 1. NARMA(p,q) recurrent perceptron

ceptron are

$$\begin{aligned} y(k) &= \Phi(v(k)) \\ v(k) &= w(k)^T \cdot u(k), \end{aligned} \quad (5)$$

where $u(k) = [y(k-1), \dots, y(k-q), 1, x(k-1), \dots, x(k-p)]^T$, and w is the weight vector. The Bounded Input Bounded Output (BIBO) stability of (5) is preserved due to the saturation type nonlinearity Φ in (5), which is typically the logistic function $\Phi(v) = \frac{1}{1+e^{-\beta v}}$, with slope β . Based upon (4), it can be shown that convergence/divergence of such a predictor [6], as well as learning [7], rests upon the choice of β . It also defines the width of the pseudo-linear range of the logistic function. For nonlinear prediction, in particular, it is important to have β optimal, which has so far been done empirically.

III. LOGISTIC FUNCTION AND PDF

As the pseudo-linear range of the function (i.e. "bandwidth"), depends on the value of slope β , it would be beneficial to establish a relationship between some features of a nonlinear and nonstationary signal in hand, and a parameter of a logistic function used in neurons of an RNN. We therefore investigate the first derivative of the logistic function (3).

Observation 1: The area under the first derivative Φ' of the general logistic function

$$\Phi'(x) = \frac{\beta e^{-\beta x}}{(1 + e^{-\beta x})^2} \quad (6)$$

is constant and equals 1.

Proof:

The goal is to calculate the integral $I = \int_{-\infty}^{+\infty} \Phi'(x) dx$. By the substitution method, a dummy variable t can be introduced as $t = e^{-\beta x} \Rightarrow dt = -\beta e^{-\beta x} dx$. Integral I can now be expressed as

$$I = \int_{-\infty}^{+\infty} \Phi'(x) dx = \int_{+\infty}^0 -\frac{dt}{(1+t)^2} = \left. \frac{1}{1+t} \right|_{+\infty}^0 = 1 - \frac{1}{1+\infty} = 1 \quad (7)$$

which does not depend on any parameter in the logistic function, such as slope, or bias. \square

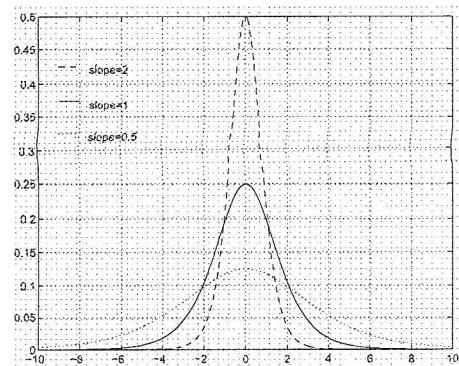
Since independently of the slope β in the logistic function Φ , the area under its first derivative Φ' equals unity (Figure 2(a)), the result from Observation 1 resembles the behaviour of a Probability Density Function (PDF). A PDF has the property that the area under the PDF equals unity, independent of the effective width of the PDF (defined by the variance). If a correspondence between the PDF of the first derivative of the logistic function and the PDF of a real nonlinear signal could be established, it might offer some new techniques for RNN applications.

IV. THE SIZE OF β AND PDF

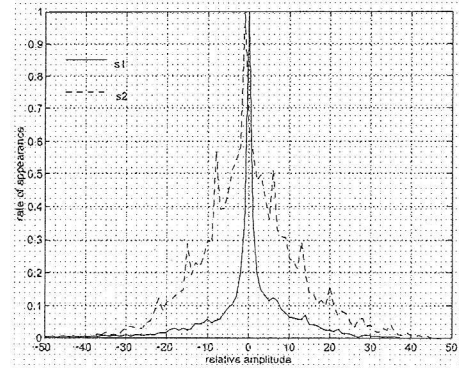
A theoretical analysis of a relationship connecting β and PDF is rather difficult. In order to depict empirically the connection between the slope β in the logistic function and a PDF of a real signal, we plot the PDF function for the amplitudes of two speech signals [2], denoted by $s1$ and $s2$, and show that there is a relationship between that PDF, and the first derivative of the logistic function (Figure 2(a)). The sample PDFs of two speech signals $s1$, and $s2$ are shown in Figure 2(b). Signal $s2$ has a wider PDF than $s1$. It is therefore expected that in order to establish a relationship between the diagram shown in Figure 2(b) to that shown in Figure 2(a), the value of slope β for the RNN based prediction of signal $s1$ should be greater than that for $s2$. Indeed, a simulation showed that the optimal slope was $\beta = 1$ for speech signal $s1$, whereas $\beta = 0.91$ for $s2$. Similar behaviour has been registered for a set of eight speech signals coming from different speakers.

V. CONCLUSIONS

A connection between the slope β of the logistic nonlinear activation function of a neuron, and a Probability Density Function (PDF) of a nonstationary input signal has been established for nonlinear prediction performed by a recurrent neural network. It has been shown, that an estimate of the size of β can be made based upon the knowledge of the PDF of a nonstationary input signal. As β is closely related to the learning process of a recurrent



(a) First derivative of the logistic function for different slopes β



(b) PDF of two speech signals

Fig. 2. PDFs and Φ' for two speech signals

neural network, that helps in achieving optimal nonlinear prediction.

LIST OF FIGURES

| | | |
|---|---|----|
| 1 | NARMA(p,q) recurrent perceptron | 66 |
| 2 | PDFs and Φ' for two speech signals | 67 |

REFERENCES

- [1] M. B. Priestley, *Non-linear and Non-stationary Time Series Analysis*. Academic Press, London, 1991.
- [2] J. T. Connor, R. D. Martin, and L. E. Atlas, "Recurrent neural networks and robust time series prediction," *IEEE Transactions on Neural Networks*, vol. 5, no. 2, pp. 240-254, 1994.
- [3] S. Haykin and L. Li, "Nonlinear adaptive prediction of nonstationary signals," *IEEE Transactions on Signal Processing*, vol. 43, no. 2, pp. 526-535, 1995.
- [4] D. P. Mandic and J. A. Chambers, "Toward an optimal PRNN based nonlinear predictor," *IEEE Transactions on Neural Networks*, vol. 10, no. 6, pp. 1435-1442, 1999.
- [5] D. P. Mandic and J. A. Chambers, "Relationship between the slope of the activation function and the learning rate for the RNN," *Neural Computation*, vol. 11, no. 5, pp. 1069-1077, 1999.
- [6] D. P. Mandic and J. A. Chambers, "Exploiting inherent relationships in RNN architectures," *Neural Networks*, vol. 12, no. 10, pp. 1341-1345, 1999.
- [7] D. P. Mandic and J. A. Chambers, "A posteriori real time recurrent learning schemes for a recurrent neural network based non-linear predictor," *IEE Proceedings-Vision, Image and Signal Processing*, vol. 145, no. 6, pp. 365-370, 1998.

- [7] R. Williams and D. Zipser, "A learning algorithm for continually running fully recurrent neural networks," *Neural Computation*, vol. 1, pp. 270-280, 1989.

A BLOCK DIAGRAM SIMULATION APPROACH FOR ALGEBRAIC EQUATIONS ROOTS LOCALIZATION

Bratislav Danković, Dragan Antić, Saša Dimitrijević
 Faculty of Electronic Engineering, University of Niš, Yugoslavia
 Beogradska 14, 18000 Nis, E-mail: dantic@elfak.ni.ac.yu*

Abstract - A symbolic method for determining solutions of algebraic equations with complex coefficients is presented in this paper. This method is based on digital simulation of n -integrators system conducted in block diagram simulation languages. Simulations are performed repeatedly for different sets of parameters. This method is used as an effective tool to construct solutions of fifth order algebraic equation with complex coefficients.

Keywords: Algebraic Equation, Complex Coefficients, Roots, Simulation

I INTRODUCTION

There are a lot of methods for numerical solving of algebraic equation with complex coefficients. Most of the methods reduce solving equation with complex coefficients to solving a system of algebraic equations with real coefficients. These methods are in most cases iterative. The zeros of the algebraic equation with complex coefficients can also be found in a successive manner or iteratively (see [6,7]). Recently, many methods for determining zeroes of algebraic equations with complex coefficients have been implemented into the software packages, for instance *Mathematica*, with the use of complex arithmetics.

This paper presents a new approach for localizing roots of complex coefficients algebraic equation based on simulation [1-4]. The procedure is used for n -th order algebraic equation, in the form:

$$f(z) = a_0 + a_1 z + \dots + a_{n-1} z^{n-1} + z^n \quad (1)$$

where a_j , $j = 0, 1, \dots, n-1$ are complex coefficients in the form $a_j = b_j + i c_j$, n is equation order and $z = x + iy$ is a complex variable. The technique relates solving algebraic equation:

$$f(x + iy) = 0 \quad (2)$$

what can be written in the form:

$$\operatorname{Re}\{f(x + iy)\} + i \operatorname{Im}\{f(x + iy)\} = 0 \quad (3)$$

The real part of Equation (3) can be written with respect to coefficients vector $\mathbf{a} = (a_0, a_1, \dots, a_{n-1})$:

$$\operatorname{Re}\{f(x + iy)\} = p_{n-1}(\mathbf{a}, y)x^{n-1} + \dots + p_0(\mathbf{a}, y) \quad (4)$$

or its real and imaginary parts $\mathbf{b} = (b_0, b_1, \dots, b_{n-1})$ and $\mathbf{c} = (c_0, c_1, \dots, c_{n-1})$, respectively:

$$\operatorname{Re}\{f(x + iy)\} = p_{n-1}(\mathbf{b}, \mathbf{c}, y)x^{n-1} + \dots + p_0(\mathbf{b}, \mathbf{c}, y) \quad (5)$$

The imaginary part of Equation (3) can be written in the same form but with different coefficients values:

$$\operatorname{Im}\{f(x + iy)\} = x^n + q_{n-1}(\mathbf{a}, y)x^{n-1} + \dots + q_0(\mathbf{a}, y) \quad (6)$$

The condition (3) is fulfilled if both absolute values of real and imaginary part are equal to zero:

$$|\operatorname{Re}\{f(x + iy)\}| + |\operatorname{Im}\{f(x + iy)\}| = 0 \quad (7)$$

Considering that this is an approach for localization of algebraic equation (1) roots based on simulation, Equation (7) model will be:

$$\varepsilon = \min_{x, y} (|\operatorname{Re}\{f(x + iy)\}| + |\operatorname{Im}\{f(x + iy)\}|) \quad (8)$$

The x, y values which correspond to the minimum will be the roots of Equation (1).

$$\varepsilon = \min_{x, y} (|p_{n-1}(\mathbf{b}, \mathbf{c}, y)x^{n-1} + \dots + p_0(\mathbf{b}, \mathbf{c}, y)| + |x^n + q_{n-1}(\mathbf{b}, \mathbf{c}, y)x^{n-1} + \dots + q_0(\mathbf{b}, \mathbf{c}, y)|) \quad (9)$$

* Corresponding author

II ROOTS LOCALIZATION

In [8], the author has shown that all roots of polynomial f defined as:

$$f(z) = a_0 + a_1 z + \cdots + a_{n-1} z^{n-1} + z^n \quad (10)$$

belong to the disk D :

$$D = \left\{ z \mid |z + 0.5a_{n-1}| \leq 0.5|a_{n-1}| + \alpha M \right\} \quad (11)$$

where:

$$M = \sum_{j=2}^n |a_{n-j}|^{\frac{1}{j}} \quad (12)$$

$$\alpha = \begin{cases} 0, & \text{if } P(z) = a_{n-1} z^{n-1} + z^n \\ \max_{2 \leq j \leq n} \left(M^{-1} |a_{n-j}|^{\frac{1}{j}} \right)^{\frac{j-1}{j}}, & \text{otherwise} \end{cases} \quad (13)$$

This result will be used to determine the interval within which complex solutions of algebraic Equation (1) can be found:

$$|z| \leq R \quad (14)$$

III SIMULATION PARAMETERS

Transformation of time base in such a way that x values correspond to current time in the simulation is shown in Figure 1.

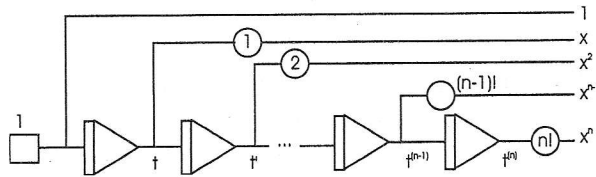


Figure 1: Time base transformation into x -domain

Simulation is conducted using block diagram simulation languages (SIMULINK, etc.) where $x = \text{time}$. In this manner, x values are within the interval $[-R, R]$, considering that simulation ends at R seconds. As a result of simulation value ε for $y = y_0 = \text{const}$ is obtained. Basic system elements are integrators, summatotors and gain elements where all parameters are constant for one simulation cycle:

$$p_i(\mathbf{a}, y_0) q_i(\mathbf{a}, y_0) = \text{const}, \quad i = 0, \dots, n-1 \quad (15)$$

A simulation scheme for 5-th order equation designed in SIMULINK is shown in Figure 2. This procedure can be easily expanded to higher order equation.

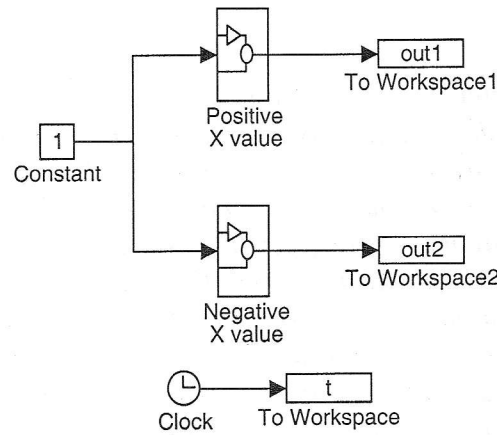


Figure 2: Simulation scheme for solving algebraic equation with complex coefficients

First simulation is conducted using initial value $y_0 = -R$. Simulation parameters for the fifth order algebraic equation with complex coefficients can be calculated based on following equations:

$$p_0(\mathbf{b}, \mathbf{c}, y) = y^5 + c_4 y^4 - b_3 y^3 - c_2 y^2 + b_1 y + c_0 \quad (16a)$$

$$p_1(\mathbf{b}, \mathbf{c}, y) = 4b_4 y^3 - 3c_3 y^2 + 2b_2 y + c_1 \quad (16b)$$

$$p_2(\mathbf{b}, \mathbf{c}, y) = -10y^3 - 6c_4 y^2 + 3b_3 y + c_2 \quad (16c)$$

$$p_3(\mathbf{b}, \mathbf{c}, y) = 4b_4 y + c_3 \quad (16d)$$

$$p_4(\mathbf{b}, \mathbf{c}, y) = 5y \quad (16e)$$

$$q_0(\mathbf{b}, \mathbf{c}, y) = b_4 y^4 + c_3 y^3 - b_2 y^2 - c_1 y + b_0 \quad (17a)$$

$$q_1(\mathbf{b}, \mathbf{c}, y) = 5y^4 + 4c_4 y^3 - 3b_3 y^2 - 2c_2 y + b_1 \quad (17b)$$

$$q_2(\mathbf{b}, \mathbf{c}, y) = -6b_4 y^2 - 3c_3 y + b_2 \quad (17c)$$

$$q_3(\mathbf{b}, \mathbf{c}, y) = -10y^2 - 4c_4 y + b_3 \quad (17d)$$

$$q_4(\mathbf{b}, \mathbf{c}, y) = b_4 \quad (17e)$$

During one simulation x takes the values from the interval $x \in [-R, R]$, since simulation starts at 0 seconds and stops at R seconds. The simulation blocks used for calculation with positive and negative x -values are shown in fig. 3. As a result of simulation, value

$$\varepsilon_0 = \min_{x \in [-R, R]} \left(\left| \operatorname{Re} \{ f(x + iy_0) \} \right| + \left| \operatorname{Im} \{ f(x + iy_0) \} \right| \right) \quad (18)$$

is obtained. At the moment ε reaches its minimum, x_0 value corresponding to the

minimum is found.

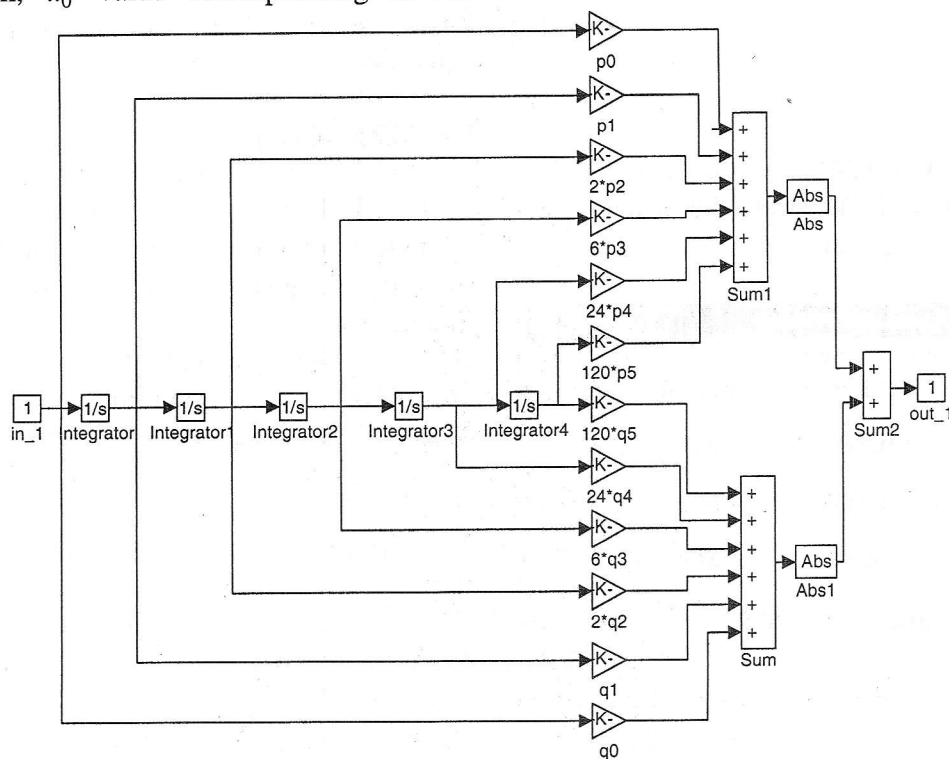


Figure 3: Simulation block for positive values of x

In the next simulation cycle, y_1 value is calculated on the basis of y_0 and predetermined step value Δy :

$$y_1 = y_0 + \Delta y \quad (19)$$

It is important to notice that Δy , as well as simulation step correspond to the desired accuracy. Simulation is again conducted for $x \in [-R, R]$ but for different parameters $p_i(a, y_1), q_i(a, y_1)$, $i = 0, \dots, n-1$. Again ε value is calculated based on Equation (9) for $y = y_1, x \in [-R, R]$:

$$\varepsilon_1 = \min_{x \in [-R, R]} \left(|\operatorname{Re}\{f(x + iy_1)\}| + |\operatorname{Im}\{f(x + iy_1)\}| \right) \quad (20)$$

If ε_1 is less than ε_{\min} (meaning that (x_1, y_1) is closer to eq. 1 root) then $\varepsilon_{\min} = \varepsilon_1$. This procedure is then repeated in the same manner for other sets of parameters:

$$y_k = y_{k-1} + \Delta y \quad (21)$$

$$p_i(a, y_k), q_i(a, y_k), i = 0, \dots, n-1 \quad (22)$$

until the following condition is fulfilled:

$$\varepsilon_{\min} \leq \delta \quad (23)$$

where δ is the desired accuracy. Repeated simulations for different values of $y = y_k = \text{const}$ are performed using MATLAB programming.

When the desired accuracy is accomplished, the obtained values $x = x_k$, $y = y_k$ will represent one of the Equation (1) roots. The procedure is then repeated for different values $y = y_{k+1} = \text{const}$. In that manner, all other roots can be localized.

IV ILLUSTRATIVE EXAMPLE

Let us consider a polynomial in the form:

$$P(z) = (z - 0.1 - i0.2)(z - 0.2 - i0.3)(z - 0.5 - i0.5) \\ (z - 0.7 - i0.8)(z - i0.9) \quad (24)$$

what is equivalent to Equation (1) with following coefficients:

$$b_0 = -0.03015;$$

$$b_1 = -0.2593;$$

$$b_2 = 2.158;$$

$$b_3 = -2.;$$

$$b_4 = -1.5;$$

```
c0= 0.04545;
c1= -0.5096;
c2= 0.11;
c3= 3.16;
c4= -2.7;
```

The polynomial (24) has been generated in this manner to demonstrate the efficiency of the proposed algorithm.

| Root: | Real Part | Imaginary Part |
|------------|-----------|----------------|
| $0.1000+i$ | 0.1000 | 0.2000 |
| $0.2000+i$ | 0.2000 | 0.3000 |
| $0.5000+i$ | 0.5000 | 0.5000 |
| $0.7000+i$ | 0.7000 | 0.8000 |
| $0+i$ | 0 | 0.9000 |

Figure 4: MATLAB results

By implementing the proposed method the coefficients $p_i(\mathbf{a}, y_1), q_i(\mathbf{a}, y_1)$, $i = 0, \dots, n-1$ are calculated for each simulation. For the desired accuracy of 0.01 the results of the proposed method are shown in Figure 4. Based on a MATLAB list, we can conclude that the solutions of Equation (24) are found with the desired accuracy.

V CONCLUSION

In this paper, a block diagram oriented approach for solving algebraic equation with complex coefficients is presented. A simulation scheme is constructed in block diagram simulation language. Simulations

are performed until all roots of algebraic equation are found. This method is used for localizing roots of fifth order algebraic equation.

REFERENCES:

- [1] N. M. Karayanakis, Computer-Assisted Simulation of Dynamic Systems with Block Diagram Languages, (CRC Press, Boca Raton, 1993).
- [2] N. M. Karayanakis, Advanced System Modelling and Simulation with Block Diagram Languages, (CRC Press, Boca Raton, 1995).
- [3] D. J. Murray-Smith, Continuous System Simulation, (Chapman & Hall, London, 1995).
- [4] F. F. Kuo, ed., Computer Simulation of Dynamic Systems, (Prentice-Hall, New Jersey, 1972).
- [5] G. Polya, G. Szego, Aufgaben und Lehrsätze aus der Analysis, (Springer-Verlag, Berlin, 1971).
- [6] G. V. Milovanovic, Numerical Analysis, I, (Naučna knjiga, Belgrade, 1988), (in serbian).
- [7] G. V. Milovanovic, M. S. Petrović, On computational efficiency of the iterative methods for simultaneous approximation of polynomial zeros, in: ACM Trans. Math. Software, No. 12 (1986) 295-306.
- [8] Q. I. Rahman, A bound for the moduli of the zeros of polynomials, in: Canad. Math. Bull. 13 (4) (1970) 541-542.
- [9] T. Yamamoto, S. Kanno, L. Atanassova, Validated Computation of Polynomial zeros by the Durand-Kerner method, in: Topic in Validated Computation, ed. by Herzberger J., (Wort-Holland, Amsterdam 1994) 27-53.

IDENTIFICATION OF THE DYNAMICAL PARAMETERS OF MANIPULATOR ACTUATOR IN THE PRESENCE OF ENCODER RESOLUTION

Petar Marić, Igor Krčmar Faculty of Electrical Engineering in Banjaluka

Abstract: Identification of the parameters of joint actuator dynamics, is analyzed in this paper. The effect of encoder resolution, concerning measurement of the angular displacement of actuator, is taken into account in this analysis. This effect and interaction among the manipulator links are introduced in the identification procedure as a colored disturbance. Also, it is shown that encoder resolution improves persistent excitation (PE) characteristics of the regressor. Nevertheless, stabilization of the recursive algorithm, proposed in this paper, is justified, by every test case presented in the paper.

1. INTRODUCTION

The form of the adopted model has essential influence on the validity of the dynamical model. The assumption, that manipulator consists of n independent systems (n joints), yields the simplest control strategy. In that case, control of each joint is performed, as it is a single input - single output (SISO) system. Interactions among the joints, during the performance of a manipulation task, are treated as disturbances. When actuator is coupled to the link, by reduction gears, these disturbances can be dumped significantly, with an appropriate control strategy.

Estimate of the parameters, of actuator dynamical model, can be computed from actuator control signals and measured values of rotor angular displacement. Measurement of rotor angular displacement, is usually performed by optical encoder. An optical encoder provides information on measured value, in digital form. Having in mind identification of the parameters of actuator dynamical model, it is natural to consider encoder resolution as a measurement error. Many papers deals with a problem of identification in the presence of colored disturbance and unmodeled dynamics. Often, it is a case, that the real system does not belong to the class of system model. Then, it is necessary to take into account the effect of unmodeled dynamics, during the process of identification [1,2]. This problem is not important, if each joint actuator is modeled separately, because, it is a well known fact, that actuator has the second order model.

When disturbance is not of a white noise type, the least squares (LS) method of identification yields biased estimate of the model parameters. It is shown, in references [3,4], how to obtain unbiased estimate, without modeling the disturbance. Algorithms are given in nonrecursive form. The advantages of recursive procedures of identification, comparing with nonrecursive ones, are well known, and they are given in the literature [5,6]. The procedure, of transformation of nonrecursive algorithm given in [4],

into appropriate recursive form, is given in reference [7].

Recursive procedure of identification, that avoids computation of matrix inversion in every iteration, is proposed in this paper. Also, influence of optical encoder resolution on the process of identification is analyzed in the paper. In the model of manipulator, interactions among joints and encoder resolution are treated as colored disturbance.

Especially, problem of insufficient persistent excitation (PE) of actuator, during real time identification, when manipulator performs a typical manipulation task, is discussed in this paper. Also, influence of encoder resolution on PE characteristics of regressor is analyzed. It is shown, that "disturbance" signal, introduced in this manner, diminish the problem of algorithm covariance matrix blow-up. On the other hand, it is still insufficient for elimination of this problem. Therefore, proposed stabilization of algorithm is justified.

2. DYNAMICAL MODEL OF MANIPULATOR

The motion of industrial robot manipulator, in a free space, without interactions with environment, may be described by the equation:

$$M(q)\ddot{q} + C(q, \dot{q})\dot{q} + F(\dot{q}) + G(q) = \tau \quad (1)$$

where q is the vector of internal (joint) coordinates, $M(q)$ is inertia tensor, $C(q, \dot{q})$ is matrix which represents centripetal and Coriolis effects, $F(\dot{q})$ is matrix of viscous friction, $G(q)$ is matrix which represents gravitational load, and τ is vector of joint generalized forces and torques. Let K_r stand for $n \times n$ matrix, which comprises reduction ratios of all reduction gears. In that case we can write:

$$K_r q = q_m, \tau_m = K_r^{-1} \tau,$$

where q_m and τ_m are vectors of joint actuator displacements, and actuator driving torques, respectively. Further, one can set

$$M(q) = \bar{M} + \Delta M(q), \quad (2)$$

where \bar{M} denotes diagonal matrix whose constant elements represent average inertia at each joint, and $\Delta M(q)$ comprises configuration-dependent terms.

Now, one can write [8]:

$$\tau_m = K_r^{-1} \bar{M} K_r^{-1} \ddot{q}_m + F_m \dot{q}_m + d \quad (3)$$

where

$$F_m = K_r^{-1} F K_r^{-1} \quad (4)$$

represents the matrix of viscous friction coefficients, and

$$d = K_r^{-1} \Delta M(q) K_r^{-1} \ddot{q}_m + K_r^{-1} C(q, \dot{q}) K_r^{-1} \dot{q}_m + K_r^{-1} G(q) \quad (5)$$

represents the contribution that depends on the configuration. Therefore, the manipulator with drives is actually composed of two subsystems. The first subsystem has τ_m as input and q_m as output, while the second subsystem has $q_m, \dot{q}_m, \ddot{q}_m$ as inputs, and d as an output. The first subsystem is linear and decoupled, since each component of τ_m influences only the corresponding component of q_m . In equation (3), d denotes the vector, whose each component represents the sum of influences, of other joints, on the corresponding joint of manipulator. Thus, a component of vector d can be regarded as a disturbance acting on the actuator of a joint. When there is a need for a faster working process, lower reduction ratios should be adopted. This, in turn, results in a greater impact of disturbance d , according to equation (5). Such an unfavorable effect is more profound in the case of joints actuated with the direct drive motors, because in this case K_r is identity matrix ($K_r = I$). The second subsystem is nonlinear and coupled. Decentralized approach to the manipulator dynamics modeling, based on the above stated considerations, is wide spread. Each joint of the manipulator is considered independently from the others, through the dynamics of its actuator. If we

consider the DC motor, with well known dynamical model, as an actuator, then dynamical model of the joint, which is in fact the model of actuator, has armature voltage as input and angle of rotation of the shaft as output.

Electrically driven manipulators are usually constructed with a DC permanent magnet torque motor, for each joint. Basically the DC torque motor is a permanent magnet, armature excited, continuous rotation motor, incorporating such features as high torque/power ratio, smooth low - speed operation, linear torque - speed characteristics, and short time constants. Use of a permanent magnet field and DC power provide maximum torque with minimum input power, and minimum weight. These features also reduce the motor inductance, and hence, the electrical time constant. The block scheme of joint i can be represented in the domain of complex variable s as in Fig. 1. In this scheme u is the armature voltage, L - armature inductance, R - armature resistance, K_{em} - proportionality constant between voltage and torque, J - effective momentum of inertia of the combined motor and load, referred to the motor shaft, f - effective viscous friction coefficient of the combined motor and load, referred to the motor shaft, K_{me} - proportionality constant between velocity and electromotive force.

Transfer function from the armature voltage to the angular displacement of motor shaft is:

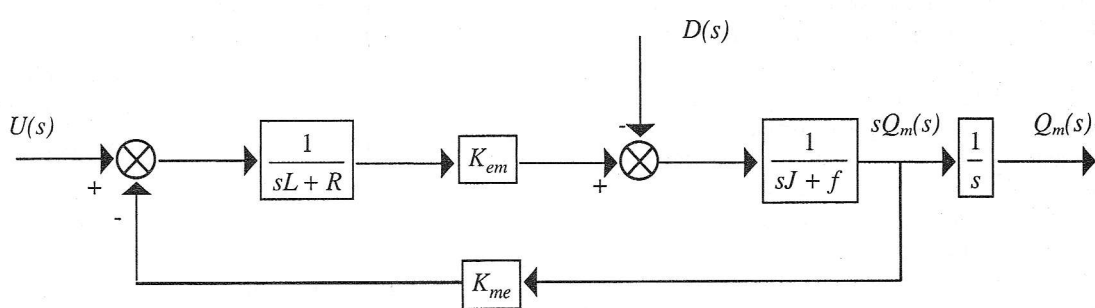


Figure 1. Block scheme of joint actuator

$$\frac{Q_m(s)}{U(s)} = \frac{K_{em}}{s(s^2 JL + s(Lf + RJ) + Rf + K_{em}K_{me})} \quad (6)$$

Since the electrical time constant of the motor is much smaller than the mechanical time constant, armature inductance effect can be neglected. This allows simplification of the above transfer function:

$$\begin{aligned} \frac{Q_m(s)}{U(s)} &= \frac{K_{em}}{s(sRJ + Rf + K_{em}K_{me})} \\ &= \frac{K}{s(sT_m + 1)} \end{aligned} \quad (7)$$

where K is motor gain constant, and T_m - motor time constant. An optical shaft encoder is a digital transducer that converts angular shaft position into

binary coded signal. This type of sensor uses an encoder disk to provide measurement of the joint coordinate (q). Since the device output is in digital form, it is often cited as one of those fortunate devices that does not require a subsequent analog-to-digital conversion of the output [9].

Optical encoders are divided into two basic categories: absolute and incremental. An absolute encoder consists of a disk with concentric tracks and a light sensor with transmitter for each track. The light source for an optical encoder, used in robotics, is a light emitting diode (LED). The optical sensors are either photodiodes or phototransistors. In order to obtain an angular position of the shaft, absolute encoder disk, usually, is coded with the Gray code. An advantage of the Gray code is that each position advance requires only one change in the digital code

(word). An absolute encoder may be turned off, without losing track of the position. Indeed, they need to be powered only when a reading is required.

The output of an incremental encoder is a pulse train, representing the overall rotation of the code disk. The rotation is expressed in the number of angular increments. This fact is, in essence, sufficient when one wants to obtain velocity data. On the other hand, the determination of an angular position requires an external digital counter, that keeps track of the number of pulses. In case of power failure, the counter may reset, thus, resulting in the loss of position information. Similarly detrimental is the fact that if an error does occur, it is propagated to all subsequent information.

An encoder can only be as good as its peripherals - the mechanical parts and processing electronics. The size and weight of an encoder, the shaft loading, end of the shaft play, and the external counter are all factors that play an important role in the quality of the encoder output. The basic quality of an encoder itself, however, is its resolution. The resolution is, in essence, the smallest unit of the measured value, that measuring device can provide, or equivalently, the smallest input increment that still provides a measurable change in output. The resolution of an absolute encoder is $r = 2^n$, where n is a number of tracks of an encoder.

The corresponding angular resolution is

$$r_a = \frac{360^\circ}{2^n} \sim \frac{2\pi}{2^n}. \quad (8)$$

The resolution of an incremental encoder is simply a number of slots per resolution

$$N = \frac{\pi r^*}{s}, \quad (9)$$

where r^* is the radial distance from the center to the middle of encoder slot, and s is the width of a slot (and the opaque segment as well) at the same distance.

3. NONRECURSIVE ESTIMATION OF PARAMETERS OF THE JOINT ACTUATOR DYNAMICS

As mentioned above, identification of parameters of the joint dynamical model should be performed in the profound presence of the non-white disturbance d .

Modeling of the i^{th} joint actuator, based on the set of measurement data $\{u(t), y(t)\}_1^N$, can be carried out as follows:

$$\begin{aligned} y(t) &= \frac{B(z^{-1})}{A(z^{-1})}(1 + \Delta(z^{-1})W(z^{-1}))u(t) + v^*(t), \\ A(z^{-1}) &= 1 + a_1z^{-1} + \dots + a_nz^{-n}, \\ B(z^{-1}) &= b_0 + b_1z^{-1} + \dots + b_mz^{-m}, \end{aligned} \quad (10)$$

where z^{-1} denotes backward in time shift operator, u denotes motor input voltage, y denotes output of the optical encoder, and v^* denotes unknown but bounded disturbance signal. Also, it is assumed that u and y are signals of limited power, i.e. $r_{yy} < \infty, r_{uu} < \infty$. Further, ΔW denotes multiplicative component, that incorporates unmodeled dynamics, characterized by stable unknown transfer function $\Delta(z^{-1})$, and known stable transfer function $W(z^{-1})$. System (10) can be described by, [9]:

$$\begin{aligned} A(z^{-1})y(t) &= B(z^{-1})(1 + \Delta(z^{-1})W(z^{-1}))u(t) \\ &\quad + v(t) \end{aligned} \quad (11)$$

where v denotes, also, unknown but bounded signal uncorrelated with input. The existence of unmodeled dynamics is not very profound, according to equation (7). Thus, appropriate discrete model can be adopted, taking into account that $W(z^{-1}) = 0$. Then the equation (11) becomes:

$$A(z^{-1})y(t) = B(z^{-1})u(t) + v(t) \quad (12)$$

where component $v(t)$ models an error of the optical encoder and sum of influences of other joints, and can be regarded as unknown colored disturbance.

Modeling of a manipulator joint of can start from the following equation:

$$\begin{aligned} y(t) + a_1y(t-1) + \dots + a_ny(t-n) &= \\ b_0u(t) + b_1u(t-1) + \dots + b_mu(t-m) + v(t) \end{aligned} \quad (13)$$

Also, following notation is introduced:

$$\begin{aligned} a &= [a_1, a_2, \dots, a_n]^T; b = [b_0, b_1, \dots, b_m]^T \\ \varphi_y(t) &= [-y(t-1), -y(t-2), \dots, -y(t-n)]^T \\ \varphi_u(t) &= [u(t), u(t-1), \dots, u(t-m)]^T \\ \varphi_p(t) &= [u(t-m-1), \dots, u(t-m-n)]^T. \end{aligned} \quad (14)$$

Definitions of the regressor and the parameter vector are as follows:

$$\varphi^T(t) = [\varphi_y^T(t) - \varphi_p^T(t); \varphi_u^T(t); \varphi_p^T(t)] \quad (15)$$

$$\theta = [a^T; b^T; a^T] \quad (16)$$

Now, the system (13) can be rewritten in the form of linear regression:

$$y(t) = \varphi^T(t)u(t) + v(t). \quad (17)$$

Vector of the system parameters a occurs twice in the vector of parameters θ , that is being estimated. This fact is used in order to determine the bias, induced by the disturbance, in the parameter estimate.

The parameter estimate obtained by nonrecursive LS method, from the set of measurement data $\{y(t), u(t)\}_1^N$, are given by:

$$\begin{aligned} \hat{\theta}(N) &= \left(\frac{1}{N} \sum_{i=1}^N \varphi(t) \varphi^T(t) \right)^{-1} \times \\ &\quad \left(\frac{1}{N} \sum_{i=1}^N \varphi(t) y(t) \right) = \hat{R}_{\varphi\varphi}^{-1}(N) \hat{R}_{\varphi y}(N) \end{aligned} \quad (18)$$

Thus, the following relation holds:

$$\lim_{N \rightarrow \infty} \hat{\theta}(N) = \theta + R_{\varphi\varphi}^{-1} R_{\varphi v} \quad (19)$$

where

$$\begin{aligned} R_{\varphi\varphi} &= \lim_{N \rightarrow \infty} \hat{R}_{\varphi\varphi}(N) = \\ &\lim_{N \rightarrow \infty} \left(\frac{1}{N} \sum_{i=1}^N \varphi(t) \varphi^T(t) \right) \quad (20) \\ R_{\varphi v} &= \lim_{N \rightarrow \infty} \left(\frac{1}{N} \sum_{i=1}^N \varphi(t) y(t) \right) \end{aligned}$$

Equation (14) can be written in the form [5]:

$$\begin{aligned} \lim_{N \rightarrow \infty} \hat{\theta}(N) &= \lim_{N \rightarrow \infty} \begin{bmatrix} \hat{\theta}_1(N) \\ \hat{\theta}_2(N) \\ \hat{\theta}_3(N) \end{bmatrix} = \begin{bmatrix} a \\ b \\ a \end{bmatrix} + \\ R_{\varphi\varphi}^{-1} \begin{bmatrix} R_{yy} \\ 0 \\ 0 \end{bmatrix} \quad (21) \end{aligned}$$

because, $v(t)$ is uncorrelated with input signal $u(t)$, thus:

$$R_{\varphi v} = [r_{yy}(1), \dots, r_{yy}(n), 0, \dots, 0] = [R_{yy}, 0]. \quad (22)$$

$\hat{\theta}_1(N)$ and $\hat{\theta}_3(N)$ denote estimates of the parameter vector a . Therefore, $\hat{\theta}(N)$ yields two estimates of a , and difference $\lim_{N \rightarrow \infty} [\hat{\theta}_1(N) - \hat{\theta}_3(N)]$ depends, only, on the bias component R_{yy} , induced by the disturbance. This fact suits $\hat{\theta}(N)$, for extraction of the bias in the parameter estimates, through the difference between two estimates of a .

If matrix Z is adopted as $Z^T = [I, 0, -I]$; $\dim(Z) = (2n + m + 1) \times n$

then from equation (18) follows:

$$Z^T \lim_{N \rightarrow \infty} \hat{\theta}(N) = Z^T R_{\varphi\varphi}^{-1} Q R_{yy} \quad (23)$$

where $Q = [I, 0]^T$; $\dim(Q) = (2n + m + 1) \times n$. A consistent estimate of R_{yy} is given by:

$$\hat{R}_{yy} = (Z^T R_{\varphi\varphi}^{-1} N Q)^{-1} Z^T \hat{\theta}(N). \quad (24)$$

It is obvious, from equation (19), that the unbiased parameter estimates are given by:

$$\begin{aligned} \hat{\theta}_u(N) &= \hat{\theta}(N) - \hat{R}_{\varphi\varphi}^{-1} N Q \hat{R}_{\varphi v}(N) \\ &= \hat{\theta}(N) - \hat{R}_{\varphi\varphi}^{-1} N Q \times \\ &(Z^T \hat{R}_{\varphi\varphi}^{-1} N Q)^{-1} Z^T \hat{\theta}(N). \quad (25) \end{aligned}$$

Further, $\hat{\theta}_0$ denotes an unbiased estimate of the vector of parameters $\theta_0 = [a, b]^T$. If matrix H is adopted as:

$$H = \begin{bmatrix} I & 0 \\ 0 & I \\ I & 0 \end{bmatrix}; \dim(H) = (2n + m + 1) \times (n + m + 1)$$

then, following relation holds: $H \hat{\theta}_0 = \theta$.

The above stated yields:

$$\begin{aligned} \hat{\theta}_0(N) &= (H^T H)^{-1} H^T (I \\ &- \hat{R}_{\varphi\varphi}^{-1} N Q (Z^T \hat{R}_{\varphi\varphi}^{-1} N Q)^{-1} Z^T) \hat{\theta}(N). \quad (26) \end{aligned}$$

Equations (18) and (26) give a nonrecursive algorithm, that yields an unbiased estimate of the parameters, for the system described with equation (1).

If matrix $\hat{R}_{\varphi\varphi}(N)$ is nonsingular, then the solution for $\hat{\theta}(N)$, according to equation (18), will exist. In the theory of identification of dynamical systems, this condition is denoted as a PE condition for a regression vector, $\varphi(t)$. This condition is usually stated as:

$$\alpha I \prec \sum_{i=t}^{t+L} \varphi(i) \varphi^T(i) \leq \beta I, \forall t \quad (27)$$

where L is an integer, and $\alpha, \beta > 0$. Condition on $\det(\hat{R}_{\varphi\varphi}(N))$ is connected with the PE characteristics of input signal. During the motion of manipulator, in many manipulation tasks, this condition is not fulfilled. In a manipulation task, it is common, that velocity has a trapezoid-like profile. A typical velocity profile, when manipulator transfers an object from one place to another, is shown at Fig. 2.

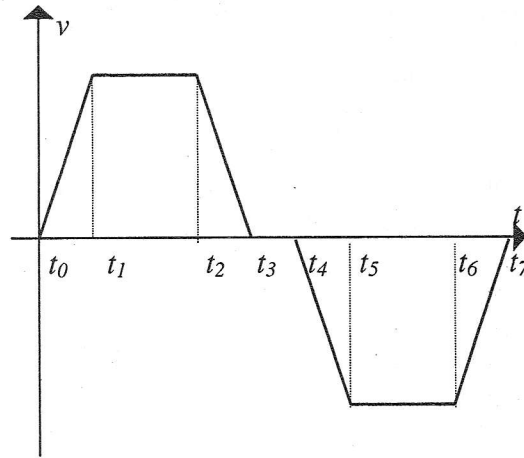


Figure 2. A typical velocity profile, during the performance of a manipulation task

The phase of motion, from $t = t_0$ to $t = t_3$, represents the motion of manipulator without the load. In the time interval $t_3 \prec t \prec t_4$, the end-effector takes the object. During the phase from t_4 to t_7 , manipulator carries the object. The time intervals $t_1 \leq t \leq t_2$, $t_3 \leq t \leq t_4$, and $t_5 \leq t \leq t_6$ correspond to the working conditions, when the input signal is constant. Regarding the PE condition, the time interval, $t_3 \leq t \leq t_4$, is specially unfavorable. During that period, the input signal equals zero.

4. RECURSIVE ESTIMATION OF PARAMETERS OF THE JOINT ACTUATOR DYNAMICS

Very often, especially in the adaptive control systems, there is a need for algorithms, that, in real time, perform estimation of the parameters of time varying system. The estimation is, by the rule, performed through the recursive procedures, because they have several advantages in comparison to nonrecursive ones.

The procedure of transformation of basic nonrecursive LS method, to recursive form (RLS), is given in several books on system identification [5,6]. Following that procedure, nonrecursive BFLS can be transformed into BFRLS.

Starting from the equation (18), and adopting that the number of measurement data is $N = t$, following equation can be written:

$$\begin{aligned}\hat{\theta}(N) &= \left(\frac{1}{t} \sum_{i=1}^t \varphi(i) \varphi^T(i) \right)^{-1} \left(\frac{1}{t} \sum_{i=1}^t \varphi(i) y(i) \right) \quad (28) \\ &= P(t) \left(\sum_{i=1}^t \varphi(i) y(i) \right)\end{aligned}$$

From the last equation, it is obvious, that the covariance matrix $P(t)$ can be computed recursively as follows:

$$P^{-1}(t) = P^{-1}(t-1) + \varphi(t) \varphi^T(t). \quad (29)$$

In order to obtain, in recursive manner, estimate of the vector of parameters θ , besides equation (29), following equations have to be set:

$$e(t) = y(t) - \varphi^T(t) \hat{\theta}(t-1), \quad (30)$$

$$K(t) = P(t) \varphi(t), \quad (31)$$

$$\hat{\theta}(t) = \hat{\theta}(t-1) + K(t) e(t), \quad (32)$$

where $e(t)$ and $K(t)$ denote prediction error and the gain of the estimator, respectively. In order to make the algorithm run, it is necessary, that the initial conditions, $P(0)$ and $\hat{\theta}(0)$, are set.

It is sufficient to have a recursive procedure for

$$(Z^T \hat{R}^{-1}(t) Q)^{-1} = \frac{t-1}{t} (Z^T \hat{R}^{-1}(t-1) Q) - \frac{Z^T \hat{R}^{-1}(t-1) \varphi(t) \varphi^T(t) \hat{R}^{-1}(t-1) Q}{t-1 + \varphi^T(t) \hat{R}^{-1}(t-1) \varphi(t)}. \quad (37)$$

Introducing $F(t) = (Z^T \hat{R}^{-1}(t) Q)^{-1}$, the last equation can be written in the form suitable for recursive

$$F(t) = \frac{t-1}{t} F(t-1) \left(I - \frac{F(t-1) Z^T \hat{R}^{-1}(t-1) \varphi(t) \varphi^T(t) \hat{R}^{-1}(t-1) Q}{t-1 + \varphi^T(t) \hat{R}^{-1}(t-1) \varphi(t)} \right). \quad (38)$$

According to the introduced notation, the equation (33) can be rewritten in the form:

computation of the correlation matrix of regressor $R_{\varphi\varphi}$, if an unbiased estimate of the parameters, given by the equation (26), would be computed recursively. According to the equation (20), an estimate of $R_{\varphi\varphi}$, can be computed as:

$$\begin{aligned}\hat{R}(t) &= \frac{1}{t} \sum_{i=1}^t \varphi(i) \varphi^T(i) \\ &= \frac{1}{t} \left(\sum_{i=1}^{t-1} \varphi(i) \varphi^T(i) + \varphi(t) \varphi^T(t) \right).\end{aligned}$$

The expression, for recursive computation of the regressor covariance matrix, is:

$$\hat{R}(t) = \frac{t-1}{t} \hat{R}(t-1) + \frac{1}{t} \varphi(t) \varphi^T(t). \quad (33)$$

Thus, an unbiased estimate of the parameters, taking into account the equation (26), can be computed as:

$$\begin{aligned}\hat{\theta}_0(t) &= (H^T H)^{-1} H^T (I - \\ &\quad \hat{R}^{-1}(t) Q (Z^T \hat{R}^{-1}(t) Q)^{-1} Z^T) \hat{\theta}(t).\end{aligned} \quad (34)$$

The algorithm, for recursive computation of an unbiased estimate of the parameters, is given by the equations (29) - (34). The algorithm demands computation of matrix inversion, in every iteration, for the matrices $P^{-1}(t)$, $\hat{R}(t)$, and $Z^T \hat{R}^{-1}(t) Q$, according to the equations (31) and (34). Inversion computation, for the first and the second matrix, can be avoided, if a well-known matrix inversion lemma is applied to the equations (29) and (33). Thus, following equations hold:

$$P(t) = P(t-1) - \frac{P(t-1) \varphi(t) \varphi^T(t) P(t-1)}{1 + \varphi^T(t) P(t-1) \varphi(t)} \quad (35)$$

$$\begin{aligned}\hat{R}^{-1}(t) &= \frac{t}{t-1} \hat{R}^{-1}(t-1) (I - \\ &\quad \frac{\varphi(t) \varphi^T(t) \hat{R}^{-1}(t-1)}{t-1 + \varphi^T(t) \hat{R}^{-1}(t-1) \varphi(t)}).\end{aligned} \quad (36)$$

Now, the following equation can be set:

$$(Z^T \hat{R}^{-1}(t) Q)^{-1} = \frac{t-1}{t} (Z^T \hat{R}^{-1}(t-1) Q) - \frac{Z^T \hat{R}^{-1}(t-1) \varphi(t) \varphi^T(t) \hat{R}^{-1}(t-1) Q}{t-1 + \varphi^T(t) \hat{R}^{-1}(t-1) \varphi(t)}. \quad (37)$$

computation, i.e. there is no need for the computation of matrix inversion. Thus, the following equation holds:

$$\begin{aligned}\hat{\theta}_0(t) &= (H^T H)^{-1} H^T (I - \\ &\quad \hat{R}^{-1}(t) Q F(t) Z^T) \hat{\theta}(t).\end{aligned} \quad (39)$$

It is a well known fact, that the gain of the RLS estimator, denoted $K(t)$, goes to zero, when the covariance matrix, $P(t)$, diminishes. This effect is known as estimator turn-off, [5]. There is the same problem in the case of BFRLS estimator. Thus, if the initial value of the parameters estimate $\hat{\theta}_0(0)$ is bad, the true value of the parameters cannot be reached. Therefore, this version of the algorithm cannot be used in the case of time varying parameters. The problem of the estimator turn-off can be solved, if RLS algorithm with forgetting factor, $\lambda \neq 1$, is employed, in the part of algorithm where, biased parameters estimate $\hat{\theta}$, is computed. Thus, the computation of the matrix $P^{-1}(t)$, according to the equations (29) and (34), has to be replaced by:

$$P^{-1}(t) = \lambda P^{-1}(t-1) + \varphi(t)\varphi^T(t). \quad (40)$$

In order to avoid the computation of matrix inversion, the last equation can be transformed to:

$$P(t) = \left(I - \frac{P(t-1)\varphi(t)\varphi^T(t)}{\lambda + \varphi^T(t)P(t-1)\varphi(t)} \right) \times \frac{P(t-1)}{\lambda}. \quad (41)$$

When $\lambda < 1$ (a typical value is adopted from the interval $0.9 < \lambda \leq 0.99$), the algorithm will perform well, if PE is adequate during the identification process. Considering implementation of the recursive identification algorithms, usually, evaluation of PE quality of the regressor is based on the trace of covariance matrix P [10], instead the equation (27). It is common, that the manipulator has a trapezoid like profile of velocity, during the motion. In that case, an actuator driving voltage and a link velocity are kept constant, on the substantial part of the manipulator trajectory. On the other hand, it is more difficult to fulfill the PE condition, in the case of the BFRLS algorithm, due to the larger regression vector $\varphi(t)$. Thus, it is very important to achieve good performance of the algorithm, in the case of the large time intervals with inadequate PE. Computation of the covariance matrix is modified, in the case of, so called, stabilized version of the adaptive estimator (SRLS). Instead of the equation (40), in the case of SRLS, there is the following equation:

$$P^{-1}(t) = (1 - \rho)P^{-1}(t-1) + \varphi(t)\varphi^T(t) + \rho\alpha I \quad (42)$$

where $\rho \in (0,1)$ and $\alpha > 0$. It is obvious, that in the case $\alpha = 0$, modification becomes the RLS algorithm with forgetting factor $\lambda = 1 - \rho$. Also, it is necessary

to avoid a computation of matrix inversion, $P^{-1}(t)$, in every iteration. This cannot be done in a usual way, using the matrix inversion lemma. Thus, there is a

solution of this problem, in [10], based on the following approximation.

Firstly, equation (42) should be rewritten as:

$$P^{-1}(t) = E^{-1}(t) + \varphi(t)\varphi^T(t) \quad (43)$$

where

$$E^{-1}(t) = \rho\alpha(I + \frac{1-\rho}{\rho\alpha}P^{-1}(t-1)). \quad (44)$$

Now, equations (43) and (44) can be transformed to the form:

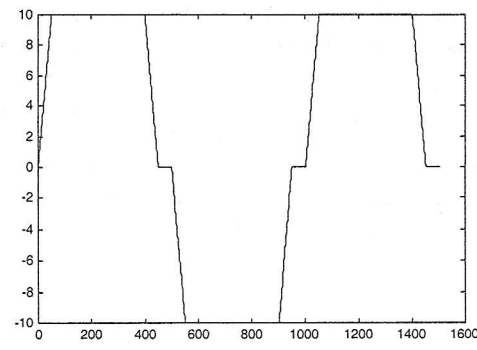
$$P(t) = \left(I - \frac{E(t)\varphi(t)\varphi^T(t)}{\lambda + \varphi^T(t)E(t)\varphi(t)} \right) \frac{E(t)}{\lambda}, \quad (45)$$

$$E(t) = \frac{P(t-1)}{1-\rho} - \frac{\rho\alpha}{(1-\rho)^2} P^2(t-1) + \dots \quad (46)$$

It is shown, in [10], that, in order to compute $E(t)$, it is sufficient to take into account the first and the second term, from the right hand side of the equation (46).

5. SIMULATION RESULTS

Manipulator PUMA 560 is modeled by software package MATLAB, Robotics Toolbox. The actuators of all PUMA 560 joints are driven by the control voltage depicted at Fig. 3.



Iterations
Figure 3. Joint control voltage[V]

Results of identification of the first joint actuator dynamics are presented in this section. Adopted values of the BFRLS algorithm parameters are: $P(0) = 10^3$, $\rho = 0.01$. Also, the second order discrete transfer function is adopted in order to model the actuator dynamics. In the first test case, encoder resolution, considering measurement of the actuator output, is not taken into account. Error of the one-step-ahead output prediction, estimates of the model parameters and the places of the discrete transfer function poles are presented at Fig. 4 - 6, respectively.

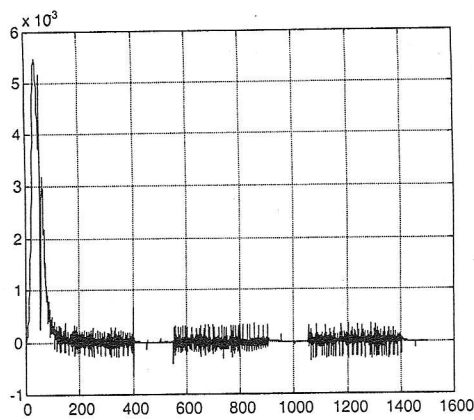


Figure 4. Prediction error

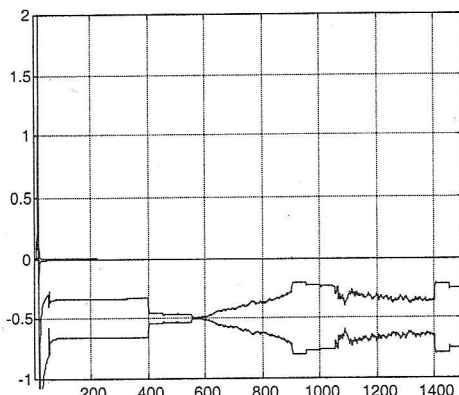


Figure 5. Parameter estimates

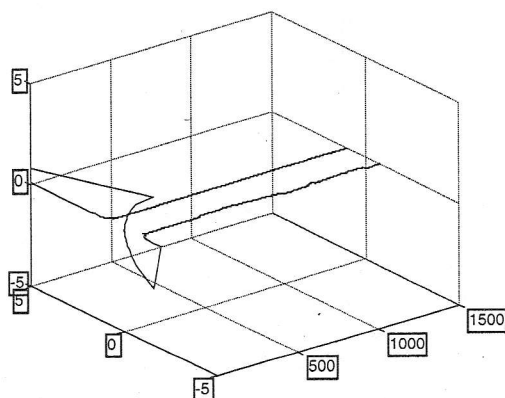


Figure 6. Poles of the model

In order to track PE characteristics of the regressor, trace of the covariance matrix $P(t)$ is presented at Fig. 7.

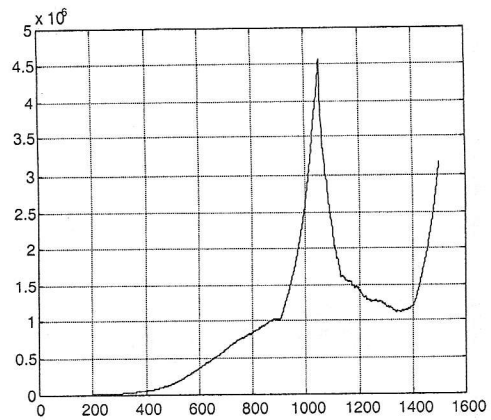


Figure 7. Trace of covariance matrix

It is obvious, that there are some time intervals where $\text{trace}[P(t)]$ exponentially grows. Fig. 5. and Fig. 7. illustrate influence of the covariance matrix variations on the variations of the estimates of the model parameters.

In the second test case, encoder resolution is taken into account. This is done by rounding a joints angular displacement data. Each data, presented in radians, is truncated, thus having the three decimal figures behind decimal point. This corresponds to the resolution of 10^{-3} radians. Fig. 8. illustrates a change in regressor PE characteristics due to adopted encoder resolution. Fig. 8. presents a trace of the covariance matrix $P(t)$.

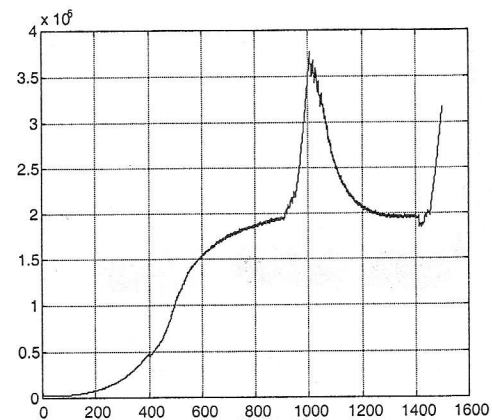


Figure 8. Trace of covariance matrix, in the presence of encoder resolution

Comparison of Fig. 7. and Fig. 8. shows improved regressor PE characteristics. Variations of a trace of the covariance matrix $P(t)$ are less profound. Hence, variations of estimates of the parameters are less profound. Estimates of the parameters are presented at Fig. 9.

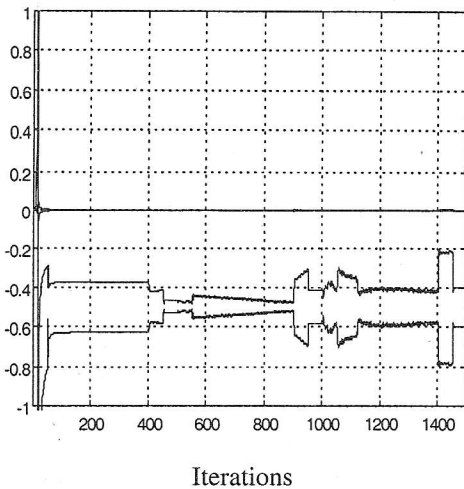


Figure 9. Parameter estimates, in the presence of encoder resolution

Therefore, a problem of covariance matrix blow-up is diminished, but it still exists.

The third test case corresponds to the BFRLS algorithm proposed in this paper. Values of the algorithm parameters are the same as in previous test cases. Value of the stabilization factor α is $\alpha = 10^{-6}$. Encoder resolution model is the same as in the second test case. Error of the one-step-ahead output prediction, estimates of the model parameters and the places of the discrete transfer function poles are presented at Fig. 10 - 12, respectively.

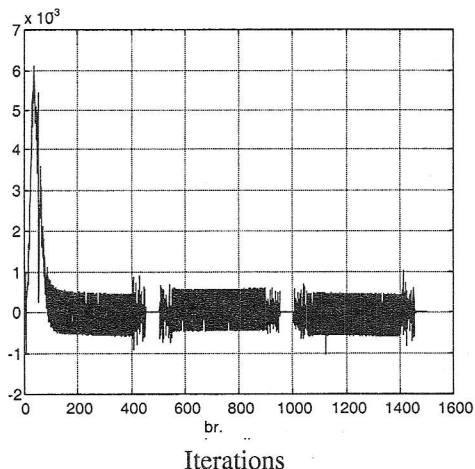


Figure 10. Prediction error

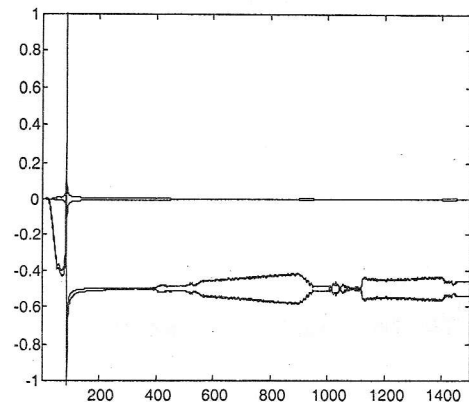


Figure 11. Parameter estimates

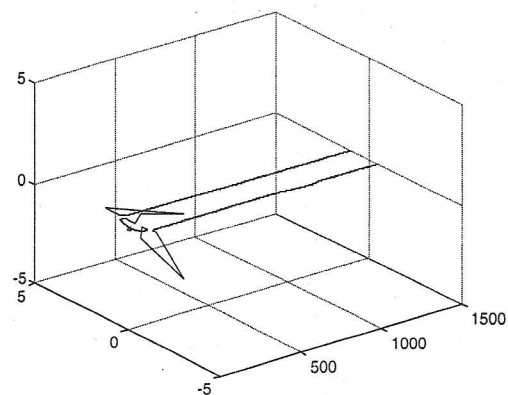


Figure 12. Poles of the model

6. CONCLUSION

Recursive algorithm, for identification of the dynamical model parameters, in the case of the system disturbed by the colored noise, is proposed in this paper. It is shown, that encoder resolution and interaction among manipulator joints can be modeled as colored disturbance, considering the model of joint actuator. Algorithm, for typical manipulation tasks, yields small variations of parameter estimates, because in stabilized version of the algorithm there is no need for a computation of matrix inversion. Simulation results confirm undertaken analysis and benefits from the proposed algorithm.

REFERENCES

- [1] Saligrama R. Venkatesh, Munther A. Dahleh, "Identification in the Presence of Classes of Unmodeled Dynamics and Noise", IEEE Transactions on Automatic Control, Vol. 42, No. 12, pp.1620-1635, December 1997.

- [2] Chun-Bo Feng, Ying Zhang, "Unbiased Identification of Systems with Nonparametric Uncertainty", IEEE Transactions on Automatic Control, Vol. 40, No. 5, pp.933-936, May 1995.
- [3] P. Stoica, T. Söderstrom, V. Simonyte, "Study of a Bias-Free Least Squares Parameter Estimator", IEE Proc. Control Theory and Applications, Vol. 142, pp. 1-6, January 1995.
- [4] Y. Zhang, T. Lie, C. Soh, "Consistent Parameter Estimation of Systems Disturbed by Correlated Noise", IEE Proc. Control Theory and Applications, vol. 144, pp. 40-44, January 1997.
- [5] T. Söderstrom, P. Stoica, *System Identification*, Prentice-Hall, Englewood Cliffs, N.J., 1988.
- [6] L. Ljung, *System Identification - Theory for the User*, Prentice-Hall, Englewood Cliffs, N.J., 1987.
- [7] P. Marić, I. Krčmar, "Bias-Free Recursive Least Squares Parameter Estimation - Computational Aspect", Proc. of 4th Conference on Informational Technologies, IT, pp. 359-362, Žabljak, 1999.
- [8] L. Sciavicco, B. Siciliano, *Modeling and Control of Robot Manipulators*, McGraw-Hill, Singapore, 1996.
- [9] Wolfram Stadler, *Analytical Robotics and Mechatronics*, McGraw-Hill, Singapore, 1995.
- [10] M. Božić, P. Marić, "Estimation of Time Varying Parameters", Proc. of 50th ETRAN Conference, vol. no. 1, pp. 429-432, Budva, 1996.

A PEDESTRIAN AND VEHICLE MOTION IDENTIFICATION BY AN "IF-THEN" RULES BASED METHOD

Milojko V. Jevtović, *VTI VJ, Beograd*
Vlastimir Pavlović, *Faculty of Electronic Engineering, Niš*

Abstract - In this paper, the original sensor signal processing method and results interpretation, enabling the pedestrian and vehicle motion identification in the observed area, are exposed. Sensors perform motion detection. The method is based on the time-domain sensor signal analysis by computing the certain parameters, and the results are interpreted, upon the beforehand defined rules. The decision rules about what is moving in the protected area are also discussed. Deciding, i.e. results interpretation, is performed by class separation from the parameter set, such as: mean-length signal duration in the observed time period, mean-time duration of the pause between the sensor successive initiations, mean-time duration of the pause between two successive passing through "zero", mean motion speed, etc. The proposed method gives positive results, unlike the attempts for solving the identification problem by using several other methods. The mentioned method has a software realization on the laboratory equipment (personal computer and digital signal processor). Its efficiency is tested in real conditions. The experimental results show that the proposed method is very efficient for solving the pedestrian and vehicle automatic identification problem.

1. INTRODUCTION

In electronic protecting system realization, the problem of provocative classification, perturbing the protected area or object security always arise. In other words, the problem is how to identify the pedestrian and vehicle motions, i.e. how to classify provocative inciting (activating) the appropriate sensors by its motions. The assumption is that the information about what is moving is contained in the sensor signal. In the previous work for solving the mentioned problem, several authors have applied a few different signal processing methods, such as: higher order spectrums [1], comparison with reference signal [2], cyclic spectrum method [3], cepstrum [4], [5] and higher order moments [6]. These methods did not give satisfactory results in the case of seismic signal. Thus, our approach to the solution of the problem was to investigate time-domain sensor signal analysis, computing certain parameters and to give results interpretation by appropriate rules. The sensor analysis method, computing parameters and decision rules are presented in this paper. The results review by real signals is also given. In addition to the commercial speed and acceleration sensors, with appropriate amplifiers, a new acceleration sensor, with piezoceramic, and a new analogue circuit are used. The characteristics of the sensor proposed by Prof. Pavlović [9] are optimized in a mechanical and electrical sense, thus, after incitement, the impulse response has a dominant first oscillation and decreasing envelope. In the absence of the incitement, it has significantly low level of

seismic noise. We emphasize that the other sensor solutions [7,8], Fig.1, with amplifier, give an impulse response, which has increasing oscillation envelope up to the peak value, after

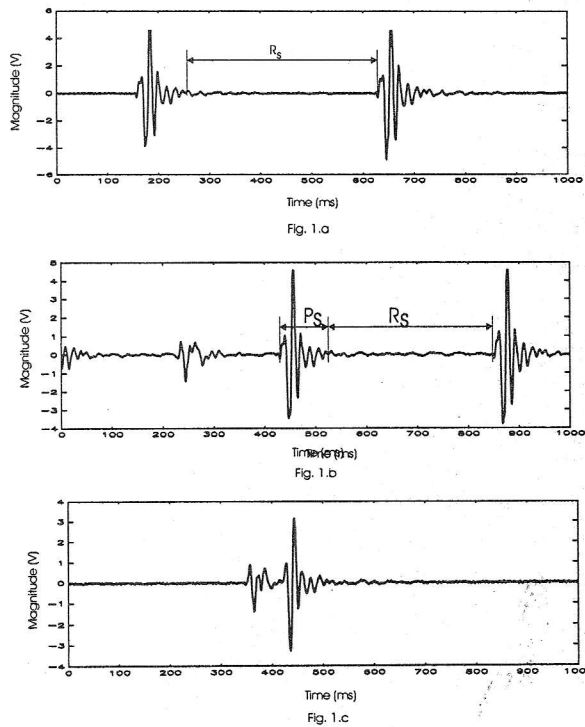


Fig. 1 Waveforms of the original seismic signals

which the envelope decreases, Fig.3.

2. SENSOR SIGNAL ANALYSIS

During pedestrian motion, the sensor is incited by a foot stroke on the ground. Fig. 1 shows the sensor's signal waveform, caused by

pedestrian motion. For such signals, a mean-length duration can be defined as:

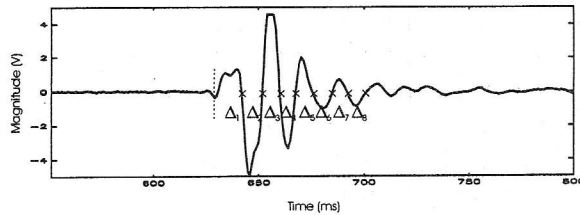


Fig. 2. Waveform of the original seismic signal

$$P_S = \frac{1}{N} (P_{S1} + P_{S2} + \dots + P_{SN}) = \frac{1}{N} \sum_{i=1}^N P_{Si} \quad (1)$$

where N is the number of pedestrian foot strokes, and P_{Si} – is the i -th stroke duration. This definition of P_S is valid for signals that do not have significant presence of reflections (Figs. 1b and c). The reflected signals influence can be avoided in two ways: by computing P_S for large number of N or by rejecting signals whose duration is less than the predefined minimal value P_{Smin} .

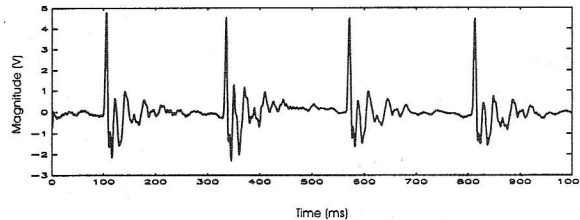


Fig. 3. Waveform of the original seismic signal

The value of P_S , depending on the moving person mass, its motion speed and ground characteristics, will be bounded:

$$P_{Smin} \leq P_S \leq P_{Smax} \quad (2)$$

for most persons moving in the observed area.

For a sensor signal, caused by pedestrian motion, the mean-time R_S , physically denoting pause duration between two steps, is defined by (see Fig.1):

$$R_S = \frac{1}{K} (R_{S1} + R_{S2} + \dots + R_{SK}) = \frac{1}{K} \sum_{i=1}^K R_{Si} \quad (3)$$

where $i=1,2,\dots,K$ is the pedestrian steps number, and R_{Si} is the time between two successive foot strokes on the ground.

The mean-time pause duration between two steps depends, of course, on motion speed (slow walk, normal walk, running) and the number of moving pedestrians (one, two or group of pedestrians). For one walking pedestrian, pause duration R_S will be bounded as:

$$R_{SK\ min} \leq R_S \leq R_{SK\ max} \quad (4)$$

while for a running pedestrian it is:

$$R_{ST\ min} \leq R_S \leq R_{ST\ max} \quad (5)$$

Foot stroke on the ground, caused by pedestrian motion, creates oscillations that the sensor detects and generates an alternating signal, which is periodic at one part (Fig.2).

Assuming that the sensor signal does not contain direct (DC) component (it can be simply eliminated, if exists) it is easy to notice that signal from Fig.2 has a certain number of passing through "zero", in Fig.2 denoted by:

$$\Delta_1, \Delta_2, \dots, \Delta_Q$$

Mean-value of interval duration between two successive sensor signal "zero" passings, can be determined from the relation:

$$\bar{\Delta}_S = \frac{1}{Q} (\Delta_1 + \Delta_2 + \dots + \Delta_Q) = \frac{1}{Q} \sum_{i=1}^Q \Delta_i \quad (6)$$

where Q is the number of "zero" passings.

Pedestrian motion speed can be determined from the motion path (trajectory) by determining two path coordinates, i.e. by measuring the distance (already known) between them and the elapsed time for the pedestrian to cross that distance.

A new method in which it is not necessary to know paths in order to determine the pedestrian motion speed is presented in this paper.

According to Fig.1 the pedestrian step duration is:

$$T_K = P_S + R_S \quad (7)$$

Step mean-duration can be evaluated from the relation:

$$T_{KS} = \frac{1}{m} \sum_{i=1}^m (P_{Si} + R_{Si}) \quad (8)$$

where m is the step number.

The step number in a time unit, measured in a time interval of τ seconds, is:

$$K_S = \frac{\tau}{T_{KS}} = \frac{\tau m}{\sum_{i=1}^m (P_{Si} + R_{Si})} \quad (9)$$

If a mean-length pedestrian step is denoted by D (regardless on a motion manner) then the pedestrian speed motion can be determined from the relation:

$$V_p = K_S D = \frac{\tau m D}{\sum_{i=1}^m (P_{Si} + R_{Si})} [m/s] \quad (10)$$

The accuracy of the determined pedestrian speed motion depends on the adopted pedestrian step mean-length value.

The vehicle motion speed is determined by measuring the time interval between the signal generation at the two sensors, placed on the path. The distance between two sensors is beforehand defined (measured).

3. DECISION RULES

Sensor signal parameters, depending on the types of stimuli (pedestrian, vehicle), lie within certain boundaries. For most of these parameters, boundaries can be determined only after a large number of experiments with real sensors. On the basis of performed experiments and obtained results, some experimental knowledge is made, which can be formulated in several rules, such as:

1. Generated sensor signal, caused by vehicle motion, is continuous and lasts longer than 3 seconds for sure.
2. Generated sensor signal, caused by pedestrian motion (one, two or group of pedestrians) has interruptions, which mean duration is longer than 30ms.
3. If one person performs normal walk (five or more steps), then the time interval between two successive foot strokes, ranges between 130ms to 800ms.
4. Pedestrian motion speed, in the case of slow walk is less than 3 km/h, in the case of normal walk it ranges between 3 to 7 km/h, while in the case of running it is greater than 7 km/h.
5. Vehicle motion speed is greater than 15 km/h.

On the basis of experiments performed with real stimuli, the other rules for processing results interpretation are defined. Using them, a decision as to what is moving in the observed, protected area can be made.

Considering the computing results of signal parameters values and the set of the aforementioned rules, the determination problem of what is moving in the protected area, can be solved by an "if-then" based method. The algorithmic approach has following form:

if

P_S at boundaries $P_{SM} \leq P_{SK} \leq P_{SN}$

and

R_S at boundaries $R_{SM} \leq R_{SK} \leq R_{SN}$

and

Δ_{PK} interval of "zero" passing

$\Delta_{MK} \leq \Delta_{PK} \leq \Delta_{NK}$

and

v_p motion speed $v_{pM} \leq v_{pK} \leq v_{pN}$

etc.

then

the motion provocative:
normal walking PEDESTRIAN

The second example, for the running pedestrian in the protected area, is:

if

P_S at boundaries $P_{SMt} \leq P_{St} \leq P_{SNt}$

and

R_S at boundaries $R_{SMt} \leq R_S \leq R_{SNt}$

and

Δ_{Pt} interval of "zero" passing

$\Delta_{Mt} \leq \Delta_{Pt} \leq \Delta_{Nt}$

and

v_{pt} running speed $v_{pMt} \leq v_{pt} \leq v_{pNt}$

etc.

then

the motion provocative:
running PEDESTRIAN

For the vehicle motion, algorithmic approach has the form:

if

sensor signal continual $P_S > 3s$

and

sensor signal R_S perpetual $R_S = 0s$

and

Δ_{Pk} interval of "zero" passing

$\Delta_M \leq \Delta_{PK} \leq \Delta_N$

and

v_{pv} motion speed $v_{vM} \leq v_{vK} \leq v_{vN}$

etc.

then

the motion provocative:
VEHICLE

Extensions of the above algorithmic approaches to a group of pedestrians, group of vehicles etc. can be realized in a similar way.

4. RESULTS

On the basis of the proposed method, a software module for pedestrian and vehicle motion identification was developed. It was installed on a personal computer with digital signal processor connected with a set of sensors array via (by) the low-pass amplifiers and filters. Two types of sensors, electrodynamics (geophone) and piezoelectric, are used in the investigation.

Testing of the method proposed for pedestrian and vehicle motion identification is performed in real conditions, inciting sensors by pedestrian and vehicle motion. Experiment is performed by motion of ten (10) different pedestrians and two

groups of pedestrians in the protected area. They were walking slowly, normal and fast (running). Three-hundred-forty-five (345) passings through protected area were performed. Successful identification of 337 pedestrian passings was achieved. Eight passings by slow walk were not identified, due to large pedestrian distance from sensors (on the sensor sensitivity threshold). Pedestrian motion identification results are presented in Table 1. The decision quality of vehicle motion identification was examined, also. All of performed 30 vehicle passings, were successfully identified.

A measuring of the pedestrian speed in the case of slow and normal walk and running is particularly performed by the proposed method.

Measured results for three pedestrian motion speeds, whereby each one passed the protected area for 30 times, are given in Table 2. Simultaneous measuring of the passed paths length and the elapsed time for those paths that were passed, have confirmed that the proposed method offers satisfactory results.

5. CONCLUSION

The proposed method for pedestrian and vehicle motion identification, based on time-domain sensor signal analysis, computing certain parameters and interpreting the results on the basis of the already defined rules, offers positive results for the decision about what is moving through the protected area.

Using the new sensor with the appropriate analogue amplifier Prof. Pavlovic's, positive identification results, by the described new method, are obtained.

Table 1. The results of identification

| Ser. no. | Incitation provocativ e | Normal walk | | | Slow walk | | | Running | | |
|-------------|-------------------------------|---------------|--------------|--------|---------------|-------------|--------|---------------|-------------|--------|
| | | No. incit. | Identif. no. | | No. incit. | Identif. No | | No. incit. | Identif. No | |
| | | | Succes. | Unsuc. | | Succes. | Unsuc. | | Succes. | Unsuc. |
| 1 | Pedestr. 1 | 10 | 10 | 0 | 10 | 9 | 1 | 10 | 10 | 0 |
| 2 | Pedestr. 2 | 10 | 10 | 0 | 10 | 9 | 1 | 10 | 10 | 0 |
| 3 | Pedestr. 3 | 10 | 10 | 0 | 10 | 9 | 1 | 10 | 10 | 0 |
| 4 | Pedestr. 4 | 10 | 10 | 0 | 10 | 9 | 1 | 10 | 10 | 0 |
| 5 | Pedestr. 5 | 10 | 10 | 0 | 10 | 9 | 1 | 10 | 10 | 0 |
| 6 | Pedestr. 6 | 10 | 10 | 0 | 10 | 10 | 0 | 10 | 10 | 0 |
| 7 | Pedestr. 7 | 10 | 10 | 0 | 10 | 10 | 0 | 10 | 10 | 0 |
| 8 | Pedestr. 8 | 10 | 10 | 0 | 10 | 10 | 0 | 10 | 10 | 0 |
| 9 | Pedestr. 9 | 10 | 10 | 0 | 10 | 10 | 0 | 10 | 10 | 0 |
| 10 | Pedestr. 10 | 10 | 10 | 0 | 10 | 10 | 0 | 10 | 10 | 0 |
| 11 | 2pedestrns. | 10 | 10 | 0 | 10 | 10 | 0 | 10 | 10 | 0 |
| 12 | Ped. group | 5 | 5 | 0 | 5 | 5 | 0 | 5 | 4 | 1 |

Table 2. The measured pedestrian motion speeds

| Motion speed km/h | | | | | | | | |
|-------------------|------|------|------------|------|-------|------------|------|-------|
| Pedestr. 1 | | | Pedestr. 2 | | | Pedestr. 3 | | |
| SW | NW | RUN | SW | NW | RUN | SW | NW | RUN |
| 2.76 | 3.63 | 7.43 | 3.45 | 5.87 | 10.09 | 2.58 | 3.28 | 14.90 |
| 2.94 | 3.63 | 7.43 | 3.63 | 5.35 | 11.40 | 2.71 | 3.92 | 16.10 |
| 2.25 | 4.49 | 9.33 | 5.01 | 4.66 | 9.67 | 2.69 | 3.45 | 13.60 |
| 3.97 | 2.42 | 7.94 | 2.25 | 3.90 | 10.07 | 2.91 | 4.10 | 13.10 |
| 3.45 | 3.11 | 7.08 | 4.66 | 6.22 | 10.04 | 3.10 | 3.28 | 10.70 |
| 2.08 | 2.59 | 6.91 | 2.94 | 6.04 | 13.03 | 2.45 | 3.92 | 13.00 |
| 2.94 | 3.11 | 7.77 | 2.25 | 7.94 | 11.10 | 2.41 | 3.45 | 12.40 |
| 2.59 | 2.59 | 9.33 | 2.59 | 5.30 | 11.60 | 2.71 | 4.11 | 11.60 |
| 3.11 | 2.94 | 8.29 | 2.42 | 4.60 | 13.10 | 2.81 | 3.28 | 15.70 |
| 2.76 | 2.25 | 8.12 | 1.21 | 7.94 | 12.40 | 2.81 | 4.10 | 11.60 |

REFERENCES

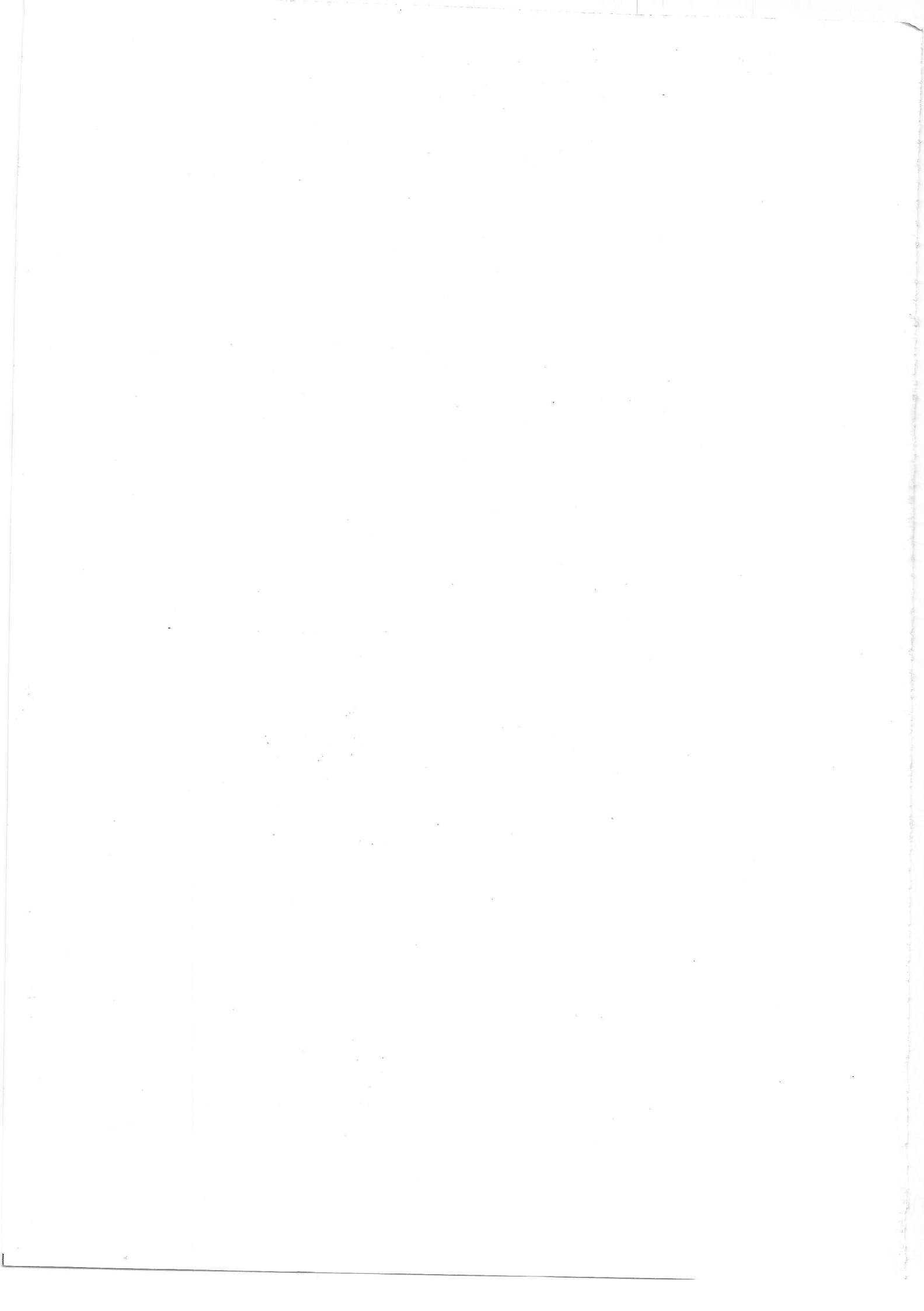
- [1] C. Nikias, J. Mendel: *Signal processing with higher order spectra*. IEEE Signal Processing Magazine, July, 1993.
- [2] G.Papadopoulos, K. Efsthathion, Yiqi Li, A. Delias: *Implementation of an intelligent instrument for passive recognition and two-dimensional location estimation of acoustic targets*. IEEE Trans. on Instrumentation Publishers B.V.
- [3] A.Oppenheim,R.Schafer: *Digital Signal Processing*. Prentice-Hall, Inc, Englewood Cliffs, New Jersey, 1975.
- [4] G.R. Reddy, V.V. Rao: *On the computation of complex cepstrum through differential cepstrum*. Signal Processing 13, Vol. 13, No 1, July 1987, Elsevier Science
- [5] A. Suen, J. Wang, Y. Chiang: *A Cepstrum chi: Architecture and implementation*. IEEE International Symposium on Circuits and Systems, Washington USA, April 29-May 3 1995.
- [6] Chrysostomos I. Nikias and Athina P. Petropoulou: *Higher-order spectra analysis*. Prentice Hall, Englewood Cliffs, 1993.
- [7] R.B. Randall: *Frequency analysis*, Brüel&Kjaer, September 1987.
- [8] A.J. Pointon: *Piezoelectric devices*. IEE PROC, Vol. 129, Pt. A. No. 5, July 1982 pp 285-307.
- [9] V.D. Pavlović: *Some problems in designing seismic signal analogue amplifier*. To be published.

SW – slow walk

NW – normal walk

RUN - runing





INSTRUCTIONS FOR AUTHORS

In the journal "Electronics", we publish the scientific and professional papers from different fields of electronics in the broadest sense like: automatics, telecommunications, computer techniques, energetic, nuclear and medical electronics, analysis and synthesis of electronic circuits and systems, new technologies and materials in electronics etc. In addition to the scientific, reviewal and professional papers, we present new products, new books, M. Sc. and Ph. D. theses.

In order to enable the unification of the technical arrangement of the papers, to simplify the printing of the review "ELECTRONICS", we are giving this instruction for the authors of the papers to be published in this professional paper.

The papers are to be delivered to the editor of the journal by the e-mail or to the address of the Faculty of Electrical Engineering on a floppy and printed in three folds.

All of the three folds are to be printed on one side of the paper A4 format, 210x297 mm, i.e., 8.27" width and 11.69" height, upper and lower margins of 1", left and right margins of 1" and the header and footer are 0,5". The paper may be written in Serbian or English language. Obligatory, the paper has to be written in two columns with the spacing between columns of 0.5 cm. Our suggestion to the authors is to make their papers on a PC using the word processor Word for Windows, and for the figures to use the graphic program Corel Draw. The graphs are going from the original programs, i.e. from the programs received. The papers should not be finished at the beginning of a page. If the last manuscript page is not full, the columns on that page should be made even.

The title of the paper shall be written on the first page, in bold and 12 pts size. Also, on the first page, one line space below the title, the author's name together with the name of his institution shall be printed in the letter size of the remaining parts of the text. The remaining parts of the manuscript shall be done in two columns with 10 mm space between them. The paper shall be typed with line spacing 1 and size not less than 10 pts. After the title of the paper and the name of the author, a short content follows, written in italics. The subtitles in the text shall be written in bold, capital letters of the size as in the text (not less than 10 pts). Each paper shall, at the beginning, comprise a subtitle INTRODUCTION, and, at the end, the subtitles CONCLUSION and REFERENCES. At the end of the paper, there shall be a short abstract and the title in English accompanied with the names of authors (if the paper is not written in English).

The operators and size marks that do not use numerical values, shall be written in common letters. The size marks that can use numerical values shall be written in italics. The equations shall be written in one column with right edge numeration. If the breaking of equations or figures is not desired, those may be placed over both columns.

Illustrations (tables, figures, graphs etc.) may be wider than one column if necessary. Above a table there shall be a title for instance: Table 2. *The experimental measuring results*. The same applies to figures and graphs but the accompanying text comes underneath the figure of graphs. At the end of each paper, the used literature shall be listed in order as used in the text. The literature in the text, shall be enclosed in square brackets, for instance: ...in [2] shown is...

ELECTRONICS

Vol. 3, No. 1, June 1999

CONTENTS

| | |
|--|----|
| Preface | 1 |
| Failure Mechanisms in Power MOSFETs in Radiation Enviroment | 2 |
| <i>Predrag Habaš, Ninoslav Stojadinović</i> | |
| Modeling & simulation of AC/DC converters in modern electric drives | 14 |
| <i>Vladimir Katić, Dušan Graovac</i> | |
| Smart sensor channel modeling according to IEEE P1451 Standard..... | 30 |
| <i>Saša Ristić, Mile Stojčev</i> | |
| Symbolic Analysis of electronic circuits - Development and Application | 37 |
| <i>Predrag Petković, Dejan Tošić</i> | |
| The real-time system implementation of the control and supervision unit for the cigarette packing machine GD-X1..... | 47 |
| <i>Milun S. Jevtić, Branimir Ž. Đorđević, Andrija S. Velimirović, Vladimir D. Živković</i> | |
| Bhattacharyya distance in evaluation of the frame-based nonstationary pattern recognition methods | 55 |
| <i>Milan Marković, Milan Milosavljević, Branko Kovačević</i> | |
| Robust modified generalized likelihood ratio algorithm for speech abrupt change detection. | 62 |
| <i>Mladen Veinović, Milan Milosavljević, Zoran Banjac, Branko Kovačević</i> | |
| Nonlinear Activation Function and PDF for Nonlinear Prediction via Recurrent Neural Networks | 66 |
| <i>Danilo P. Mandić</i> | |
| A block diagram simulation approach for algebraic equations roots localization | 69 |
| <i>Bratislav Danković, Dragan Antić, Saša Dimitrijević</i> | |
| Identification of the dynamical parameters of manipulator actuator in the presence of encoder resolution..... | 73 |
| <i>Petar Marić, Igor Krčmar</i> | |
| A pedestrian and vehicle motion identification by an "if-then" rules based method..... | 82 |
| <i>Milojko V. Jevtović, Vlastimir Pavlović</i> | |